NASA Technical Memorandum 88287

Flutter Clearance of the F-14 Variable-Sweep Transition Flight Experiment Airplane – Phase I

Michael W. Kehoe

September 1987

National Aeronautics and
Space Administration

NASA Technical Memorandum 88287

Flutter Clearance of the F-14 Variable-Sweep Transition Flight Experiment Airplane – Phase I

Michael W. Kehoe
Ames Research Center, Dryden Flight Research Facility, Edwards, California

1987

National Aeronautics and
Space Administration
Ames Research Center
Dryden Flight Research Facility
Edwards, California 93523-5000

SUMMARY

An F-14 airplane was modified to become the test bed aircraft for the variable-sweep transition flight experiment (VSTFE) program. The VSTFE program is a laminar flow program designed to measure the effects of wing sweep on boundary layer transition from laminar to turbulent flow. The airplane was modified by adding an upper surface foam-fiberglass glove over a portion of the left wing. Ground vibration and flight flutter testing were accomplished to clear a sufficient flight envelope to conduct the laminar flow experiments. Flight test data indicated satisfactory damping levels and damping trends for the elastic structural modes of the airplane. The data presented in this report include frequency and damping as functions of Mach number.

INTRODUCTION

An F-14 aircraft was modified to become the test bed aircraft for the variable-sweep transition flight experiment (VSTFE) program. The VSTFE program is a laminar flow program designed to measure the effects of wing sweep on boundary layer transition from laminar to turbulent flow (refs. 1 and 2). The F-14 aircraft was selected because of its variable wing sweep capabilities, wing planform, and Mach-Reynolds number envelope. The experiment was conducted with wing sweep angles between 20° and 35°. The aircraft was modified by adding an upper wing surface foam-fiberglass glove over a portion of the left wing (fig. 1). The thickness of the glove was approximately 0.60 in.

The aeroelastic concerns for this modification were whether the resulting changes in wing weight, wing stiffness, and airfoil shape could be sufficient to adversely affect the flutter stability of the airplane. The approach taken to qualify this modification for flight was to conduct a ground vibration test (GVT) before and after glove installation. A comparison of modal parameters, including mode shapes, would then be accomplished to determine if there were any significant changes. A flight flutter program was then planned based on the GVT results.

NOMENCLATURE

CRT	cathode ray tube
G	structural damping coefficient
GVT	ground vibration test
KCAS	knots calibrated airspeed
SAS	stability augmentation system
VSTFE	variable-sweep transition flight experiment
Λ	wing sweep angle, deg

TEST OBJECTIVES

The objectives of the flutter clearance program were

1. to measure structural frequencies and mode shapes below 50 Hz for the clean airplane and the airplane with the wing glove installed,

2. to verify freedom from flutter within the flight envelope of 450 knots calibrated airspeed (KCAS) or Mach 0.90, whichever is less, for wing sweep angles of 20° to 35°, and

3. to obtain frequency and damping data for critical structural modes.

VEHICLE DESCRIPTION

The F-14 is a variable-geometry midwing airplane with leading edge slats, maneuvering flaps, and twin outward-canted vertical stabilizers and rudders. The airplane is powered by two afterburning turbofan engines. The all-movable horizontal surfaces have skins of boron-epoxy composite material.

The F-14 used for the VSTFE program had the following modifications:

1. A foam-fiberglass glove was added to the left wing beginning at wing butt line 130 and extending to wing butt line 350. The glove extended from the 5-percent chord line on the bottom of the wing, forward around the leading edge, and then aft on top of the wing, to the 60-percent chord line.

2. The wing leading edge slats were locked in the retracted position because of the glove installation.

3. The maneuvering flaps were disabled.

4. The wing fuel tanks were not used and remained empty.

5. The wing sweep override was used to maintain the sweep angle in the range of 20° to 35°. A guard was built and mounted on the wing sweep control lever to prevent inadvertent wing sweep angles beyond 35°.

TEST PROCEDURE

Ground Vibration Test

Because there were no GVT data available for the airplane on its landing gear, a GVT was first conducted with the unmodified airplane on its gear to establish a baseline. For each GVT, the landing gear struts were deflated to eliminate potential nonlinearities in the oleo-struts. The tire pressure was reduced to one-half the normal value to provide a soft support. Electrical and hydraulic power were supplied to the airplane. The wing fuel tanks were empty, and the fuselage tanks were full.

Instrumentation. — Piezoelectic accelerometers were attached to the airplane to measure the response of the structure. A force link was used to measure the input force to the structure from the electrodynamic shaker. A minicomputer-based structural analysis system (fig. 2) was used to acquire, filter, display, and record eight channels of data (one input force and seven responses) during each data acquisition.

Excitation. — Two excitation techniques were used: multishaker sine-dwell and single-shaker random. The multishaker sine-dwell technique was used to conduct frequency sweeps at various wing sweep angles and also to excite the wing fore-and-aft modes. However, the majority of the modal data was acquired using the single-shaker random approach.

The sine frequency sweeps were performed with a vertically oriented shaker placed under each wingtip to locate the approximate resonant frequencies. These sweeps were conducted with the unmodified wings swept 20°, 50°, and 68°, and the gloved wings swept 20° and 35°. All frequency sweeps were conducted from 3 to 45 Hz at a logarithmic sine sweep rate of 0.3 decade/min. These data were used only to compare with the airplane manufacturer's GVT data obtained with the airplane on a true soft support system and are not presented in the report.

For exciting the wing fore-and-aft modes, two horizontally oriented shakers were suspended from cranes and attached at the wingtips. The suspension cables were long enough to ensure that the pendulum frequency of each shaker was well below the wing fore-and-aft resonant frequencies. Both sine frequency sweep and sine-dwell modal survey data were acquired for these particular modes.

Single-input random techniques were used to excite all other structural resonant modes. For these tests, a single vertically oriented shaker was placed under the left wingtip, attached to the rear spar, and driven with a broad-band random forcing function.

Structural mode measurements. — Response data from the random excitation were acquired with the minicomputer structural analysis system for each location shown in figure 3. Transfer and coherence functions were then calculated. The coherence function was used as a measurement of the quality of the data before they were stored on the system disk. The data were sampled at 128 samples/sec using a data block size of 1024 samples (8 sec required to fill the block). The antialiasing filters were set at 50 Hz. The total number of averages used to calculate each transfer function was 500. This total included an overlap factor of eight. Overlap processing is a procedure by which a time history includes a certain amount of previously processed data and a certain amount of new data. This technique is useful when a Hanning window is used (ref. 3). A Hanning window was applied to the data to reduce leakage errors.

Once data acquisition was completed for the airplane, the modal parameters (frequency, damping, phase, and amplitude) were estimated for each mode by fitting a multiple-degree-of-freedom curve to a selected transfer function that exhibited a good response for the structural modes of interest. The estimated modal parameters, particularly phase, for each mode were examined to determine whether the curve fit was acceptable. It was necessary to examine several different transfer functions to ensure a good curve fit for all the structural modes below 50 Hz.

Once an acceptable fit was obtained for estimating the modal parameters, the modal coefficients for each mode shape were calculated by using the amplitude and phase of each measured response at the estimated resonance frequency. Animated mode shapes were then displayed to identify each mode. A more detailed example of this procedure can be found in reference 4.

After the single-point random excitation measurements were completed, the wing fore-and-aft modes were fine tuned using a coincident-quadrature analyzer by minimizing the coincident component and maximizing the quadrature component of the signal. Acceleration time histories were also used to verify phasing between the left and right sides of the airplane. Another check on the quality of the mode was to terminate electrical power to the shakers and observe the decay of the oscillations for beats. The absence of beats in the decay trace indicated that a mode was properly tuned.

Flight Flutter Test

Flutter testing was accomplished for the gloved wing configuration at altitudes of 27,500, 17,000, and 5000 ft. The planned flutter envelope expansion points at each altitude are shown in figure 4. Note that the stability augmentation system (SAS) was turned off at selected test points. Each test point was flown at wing sweep angles of 20° and 35°. The 35° wing sweep angle was flown first since it was considered to be less critical than the 20° sweep angle.

Instrumentation. — The instrumentation aboard the aircraft for flutter testing consisted of the accelerometers and position transducers indicated in figure 5. Air data parameters were obtained from a standard nose boom.

Excitation. — Random atmospheric turbulence and pilot-induced control surface pulses were used to excite the structure. Typically, 60 sec of random data were collected at each test point followed by pitch, yaw, and roll pulses in one direction. With the SAS off, only control surface pulses were used for structural excitation. The turbulence levels at 5000 ft were sufficient for good structural excitation, while the levels at 17,000 and 27,500 ft provided very little excitation.

Envelope expansion procedure. — A consistent procedure was used during the testing of the airplane. The airplane was accelerated to the specified Mach number at the test altitude. Once the airplane was stablilized, 60 sec of random data were acquired, followed by pilot-induced control surface pulses. At selected test points, control surface pulses were repeated with the SAS turned off.

Telemetered data were displayed on strip charts in the NASA Ames Research Center, Dryden Flight Research Facility, Spectral Analysis Facility. The aircraft status, which included altitude, airspeed, and Mach number, was displayed on cathode ray tube (CRT) monitors. A single selected accelerometer response (from a menu of 12) was monitored on a real-time spectrum analyzer to provide frequency domain information. A Fourier analyzer was used to provide near-real-time frequency and damping estimates for critical accelerometer responses. Clearance to proceed to the next higher Mach number test point was given by the test director in the Spectral Analysis Facility after the damping coefficients and trends for critical structural modes were observed to be satisfactory.

Postflight data analysis was performed between flights. This analysis consisted of calculating the autopower spectrum for each accelerometer response to extract improved frequency and damping values. A description of the data analysis techniques is presented in reference 5.

RESULTS

Ground Vibration Test

A comparison of the unmodified and gloved wing airplane modal data for the 20° wing sweep angle is shown in table 1. The 20° wing sweep angle was considered to be the most critical configuration for flutter. In general, there were few significant changes in modal frequencies between the unmodified and gloved wing configurations. The exceptions are discussed in the following paragraphs.

The most significant change in the modal characteristics involved the wing torsion modes. While the corresponding symmetric and antisymmetric wing torsion modes agreed very well in frequency and damping for the unmodified and modified configurations, some differences in the mode shapes were observed. The most significant difference was the addition of a new mode, at 21.26 Hz, caused apparently by the wing modification. This new mode was a decidedly asymmetric wing torsional response of only the left wing when the natural laminar flow glove was installed. Figure 6 compares the wing torsion mode shapes for the unmodified and gloved wing configurations.

Differences between the left and right wing fore-and-aft pivot mode frequencies were noted for both the unmodified and the gloved wing configurations. In both configurations, the antisymmetric mode was tuned at a higher frequency on the right wing with the laminar flow gloved configuration showing the larger discrepancy. The symmetric mode showed smaller differences between the left and right for the unmodified configuration, and no left-right anomalies were exhibited in the gloved wing configuration. Free play in the pivots most likely contributed to the difficulty of tuning these modes.

Flight Flutter Test

Plots of frequency and damping as functions of Mach number for the 20° and 35° wing sweep angles are shown in figures 7 to 30 and 31 to 54, respectively, for altitudes of 5000, 17,000, and 27,500 ft. Note that on some plots frequency and damping values are missing. These data could not be extracted due to the lack of random atmospheric turbulence for structural excitation in these instances.

In general, the damping levels and trends were satisfactory. There were some differences in modal frequency, damping, and damping trends between the 20° and 35° wing sweep data. Some modes exhibited an adverse damping trend. However, these modes exhibited moderate to heavy damping, and envelope expansion could have continued further if it were necessary.

The wing fore-and-aft modes were observed in the power spectra from the wingtip fore-and-aft accelerometers. The left wing generally responded at a lower frequency than did the right wing (fig. 55). Response frequencies tended to agree well with GVT-measured modal frequencies.

The laminar flow gloved-wing-only torsion mode was observed during flight at 27,500 and 17,000 ft for the 20° wing sweep only. Figure 56 shows the power spectra from the right and left wingtip vertical accelerometers for Mach 0.85 at 27,500 ft. Note that a 21.3-Hz mode is exhibited on the gloved wing only.

A 42-Hz spoiler resonance was observed on the left (laminar flow glove) and right (unmodified) wingtip accelerometers during the flight test program. The resonance occurred on the modified wing at a lower Mach number than on the unmodified wing. The 35° wing sweep angle exhibited the lowest Mach number at which this occurred. The onset boundaries at which this resonance occurred are shown in figure 57. These boundaries were determined by observing the frequency content of the signals from the wingtip fore-and-aft accelerometers and noting when the 42-Hz resonance occurred in the power spectra for the wing (fig. 58).

This resonance was determined to stem from the wing outboard spoilers. During the GVT, an accelerometer was placed on the outboard spoiler and a 42-Hz mode was measured (fig. 59). In addition, at Mach 0.9 and 17,000 ft, and for a wing sweep angle of 20°, the chase pilot reported seeing evidence of the wing outboard spoiler vibrating.

The resonance of the left wing spoiler occurs at a lower Mach number probably because of the 0.6-in step at the trailing edge of the glove on the upper surface of the wing. The glove, which ends just in front of the spoiler hinge line (fig. 1), created a disturbance in the airflow over the left spoiler. The spoiler resonance did not affect the flutter characteristics of the airplane.

Cleared Flight Envelope

The flight envelope cleared for the F-14 VSTFE airplane is shown in figure 60. This envelope is for any wing sweep angle from 20° to 35° with SAS either on or off. Note that the autopilot was not tested, and thus its use is restricted for this aircraft configuration unless such tests are successfully completed.

CONCLUSIONS

A ground vibration test was conducted on an unmodified F-14 airplane and an airplane modified with a laminar flow glove on the left wing to determine the change in modal characteristics that resulted from the addition of the foam-fiberglass glove. Results indicated that there were no significant changes in modal characteristics with the exception of the wing torsion modes. The airplane with the laminar flow glove installed exhibited a new (asymmetric) gloved-wing-only torsion mode in addition to the symmetric and antisymmetric torsion modes.

Flight flutter testing was accomplished for the laminar flow gloved wing at altitudes of 27,500, 17,000, and 5000 ft to maximum Mach numbers of 0.89, 0.90, and 0.74, respectively, for a wing sweep angle of 35°. For a wing sweep angle of 20°, the maximum Mach numbers tested were 0.87, 0.90, and 0.74 at altitudes of 27,500, 17,000, and 5000 ft, respectively. Damping levels and trends were satisfactory from a flutter standpoint. The test results demonstrated that the airplane can be flown safely throughout an envelope up to 450 KCAS and Mach 0.90, whichever is less, for wing sweep angles between 20° and 35°. Since the autopilot was not tested, its use is prohibited for this aircraft configuration.

A small-amplitude 42-Hz spoiler resonance was detected during the flight flutter tests. It was concluded that this resonance was not hazardous and did not affect the flutter characteristics of the airplane.

REFERENCES

1. Moes, Timothy R.; Myer, Robert R., Jr.: In-Flight Wing Pressure Distributions for the F-14A Aircraft. NASA TM-85921, 1985.

2. Rozendaal, Rodger A.: Varible Sweep Transition Flight Experiment (VSTFE)-Parametric Pressure Distribution Boundary Layer Stability Study and Wing Glove Design Task. NASA CR-3992, 1986.

3. Bendat, Julius S.; and Piersol, Allan G.: Engineering Applications of Correlation and Spectral Analysis. John Wiley and Sons, Inc., New York, 1980.

4. User Manual for Modal Analysis 8.0. General Electric CAE International, 1983.

5. Kehoe, Michael W.: AFTI/F-16 Aeroservoelastic and Flutter Flight Test Program — Phase I. NASA TM-86027, 1985.

TABLE 1. — GROUND VIBRATION TEST RESULTS AND COMPARISONS

Mode description	Unmodified airplane		Gloved airplane		Difference,[a] percent
	Frequency, Hz	Damping, G	Frequency, Hz	Damping, G	
20° wing sweep, symmetric					
First wing bending	4.707	0.028	4.621	0.024	-1.86
Second wing bending	14.391	0.041	13.978	0.039	-2.95
Wing torsion					
Left	---	---	21.257	0.068	---
Right	19.776	0.052	19.255	0.06	-2.71
Fore and aft					
Left	9.23	0.09	9.76	0.097	---
Right	9.96	0.069	---	---	---
Vertical fin bending	---	---	11.445	0.02	---
Fuselage vertical bending	7.863	0.062	7.698	0.046	-2.14
Stabilizer bending-pitch	---	---	17.076	0.053	---
Engine nacelle roll	10.77	0.052	10.263	0.055	-4.94
20° wing sweep, antisymmetric					
First wing bending	6.486	0.06	6.535	0.032	0.75
Second wing bending	16.044	0.052	16.366	0.055	1.97
Wing torsion	23.537	0.044	23.786	0.051	1.05
Fore and aft					
Left	9.34	0.078	9.39	0.058	0.53
Right	10.35	0.07	11.23	0.11	7.84
Vertical fin bending	12.589	0.086	---	---	---
Vertical fin torsion	36.67	0.035	35.305	0.044	-3.87
Fuselage torsion	8.483	0.051	8.378	0.039	-1.25
Fuselage torsion	9.881	0.062	9.658	0.026	-2.31

[a]The percentage difference is defined as $100\left[1 - \frac{\text{(Unmodified airplane)}}{\text{(Gloved airplane)}}\right]$

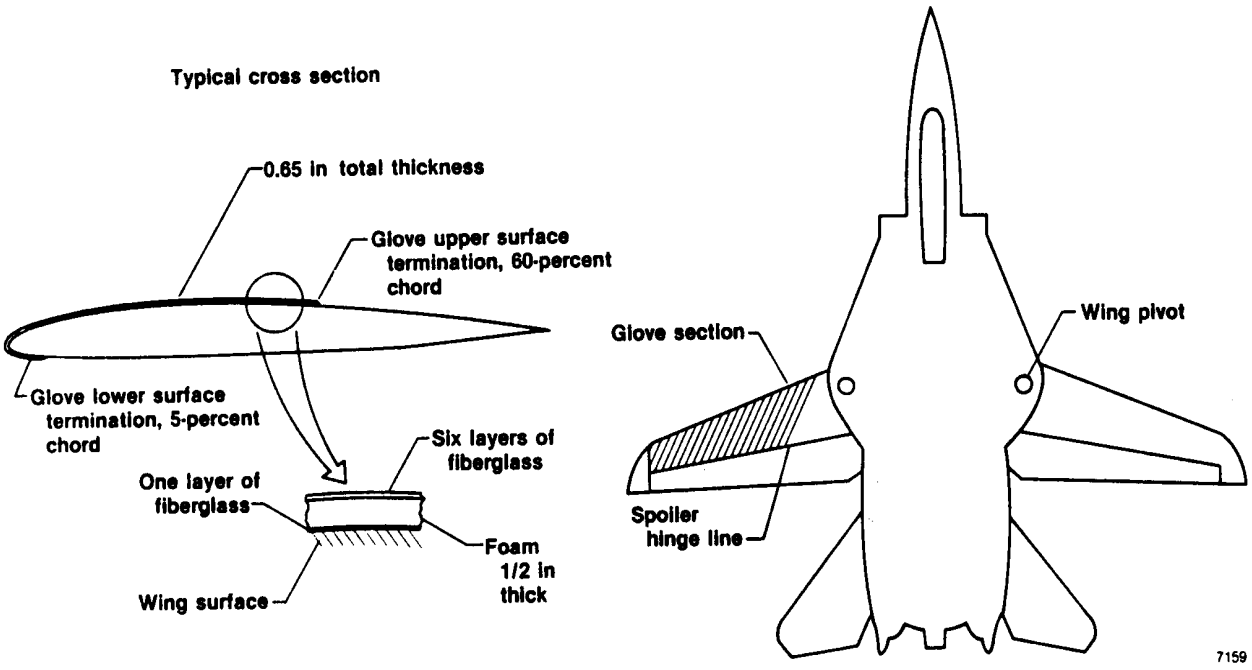

Figure 1. Typical cross section and position of the laminar flow glove.

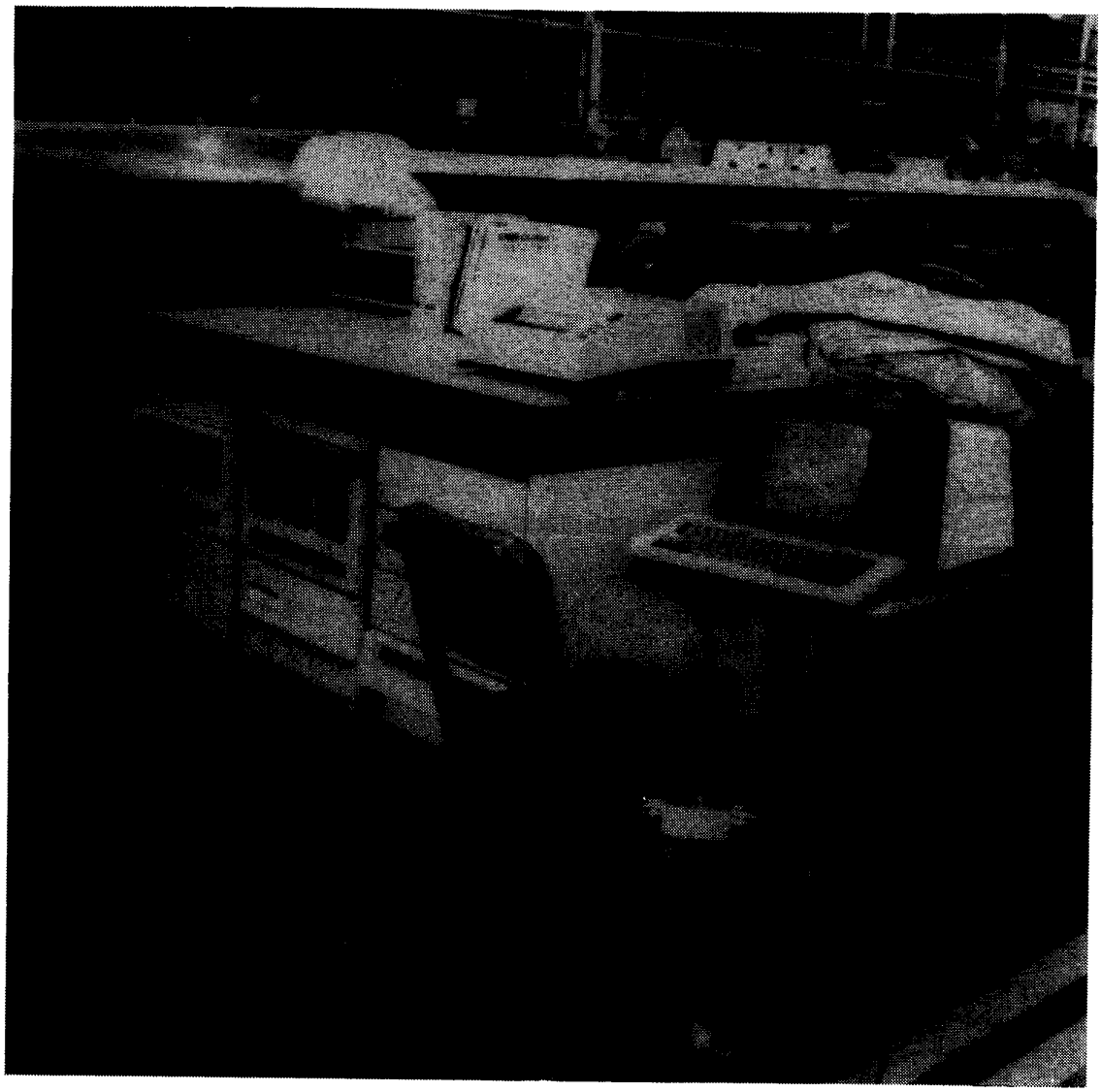

ECN 33451-004

Figure 2. Minicomputer-based structural analysis system.

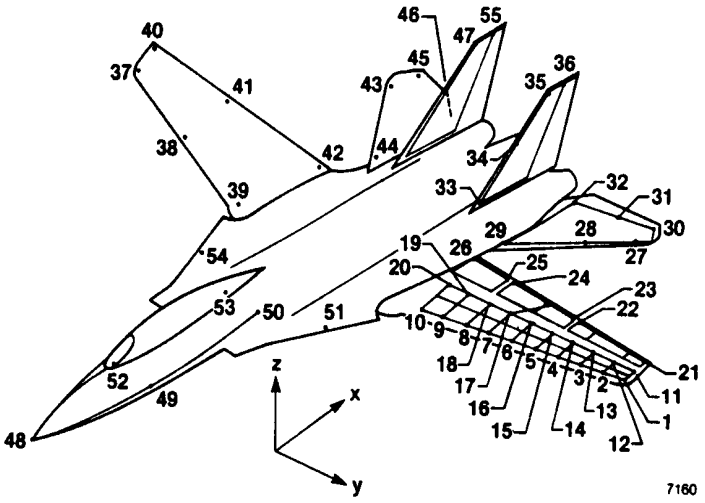

Figure 3. Accelerometer locations for mode shape measurements.

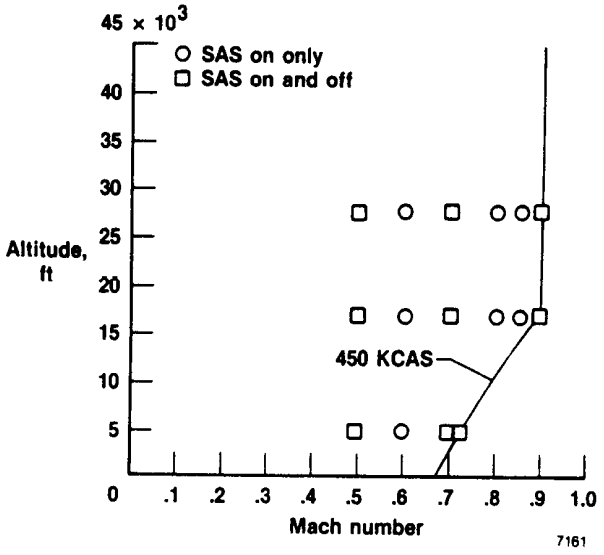

Figure 4. Planned flight flutter test points, 20° and 30° wing sweeps.

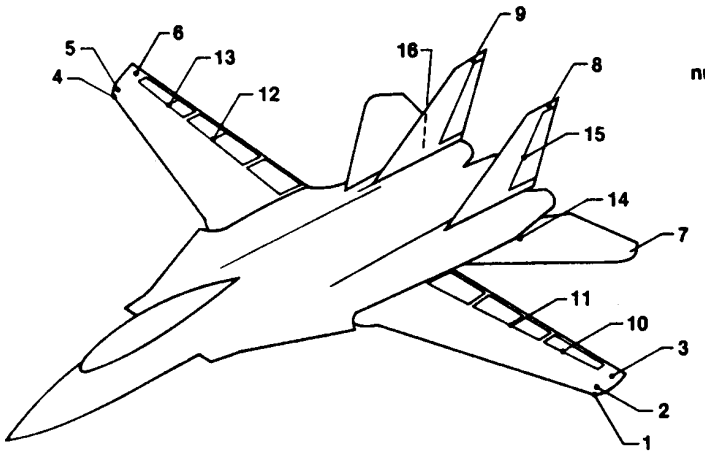

Item number	Parameter identification
1	Left wingtip fore-and-aft acceleration
2	Left forward wingtip normal acceleration
3	Left aft wingtip normal acceleration
4	Right wingtip fore-and-aft acceleration
5	Right forward wingtip normal acceleration
6	Right aft wingtip normal acceleration
7	Left horizontal stabilator normal acceleration
8	Left vertical stabilizer lateral acceleration
9	Right vertical stabilizer lateral acceleration
10	Left outboard spoiler position
11	Left inboard spoiler position
12	Right inboard spoiler position
13	Right outboard spoiler position
14	Left horizontal stabilator position
15	Left vertical stabilizer position
16	Right horizontal stabilator position

7162

Figure 5. Aircraft flight test instrumentation.

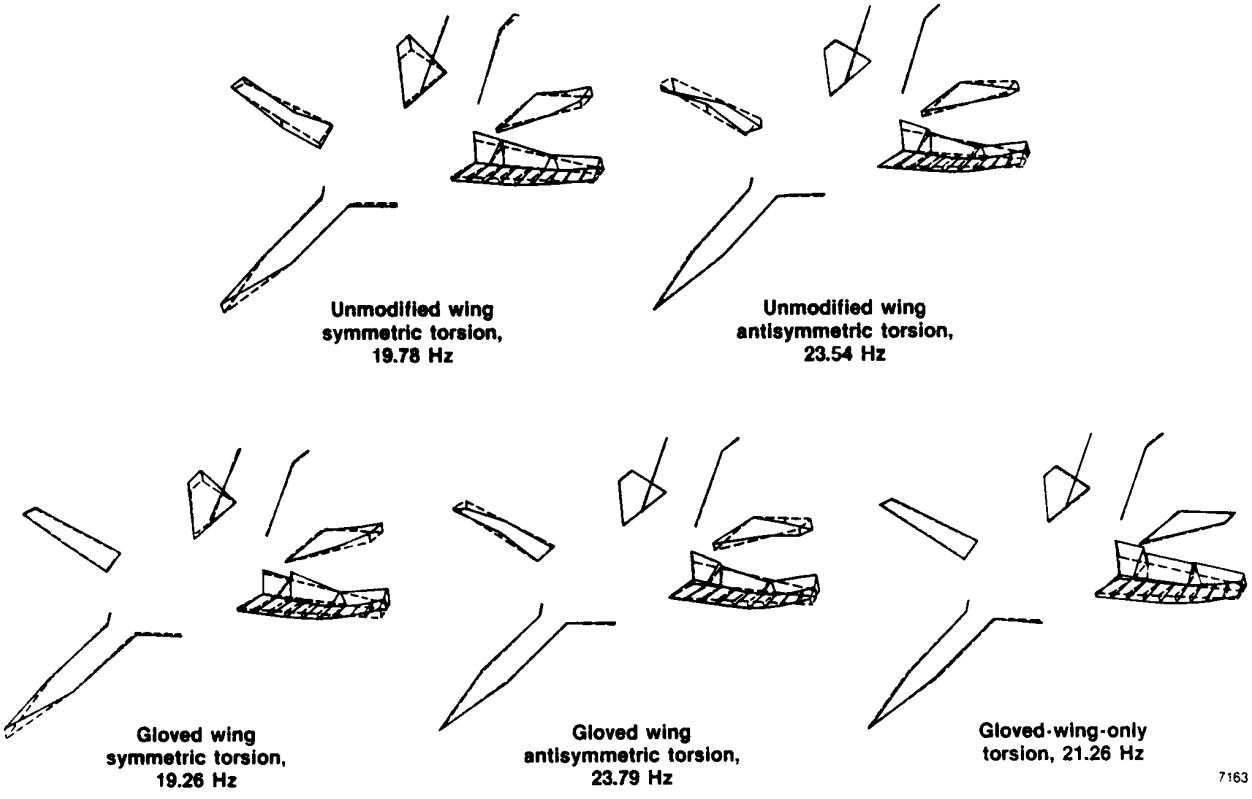

Figure 6. Comparison of wing torsion mode shapes at 20° wing sweep.

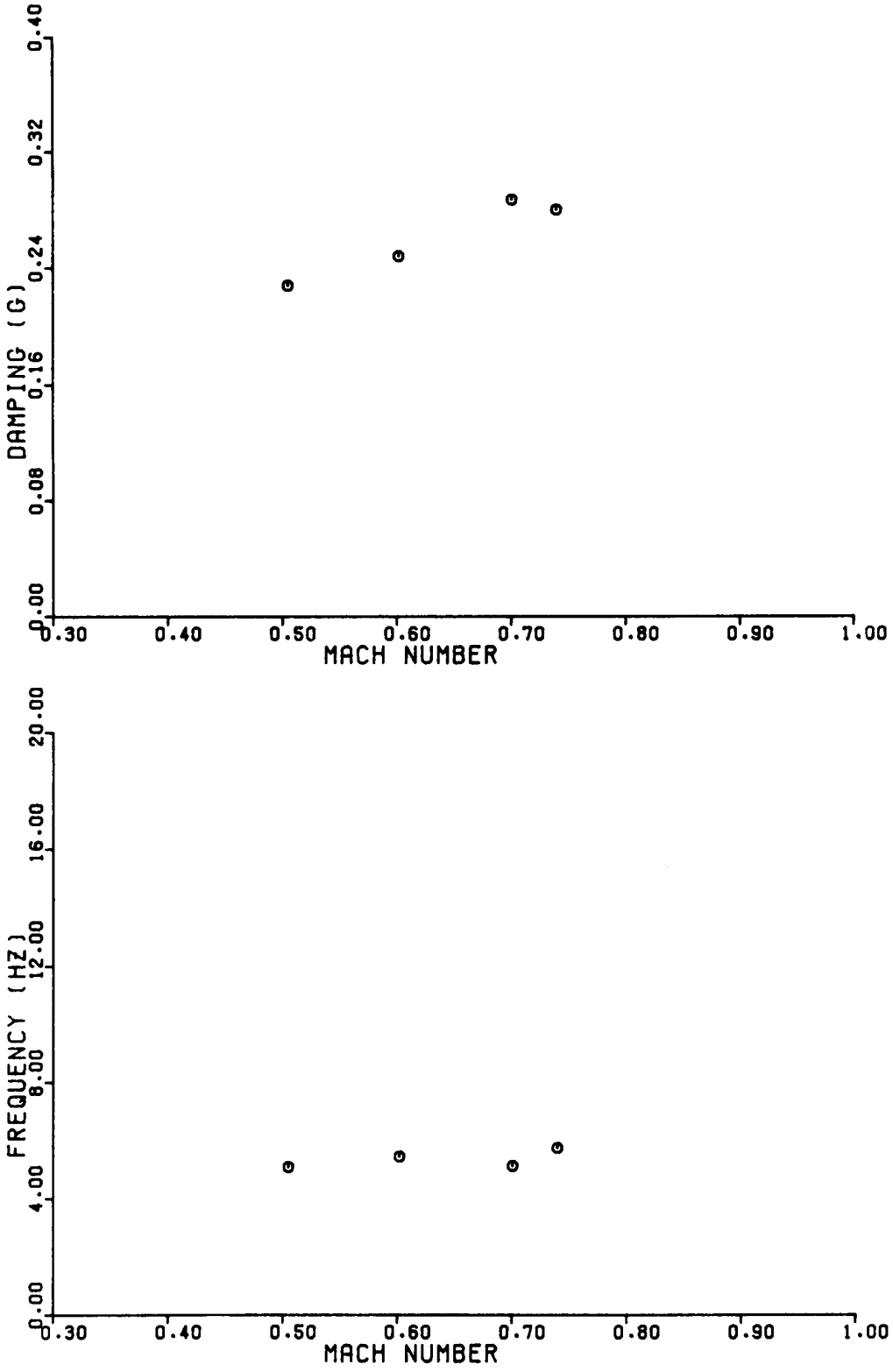

Figure 7. Symmetric wing bending modal data at 5000 ft for 20° wing sweep.

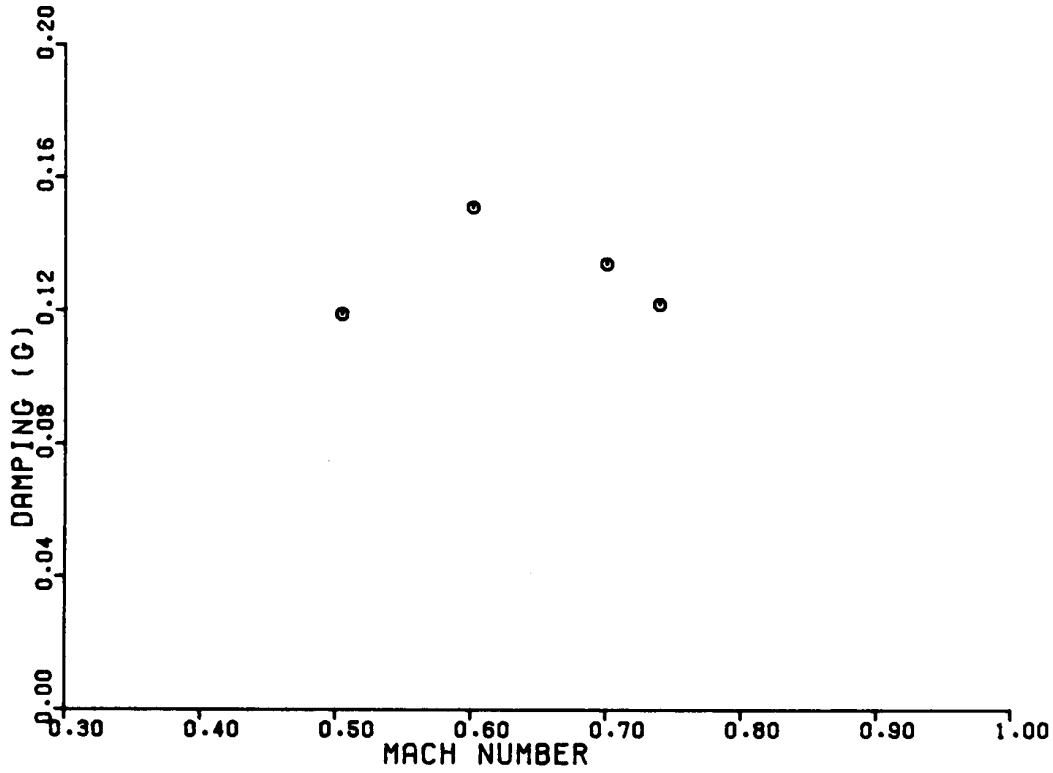

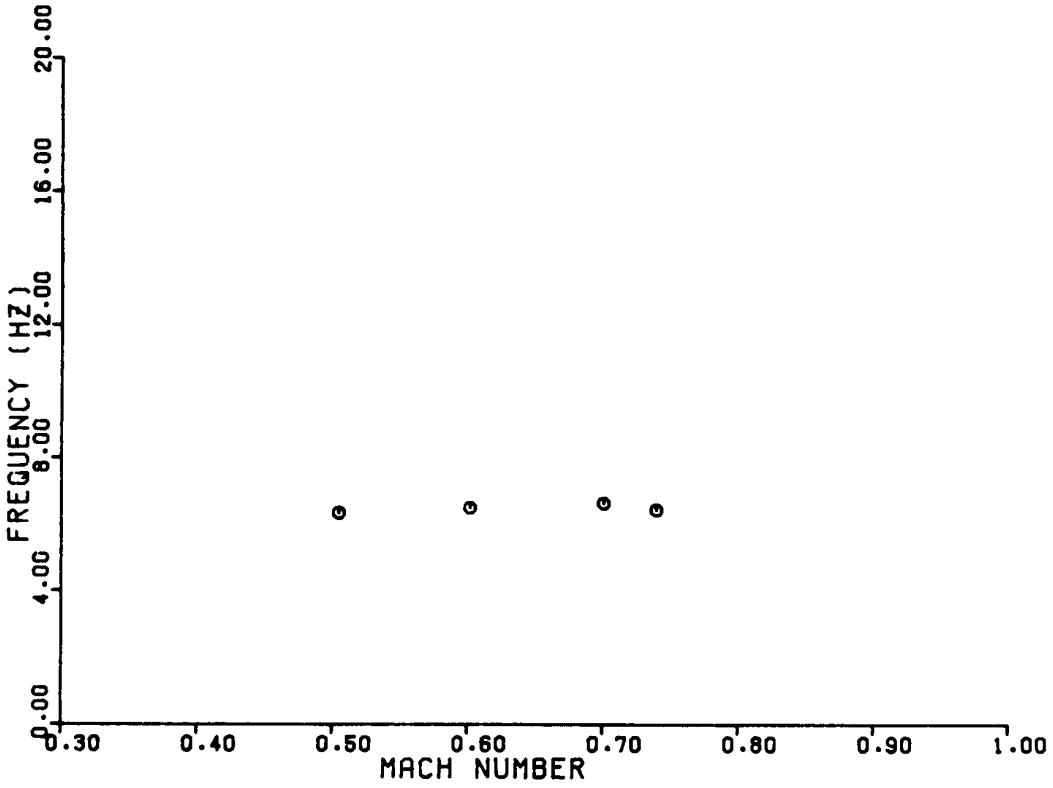

Figure 8. Antisymmetric wing bending modal data at 5000 ft for 20° wing sweep.

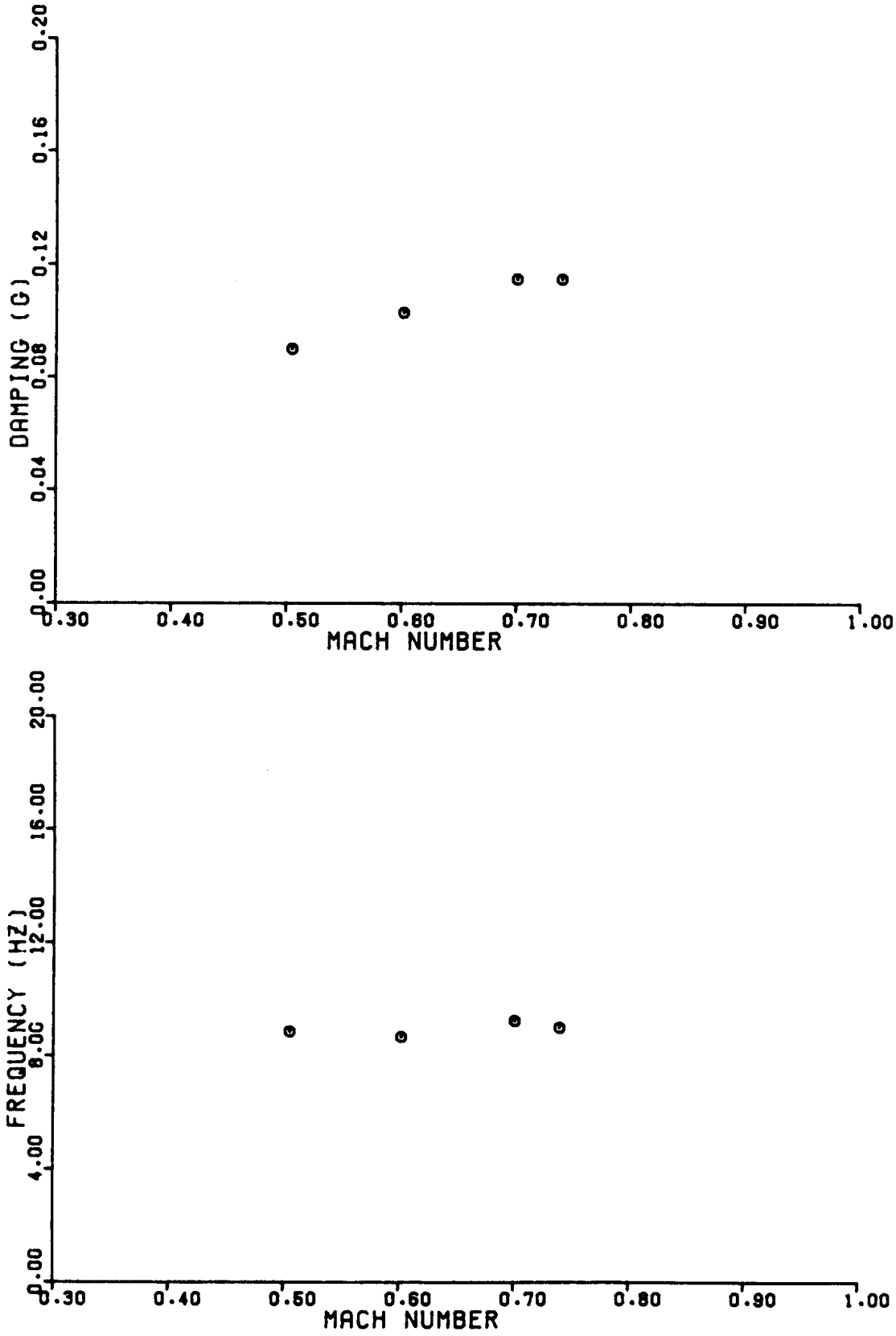

Figure 9. Left wing fore-and-aft bending modal data at 5000 ft for 20° wing sweep.

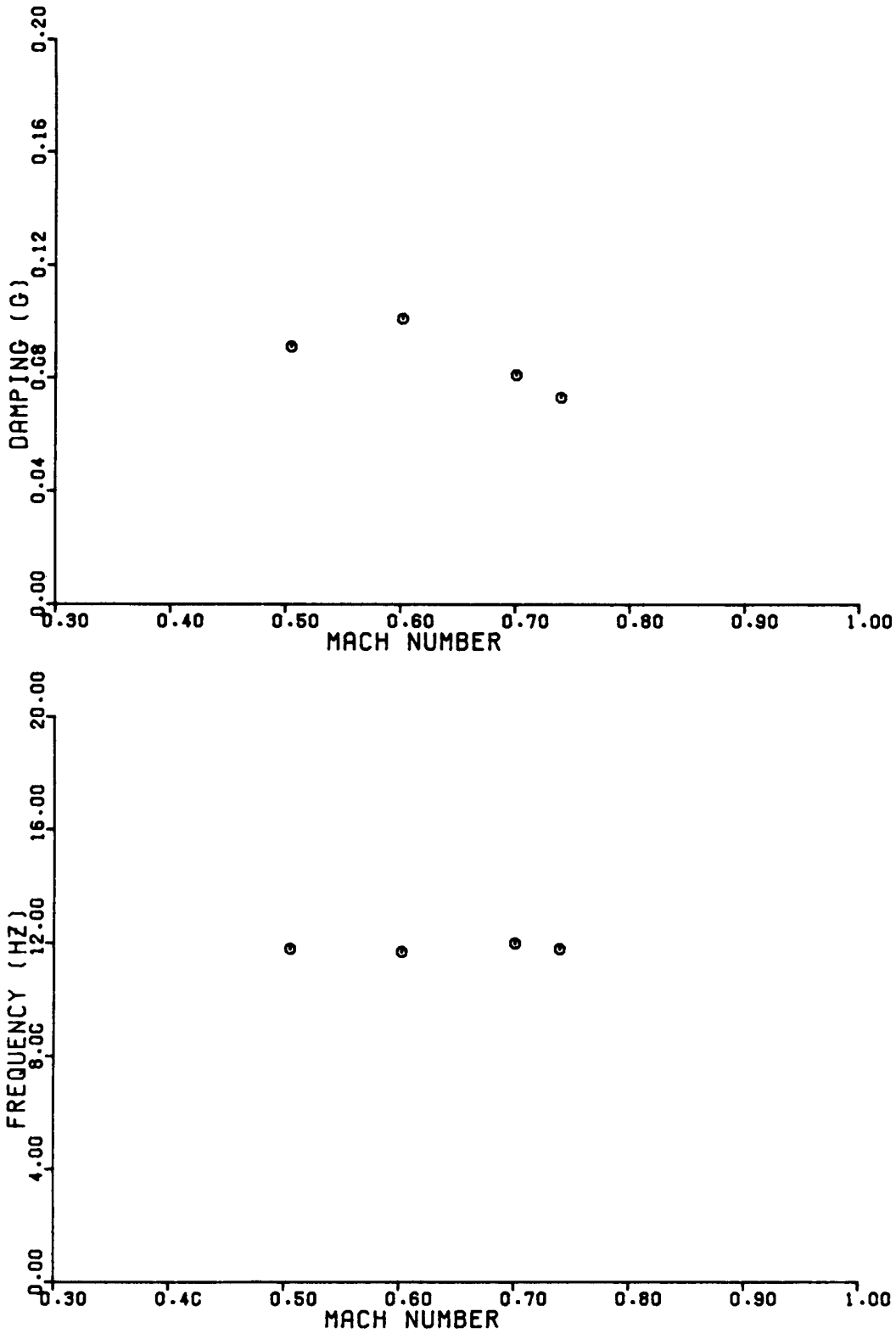

Figure 10. Right wing fore-and-aft bending modal data at 5000 ft for 20° wing sweep.

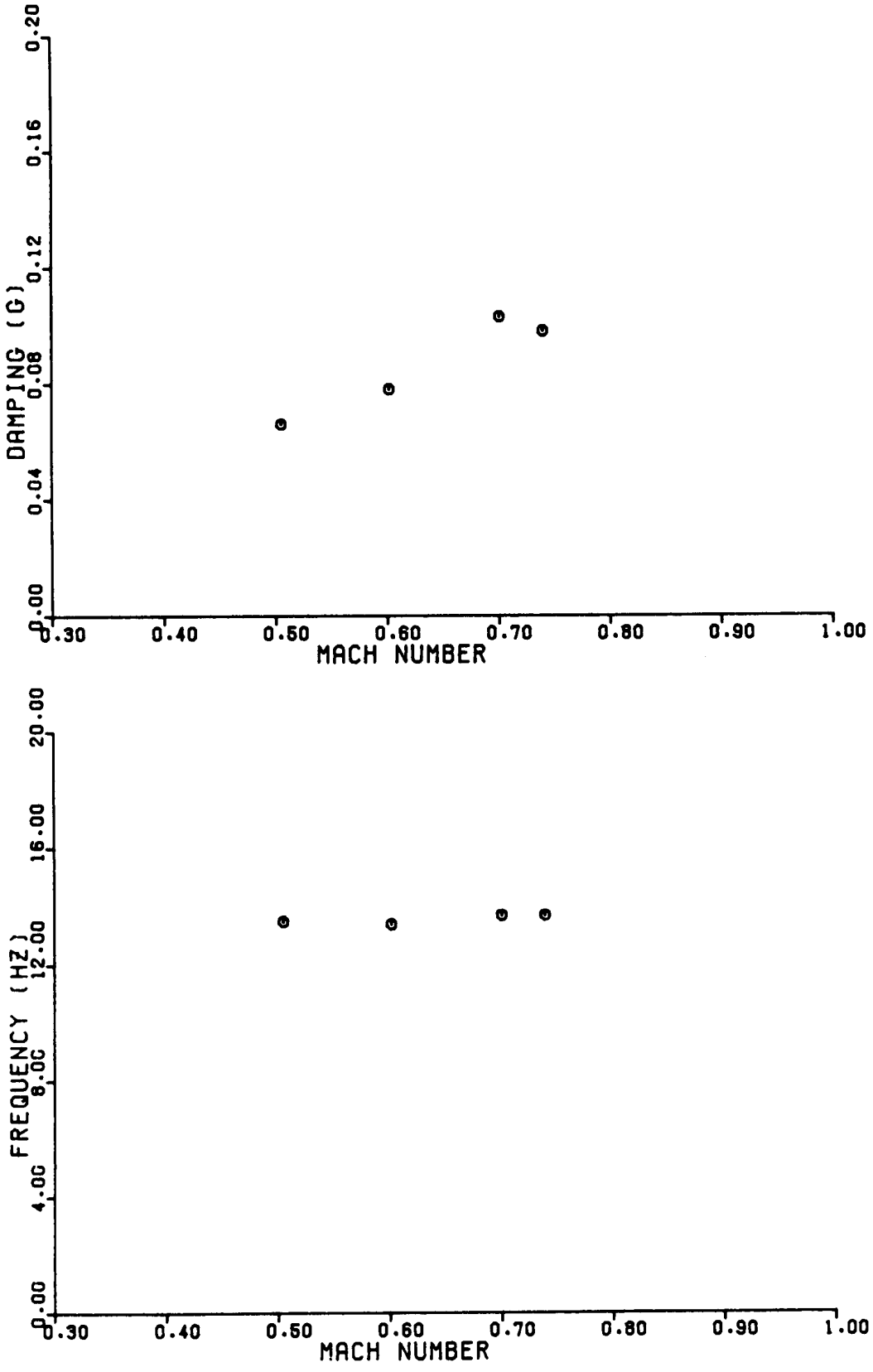

Figure 11. Vertical fin bending modal data at 5000 ft for 20° wing sweep.

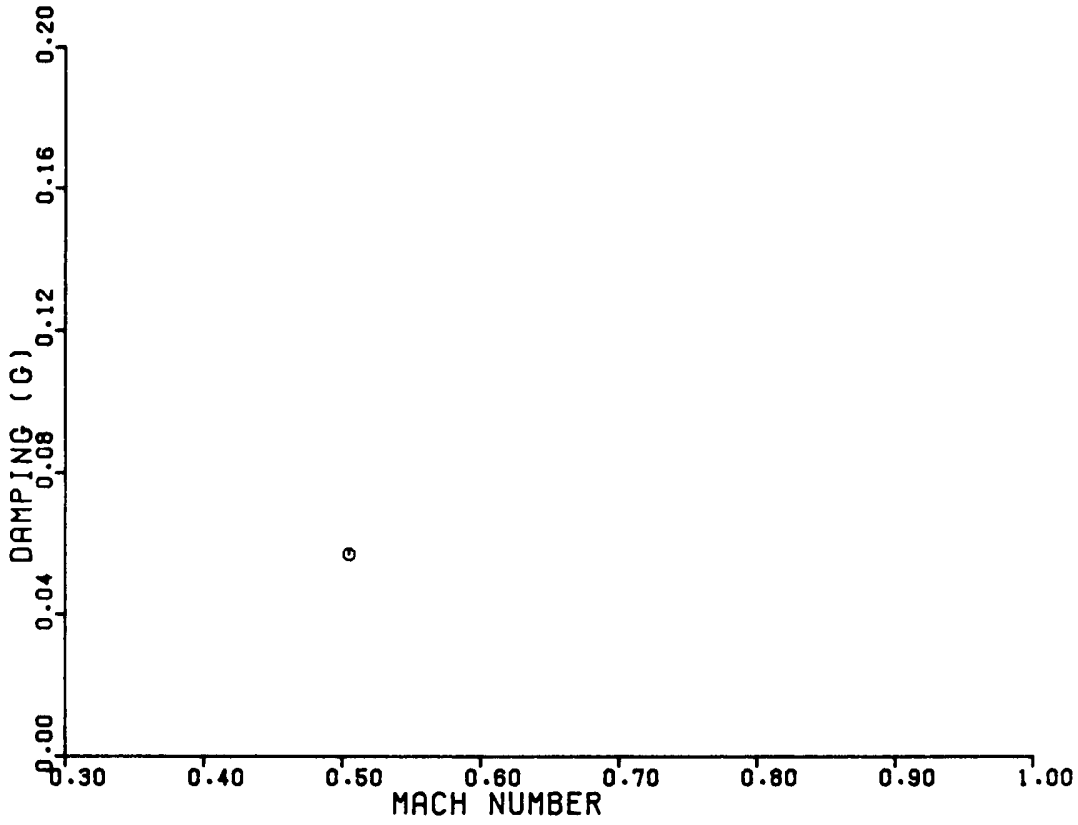

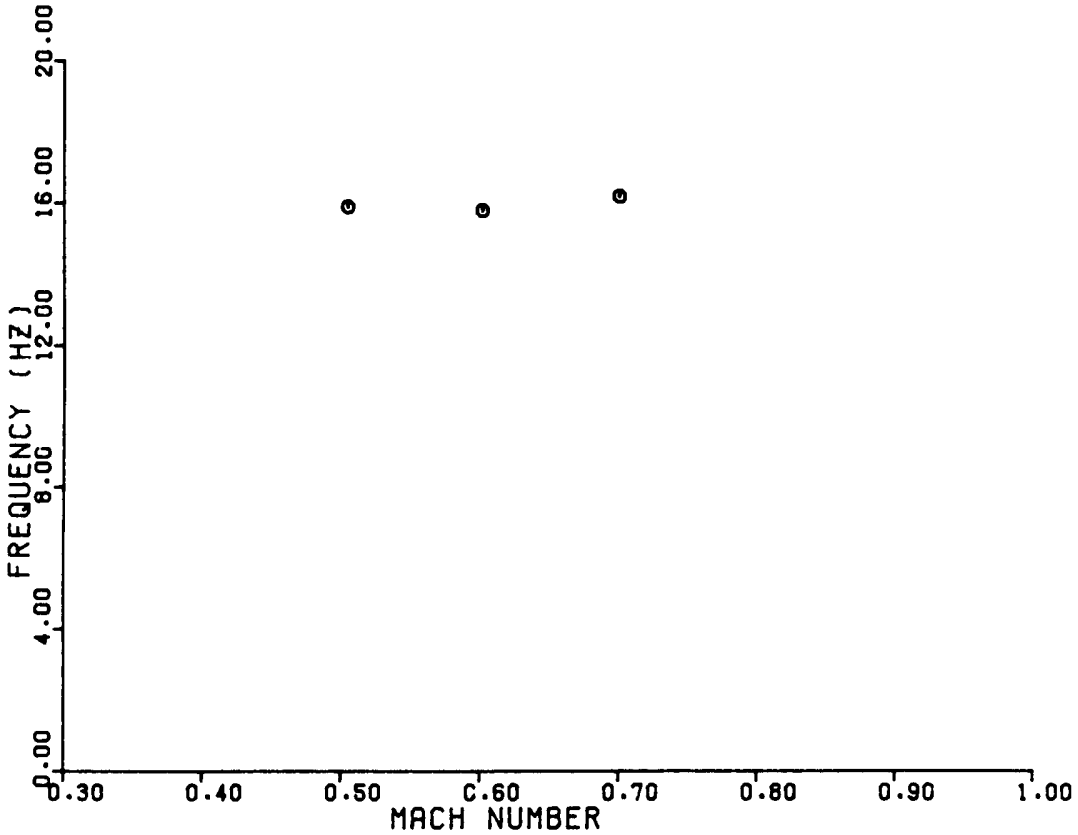

Figure 12. Second antisymmetric wing bending modal data at 5000 ft for 20° wing sweep.

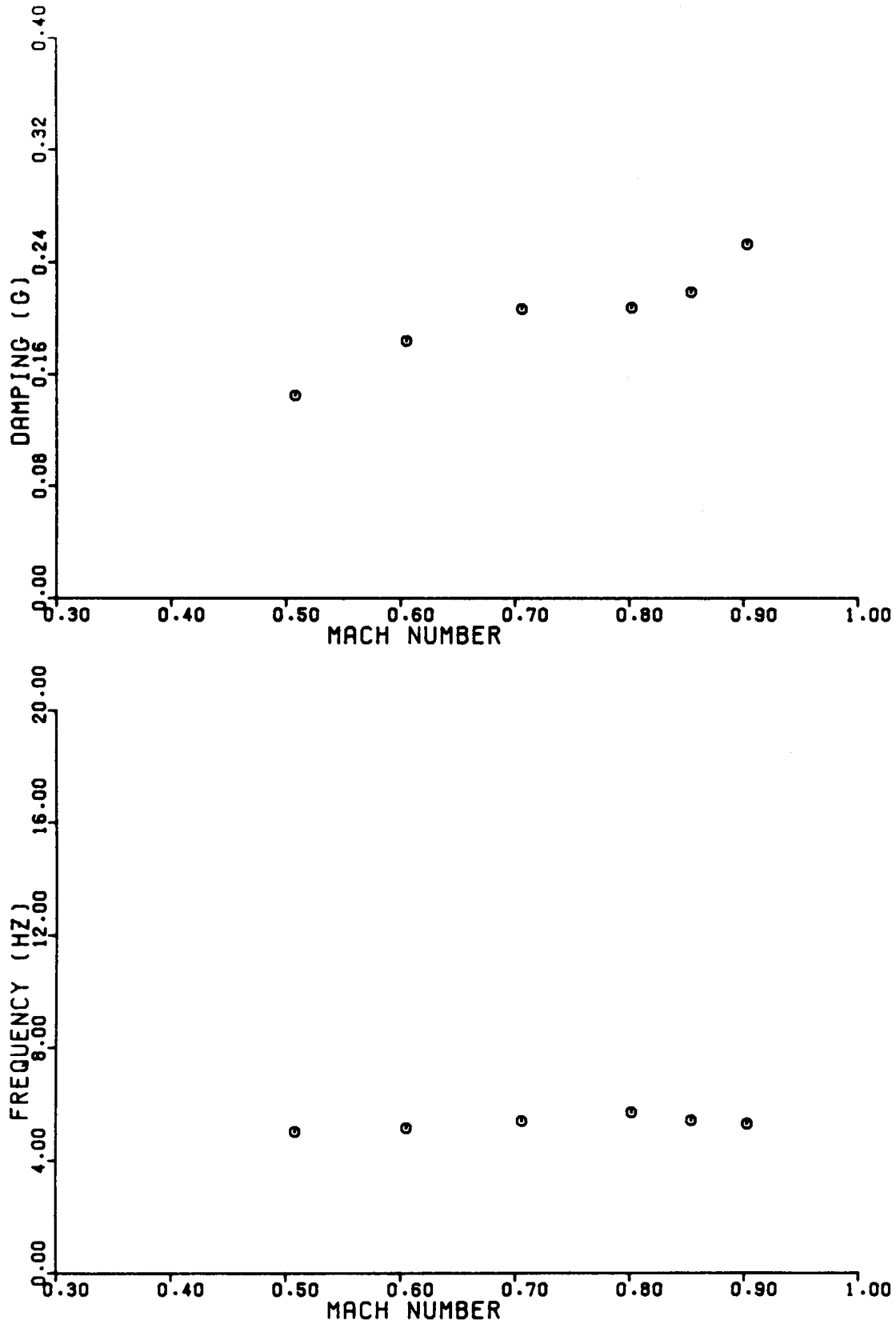

Figure 13. Symmetric wing bending modal data at 17,000 ft for 20° wing sweep.

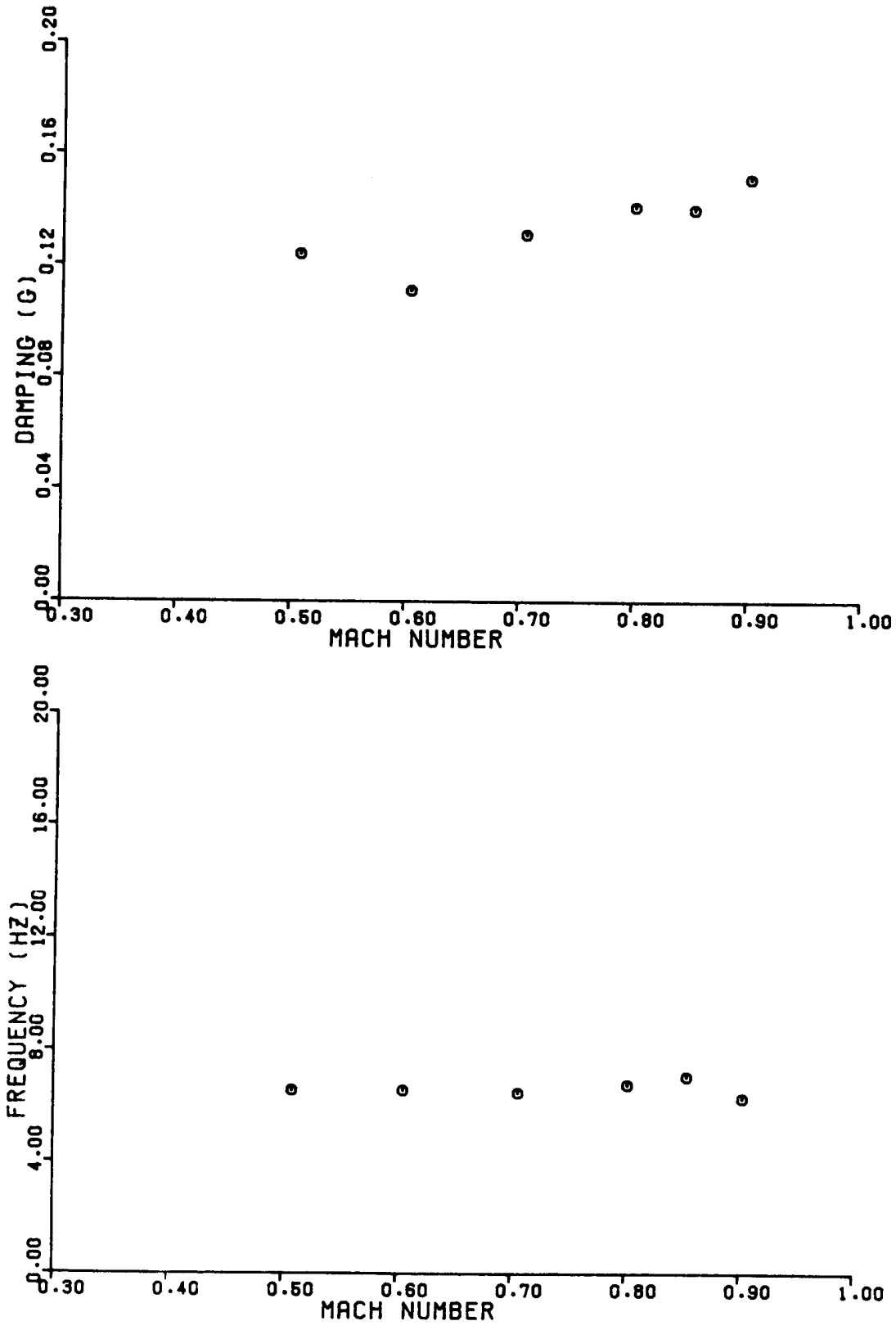

Figure 14. Antisymmetric wing bending modal data at 17,000 ft for 20° wing sweep.

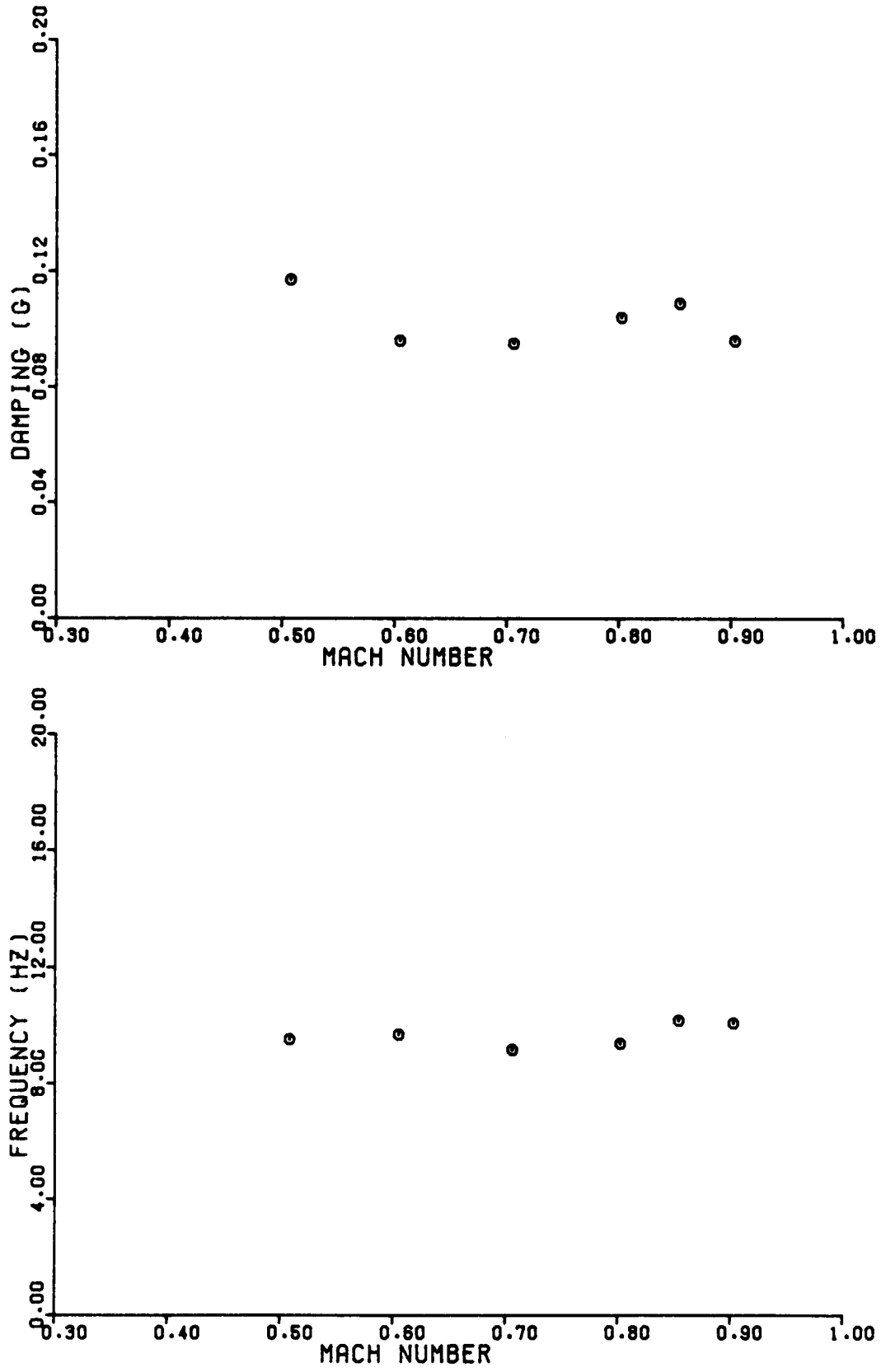

Figure 15. Left wing fore-and-aft bending modal data at 17,000 ft for 20° wing sweep.

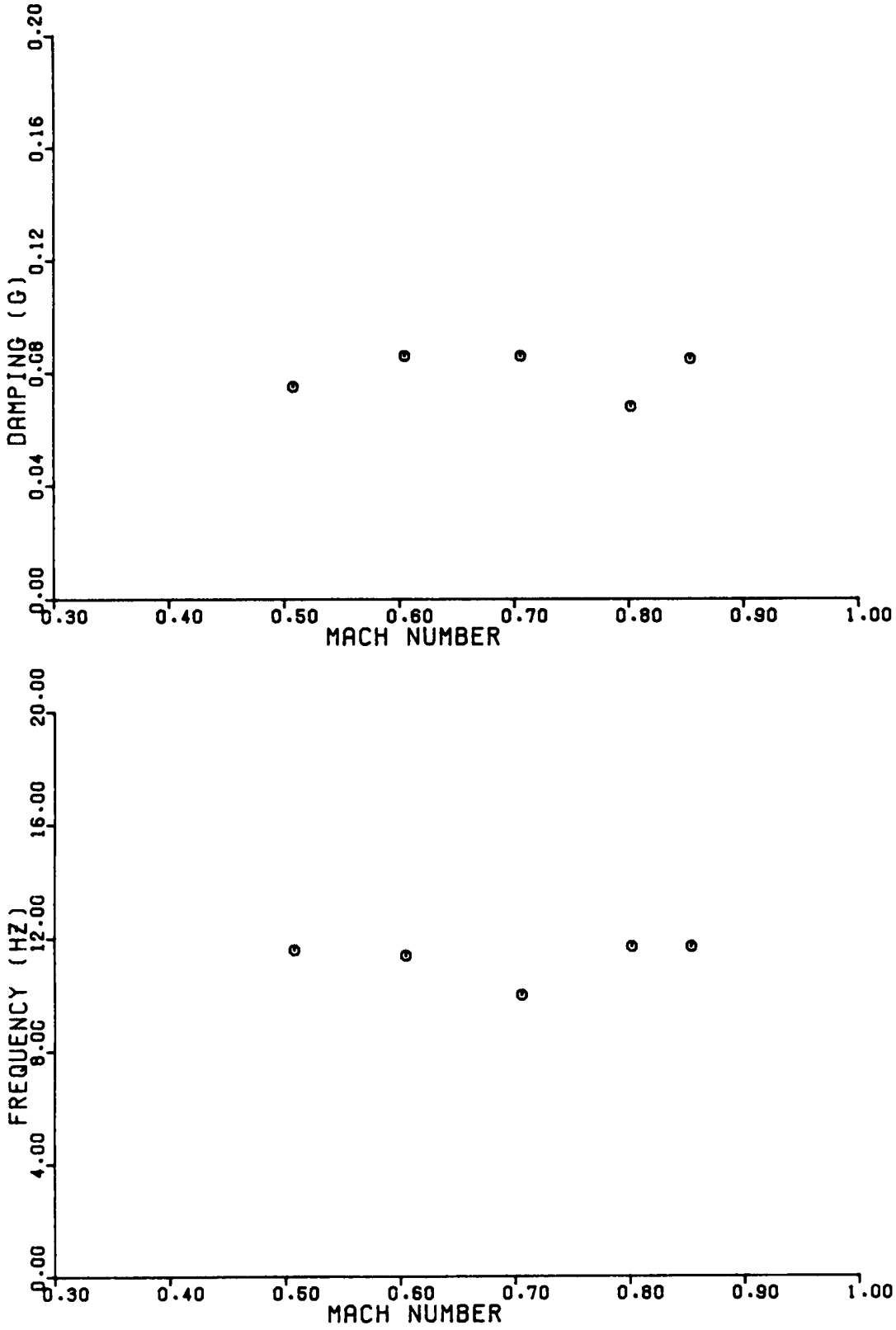

Figure 16. Right wing fore-and-aft bending modal data at 17,000 ft for 20° wing sweep.

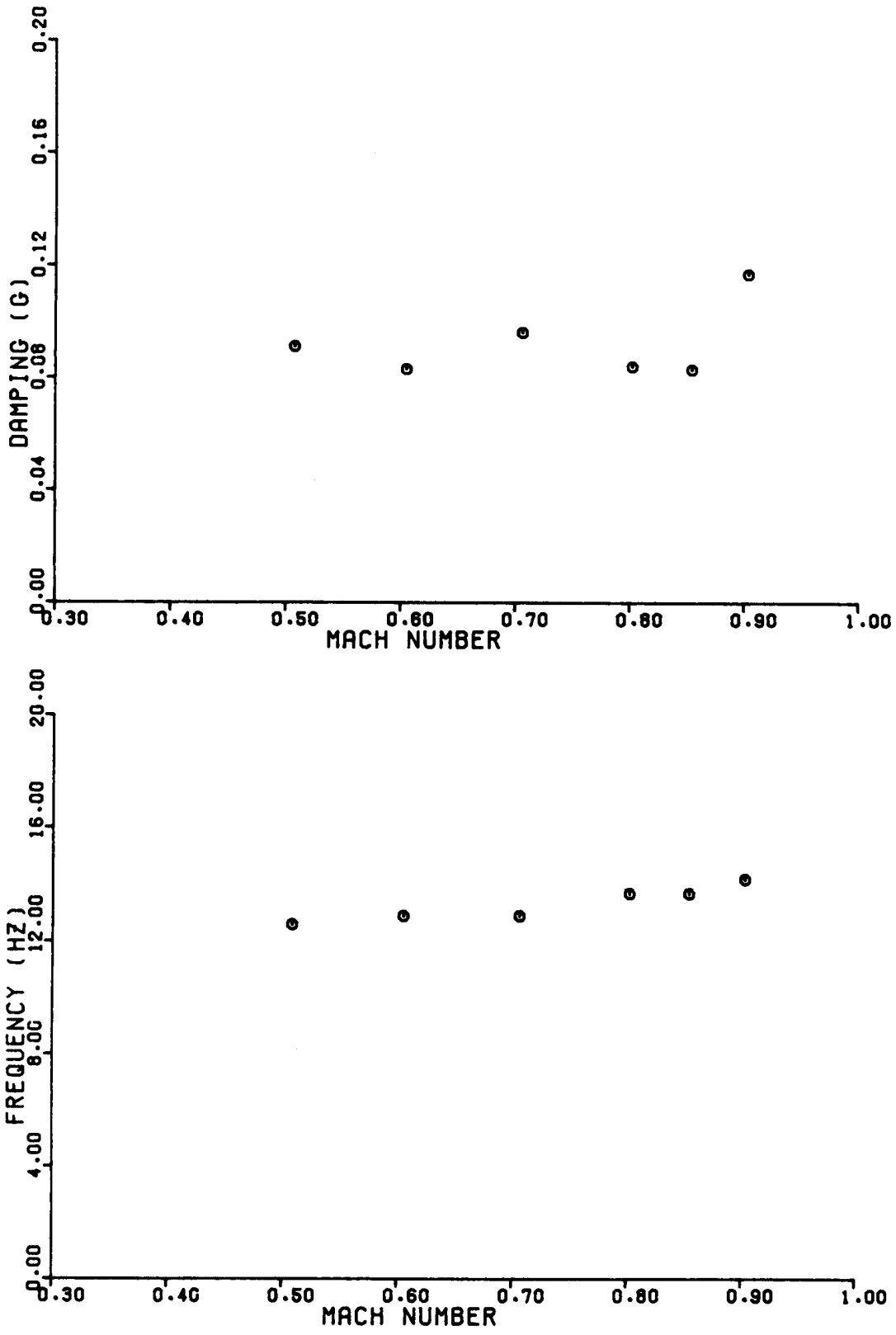

Figure 17. Vertical fin bending modal data at 17,000 ft for 20° wing sweep.

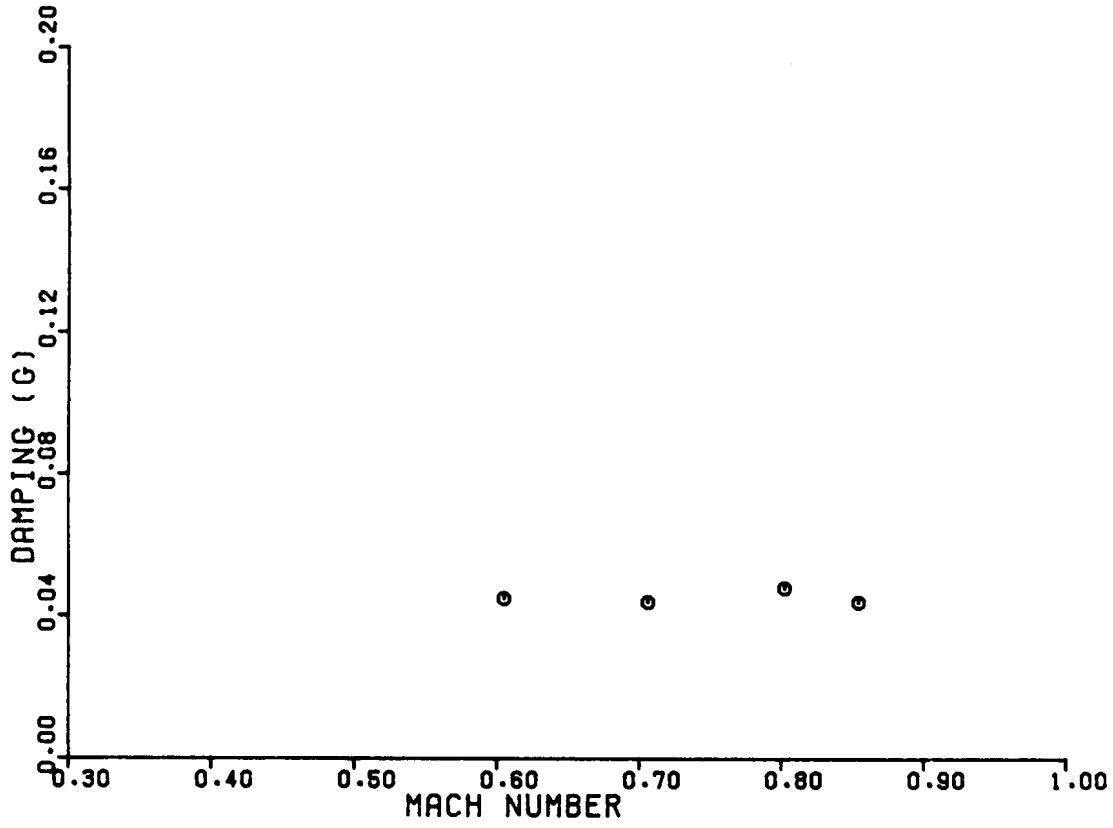

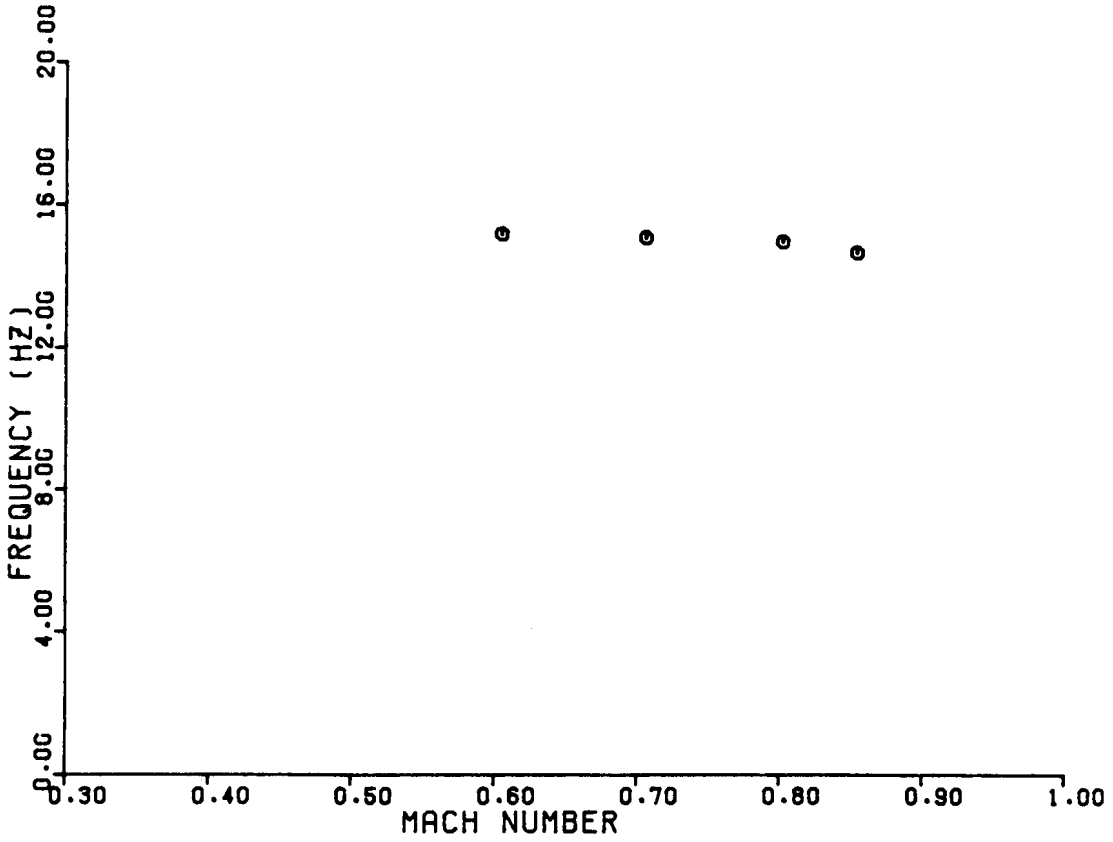

Figure 18. Second symmetric wing bending modal data at 17,000 ft for 20° wing sweep.

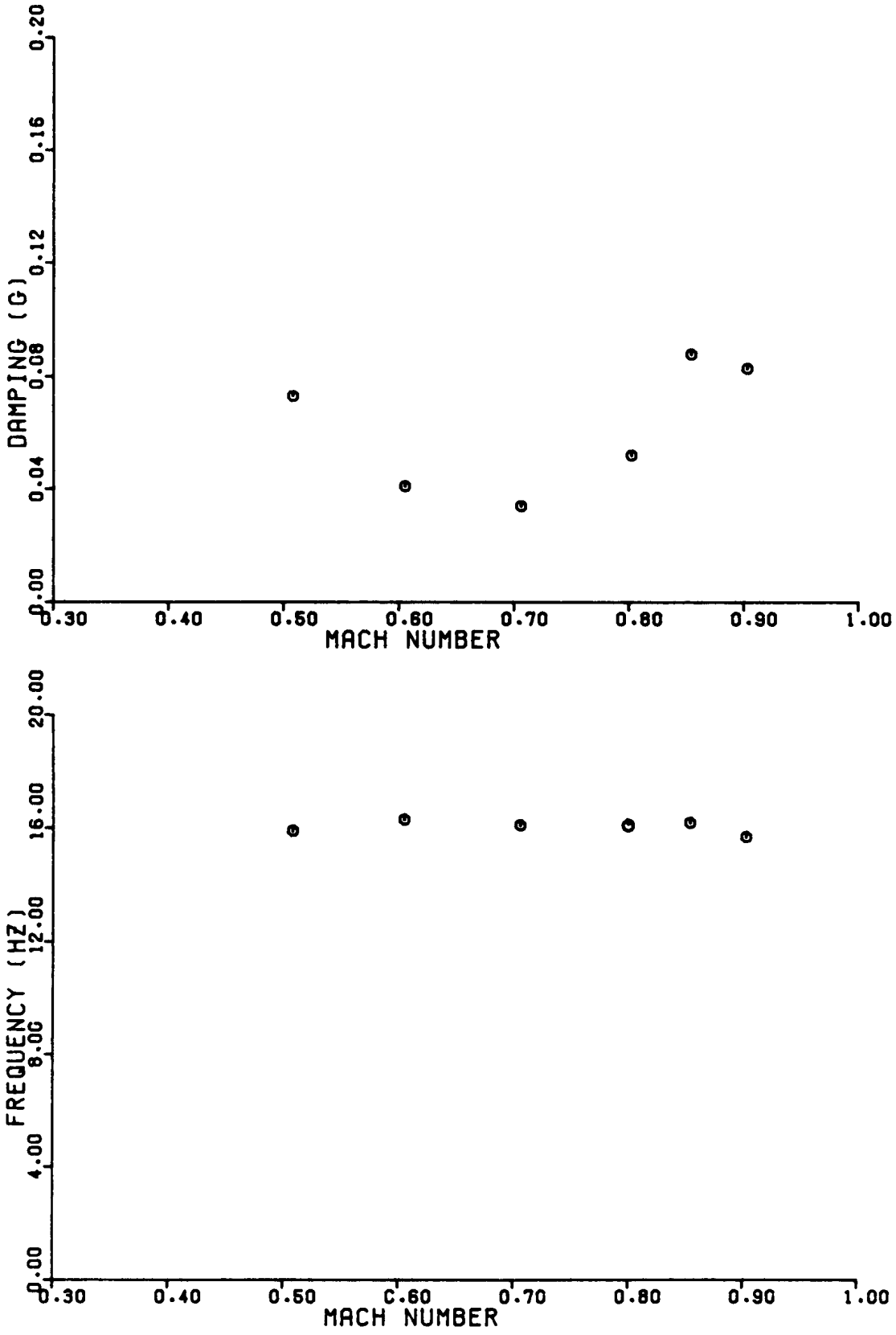

Figure 19. Second antisymmetric wing bending modal data at 17,000 ft for 20° wing sweep.

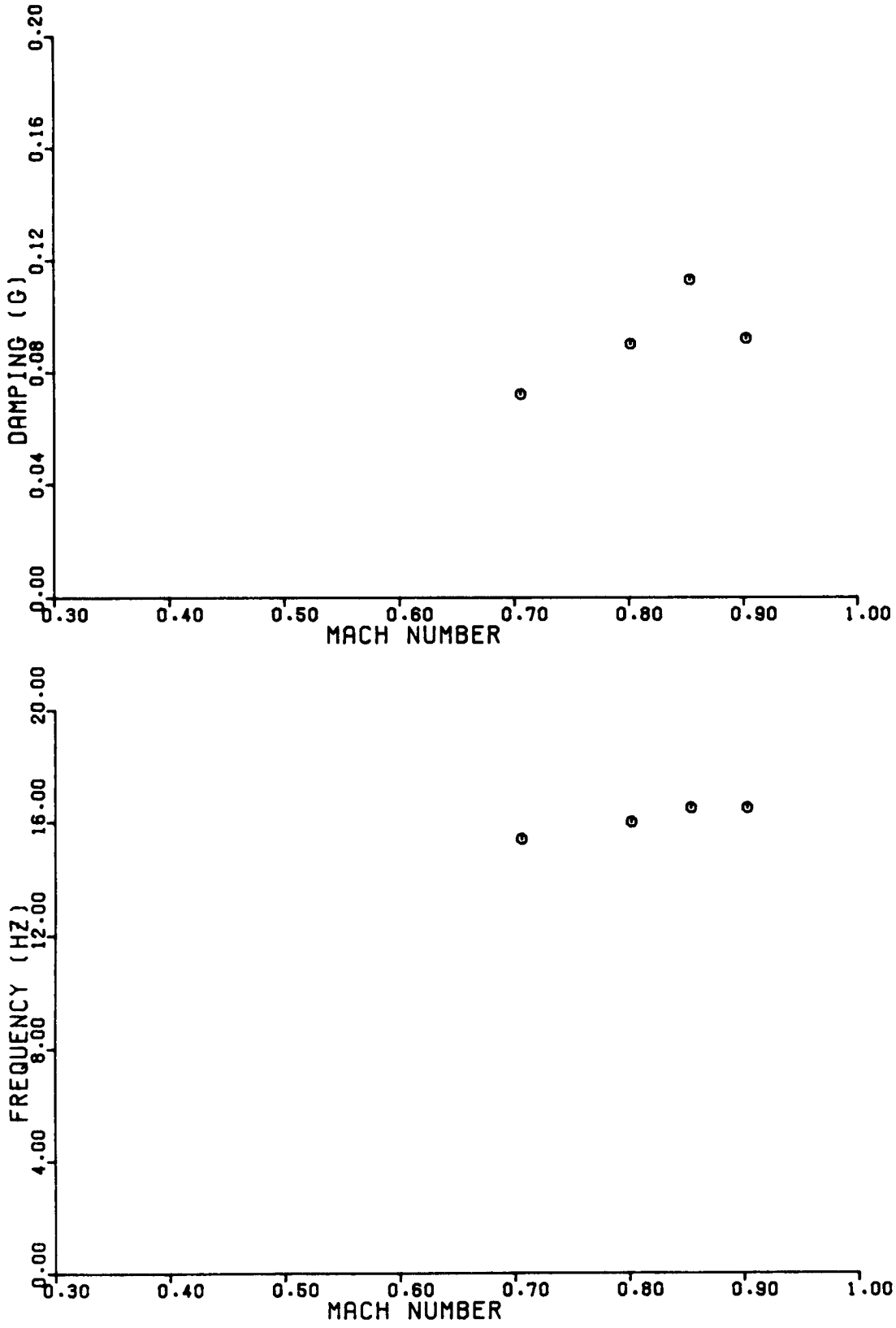

Figure 20. Horizontal stabilator bending modal at 17,000 ft for 20° wing sweep.

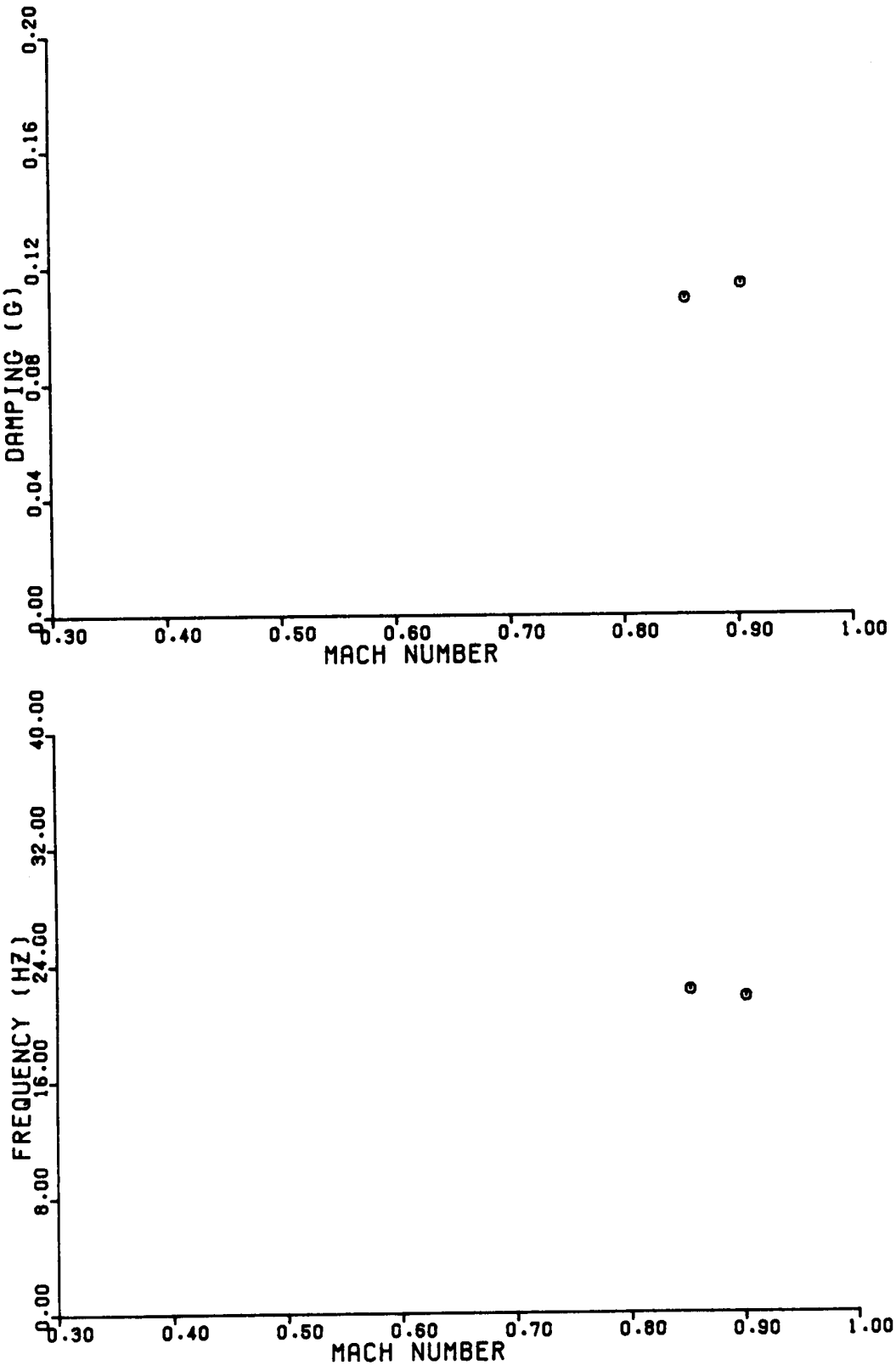

Figure 21. Left wing torsion modal data at 17,000 ft for 20° wing sweep.

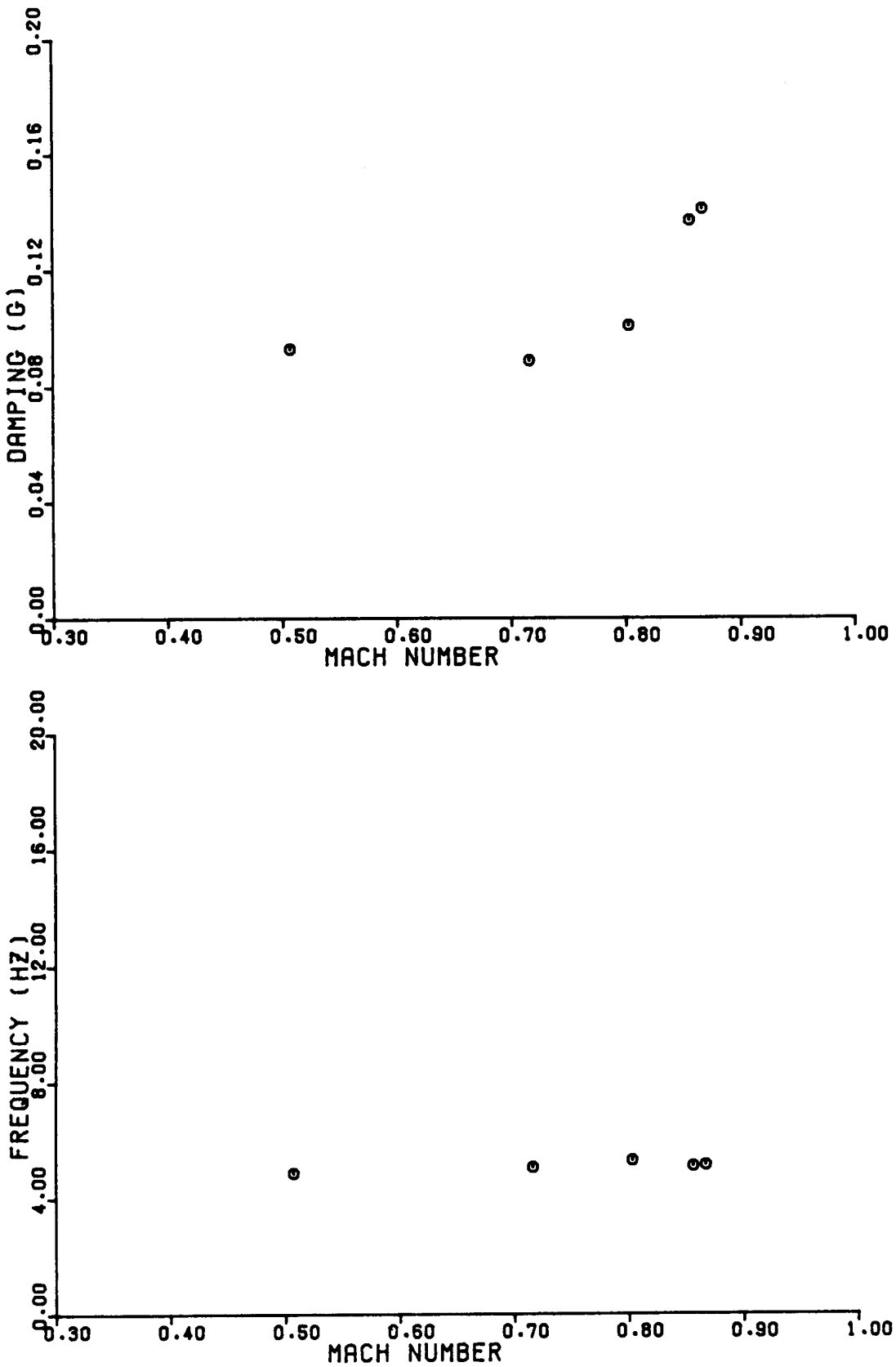

Figure 22. Symmetric wing bending modal data at 27,500 ft for 20° wing sweep.

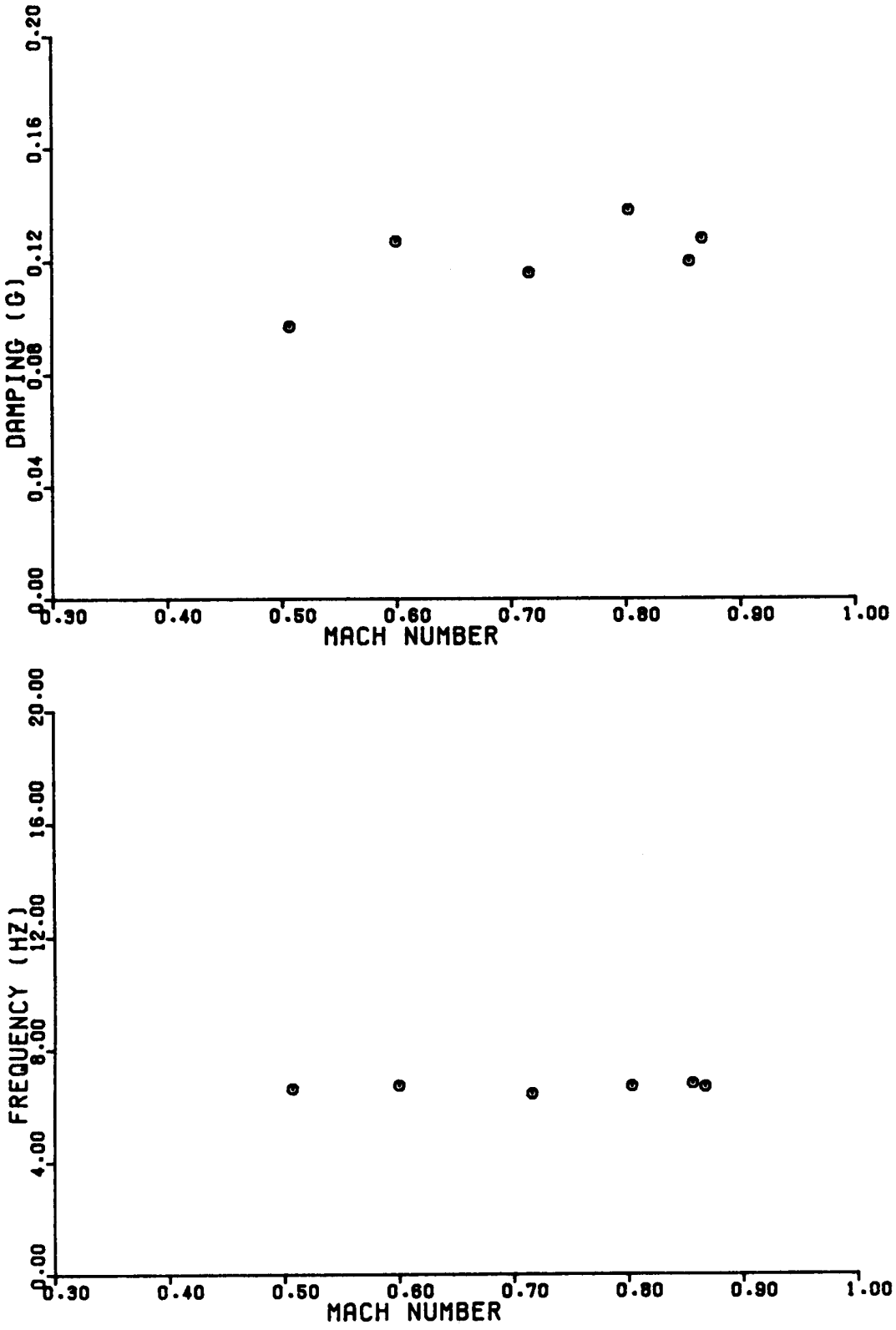

Figure 23. Antisymmetric wing bending modal data at 27,500 ft for 20° wing sweep.

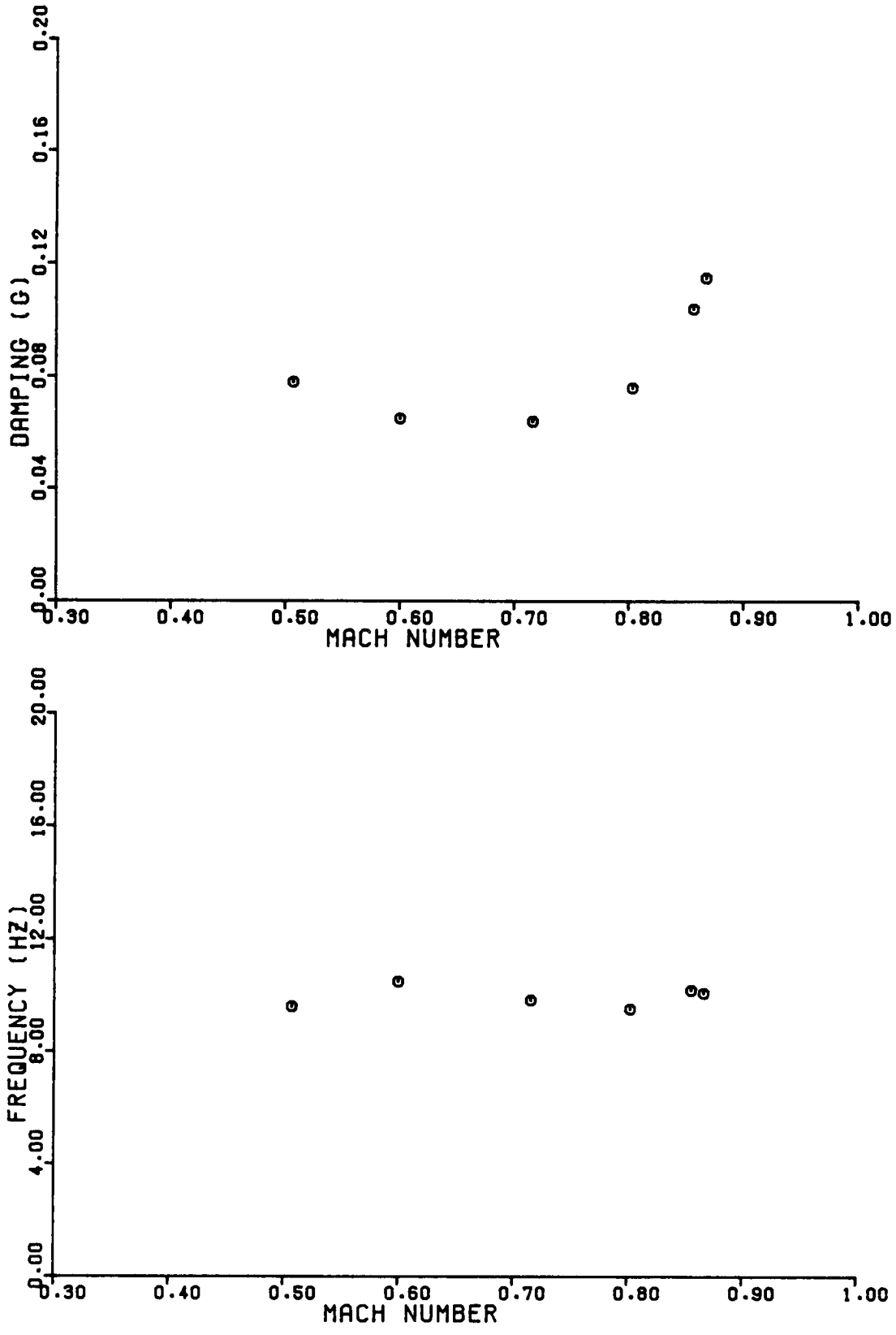

Figure 24. Left wing fore-and-aft bending modal data at 27,500 ft for 20° wing sweep.

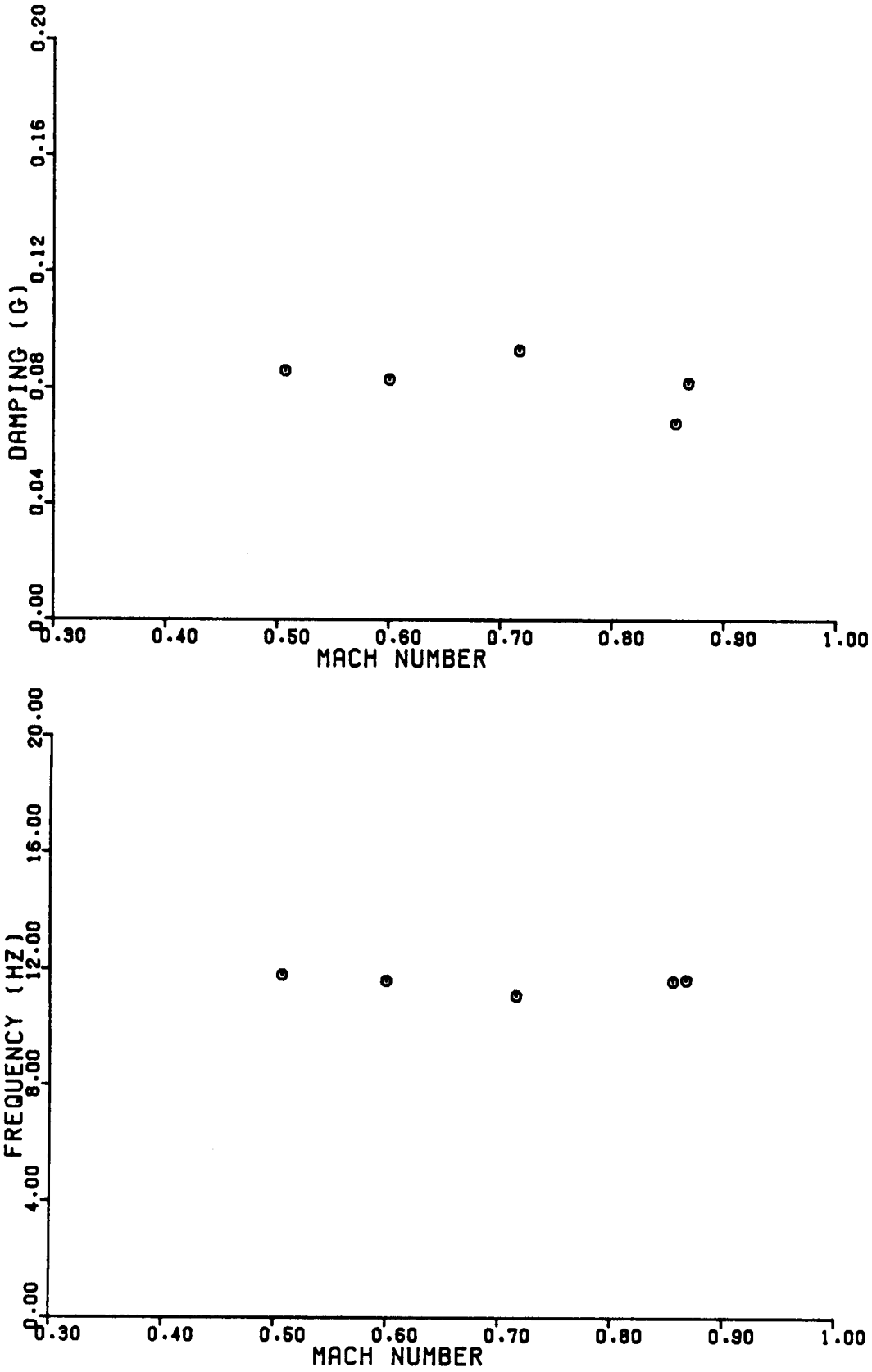

Figure 25. Right wing fore-and-aft bending modal data at 27,500 ft for 20° wing sweep.

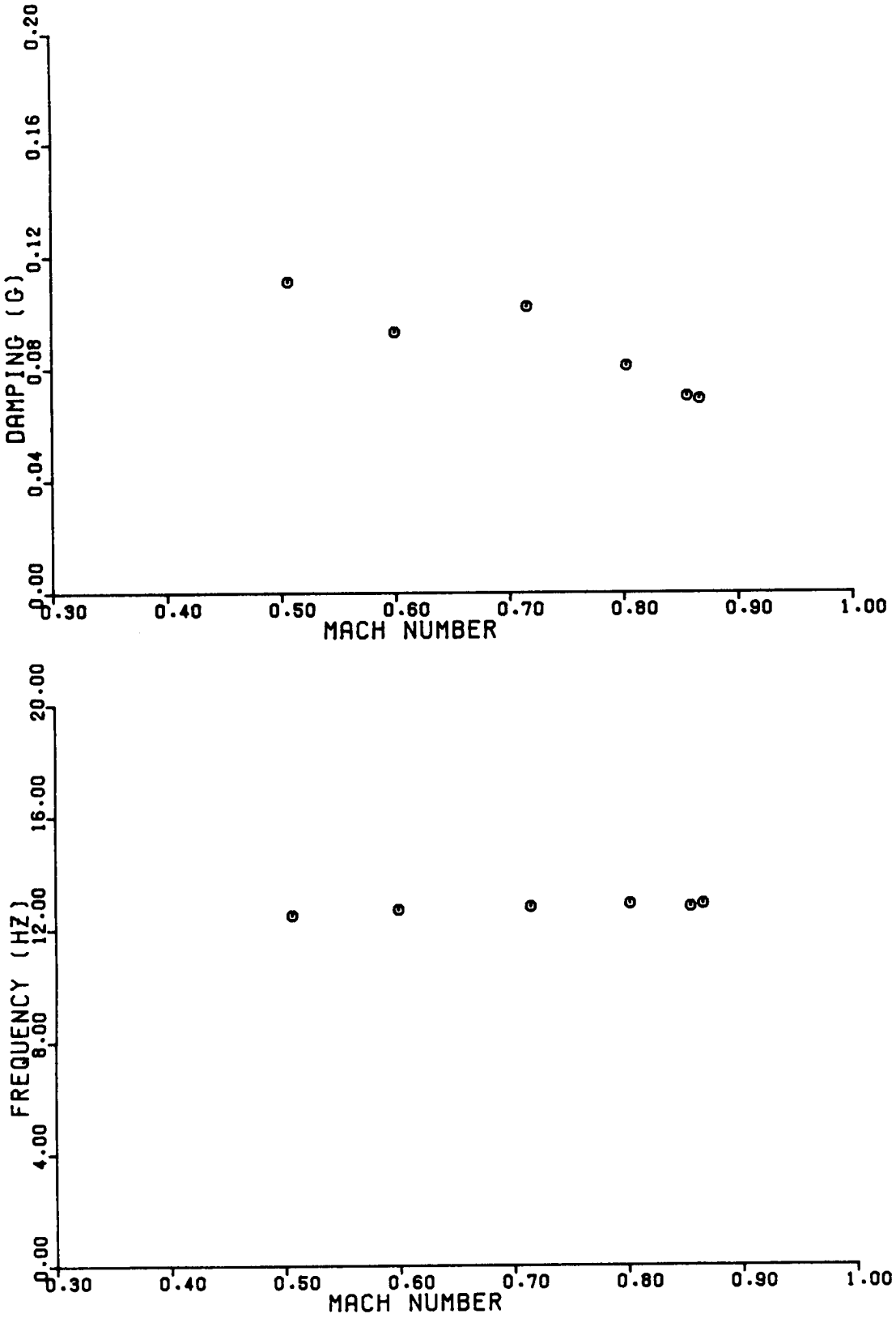

Figure 26. Vertical fin bending modal data at 27,500 ft for 20° wing sweep.

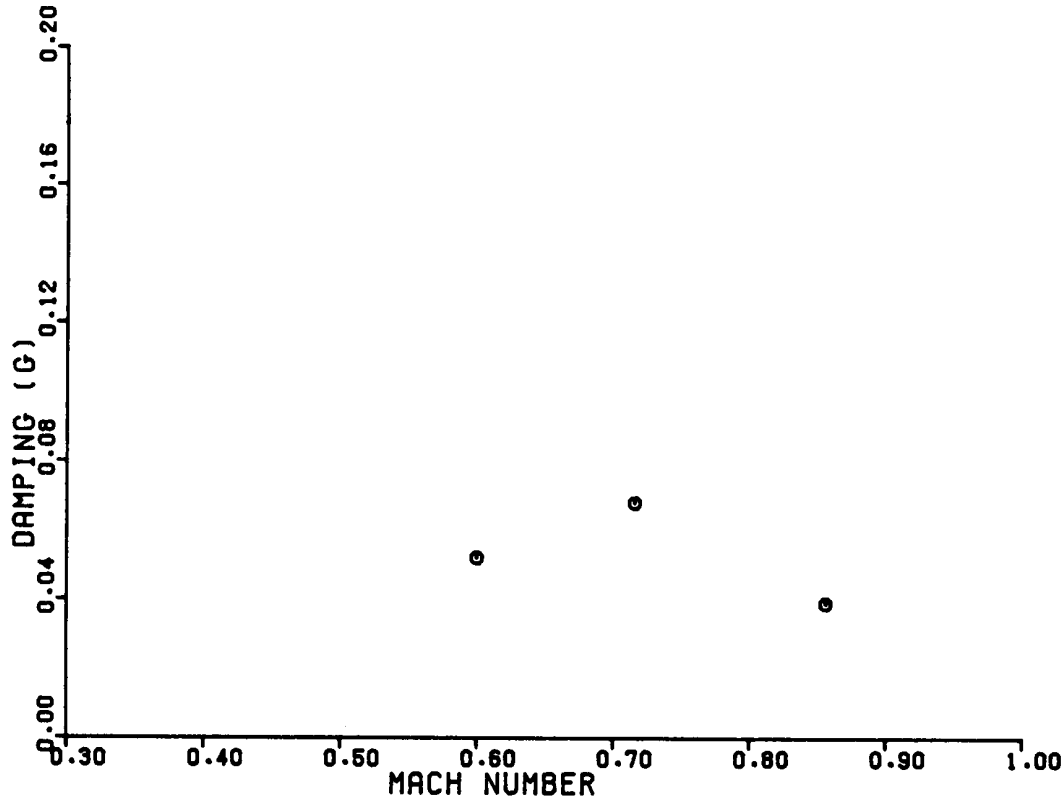

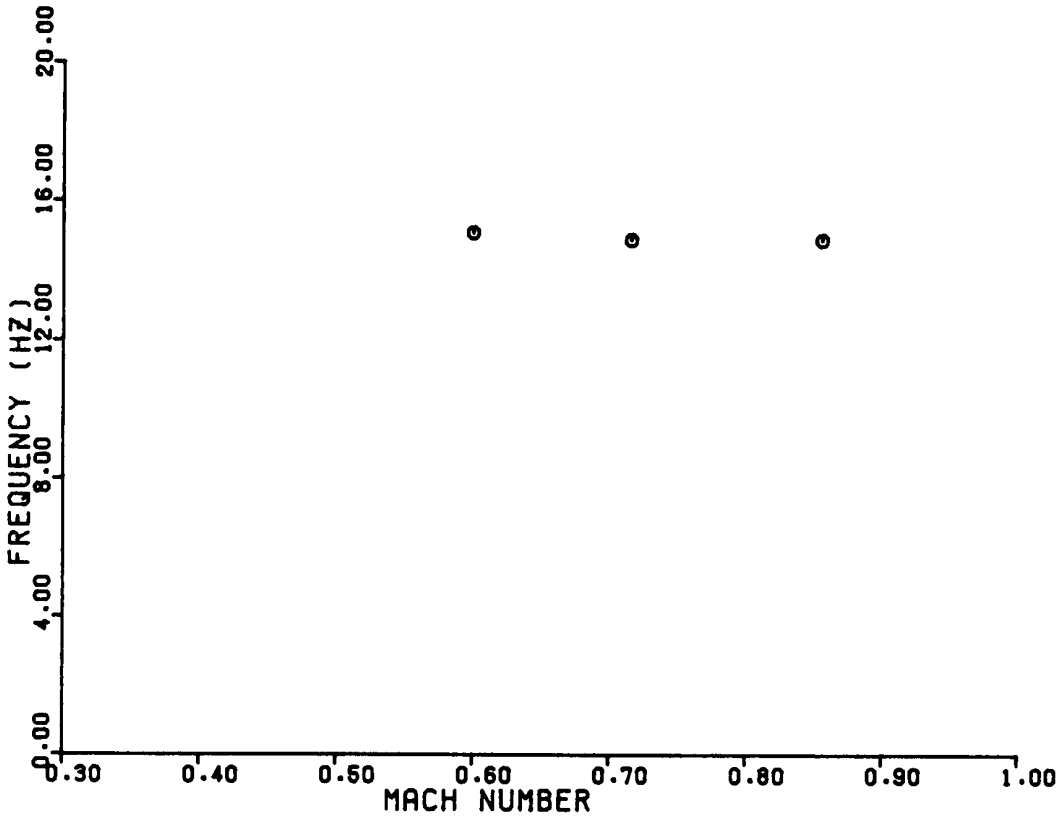

Figure 27. Second symmetric wing bending modal data at 27,500 ft for 20° wing sweep.

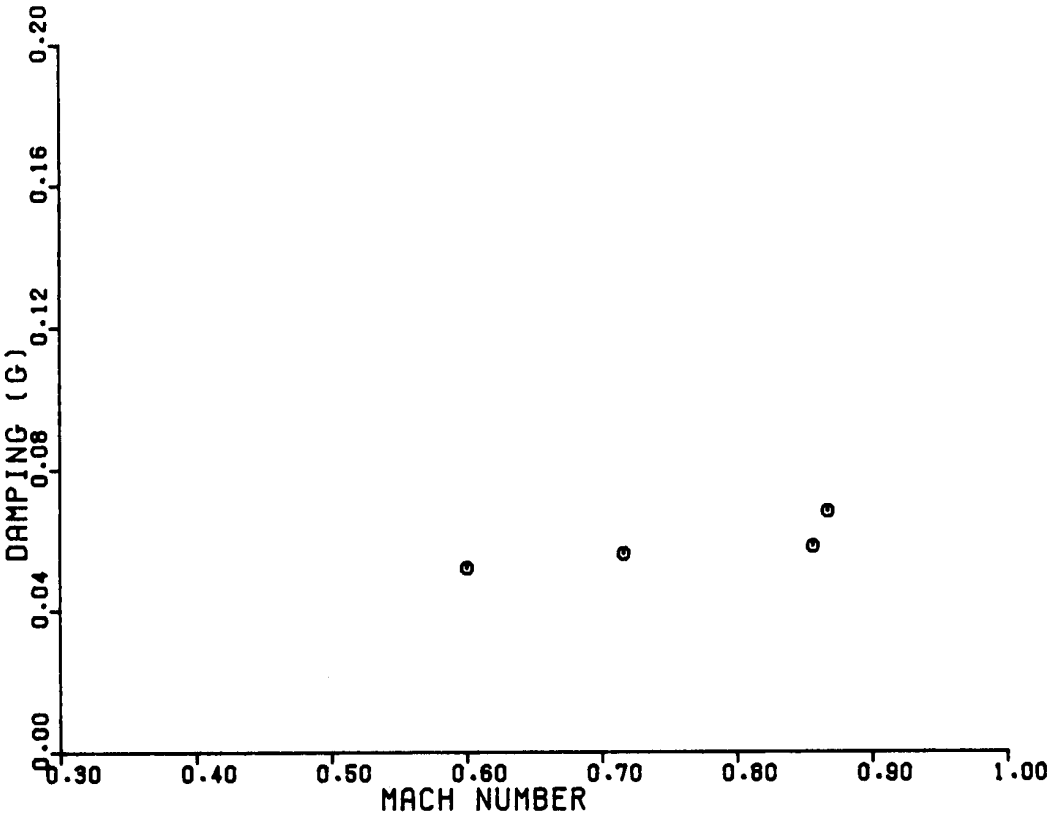

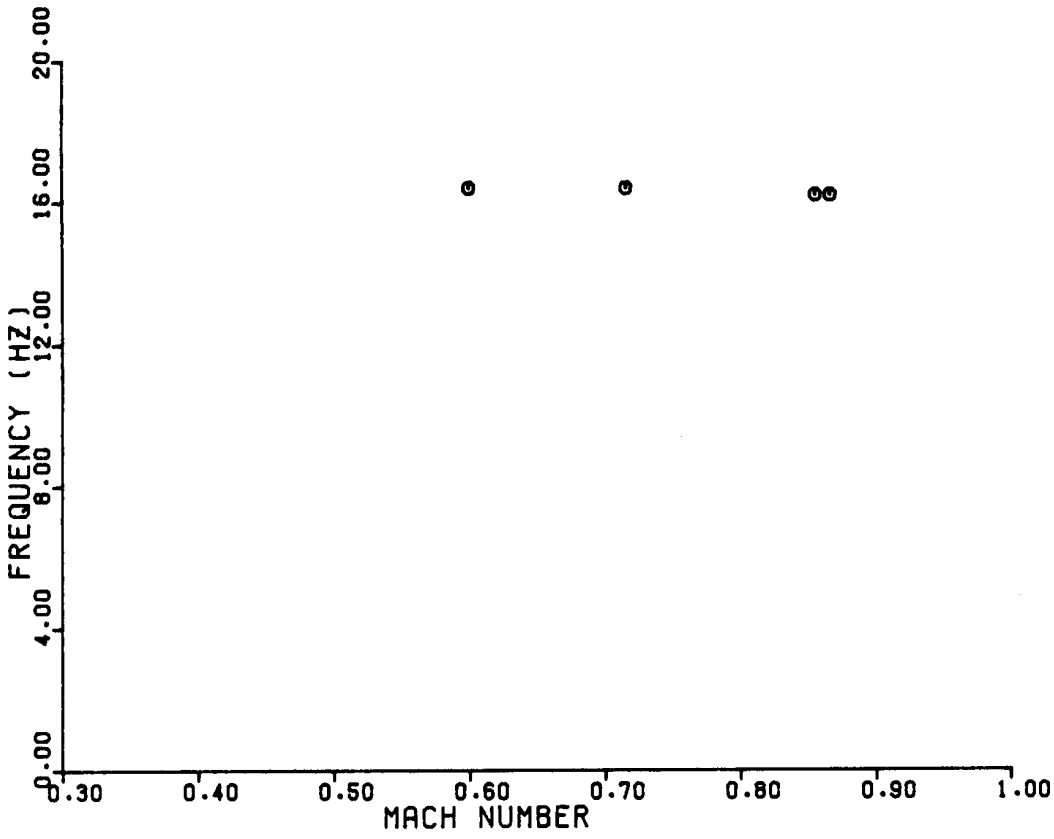

Figure 28. Second antisymmetric wing bending modal data at 27,500 ft for 20° wing sweep.

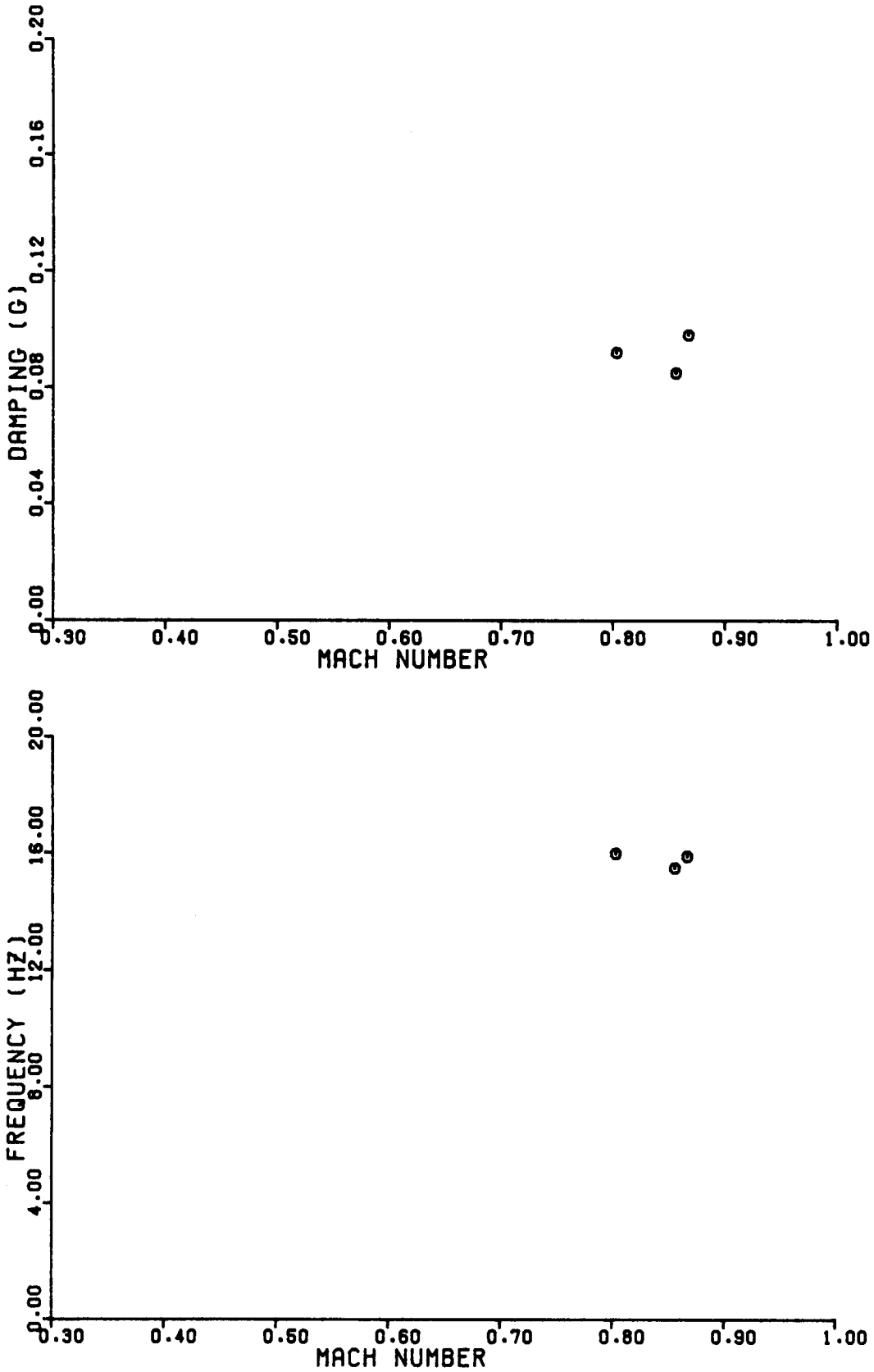

Figure 29. Horizontal stabilator bending modal data at 27,500 ft for 20° wing sweep.

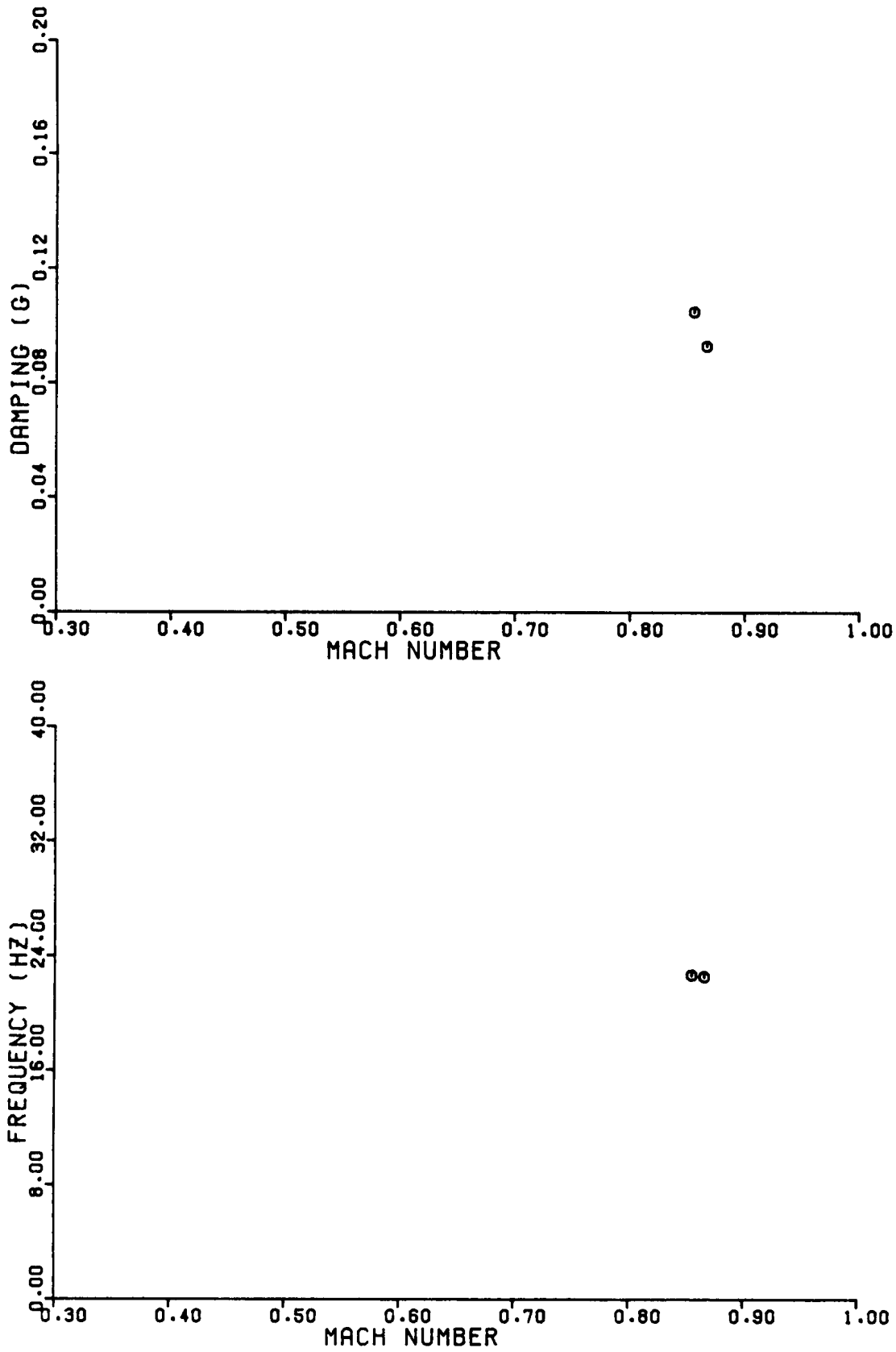

Figure 30. Left wing torsion modal data at 27,500 ft for 20° wing sweep.

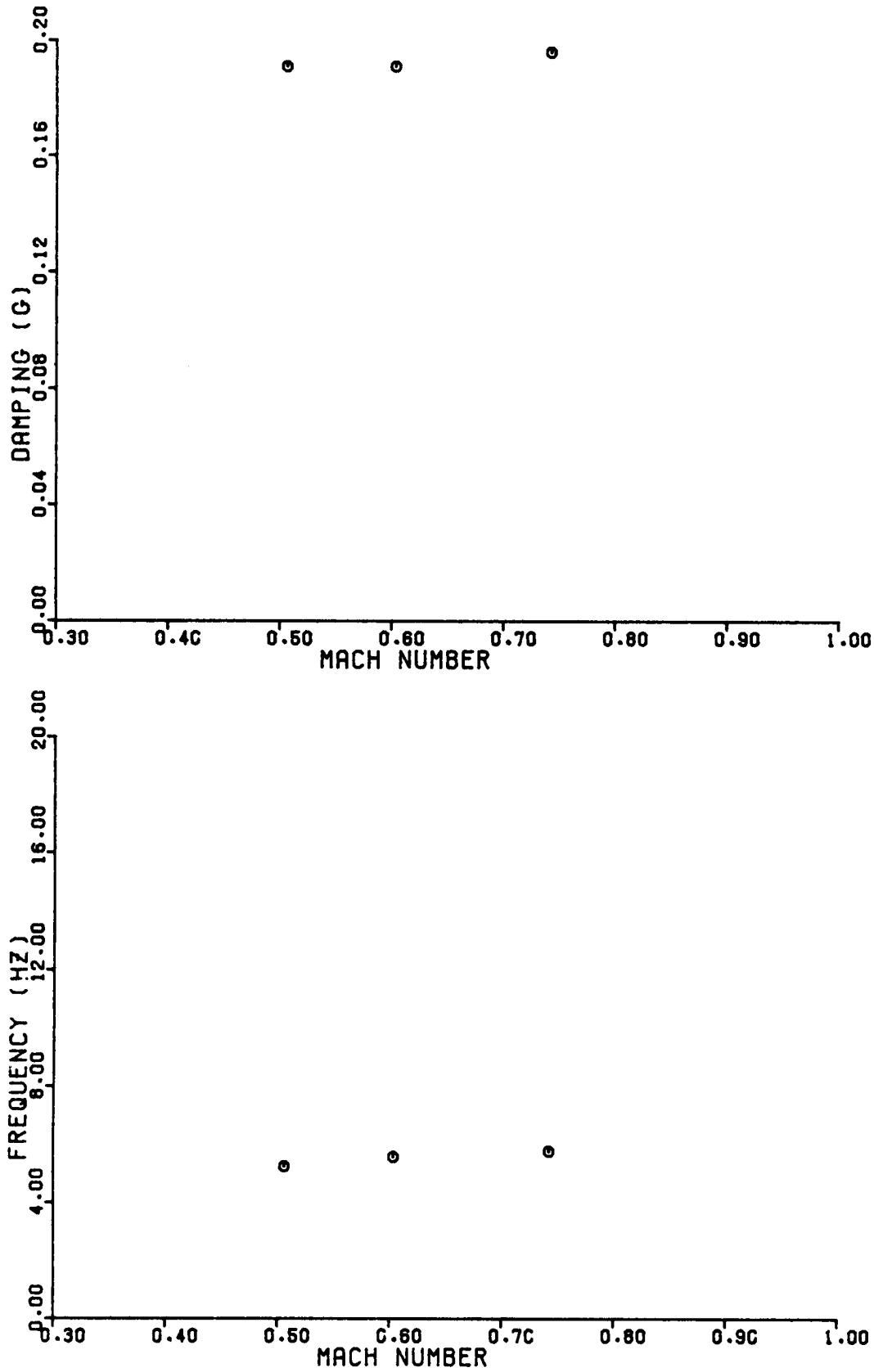

Figure 31. Symmetric wing bending modal data at 5000 ft for 35° wing sweep.

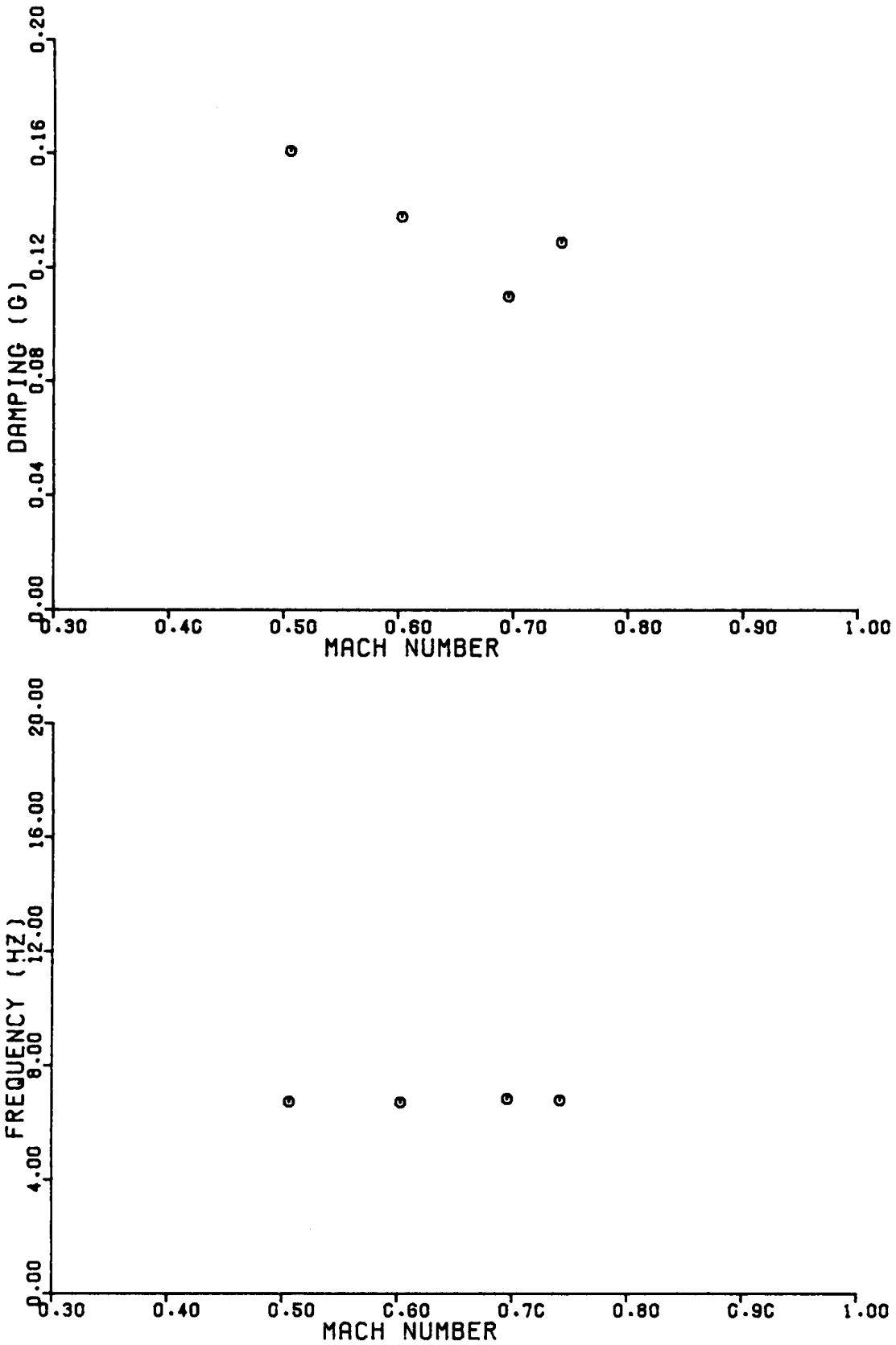

Figure 32. Antisymmetric wing bending modal data at 5000 ft for 35° wing sweep.

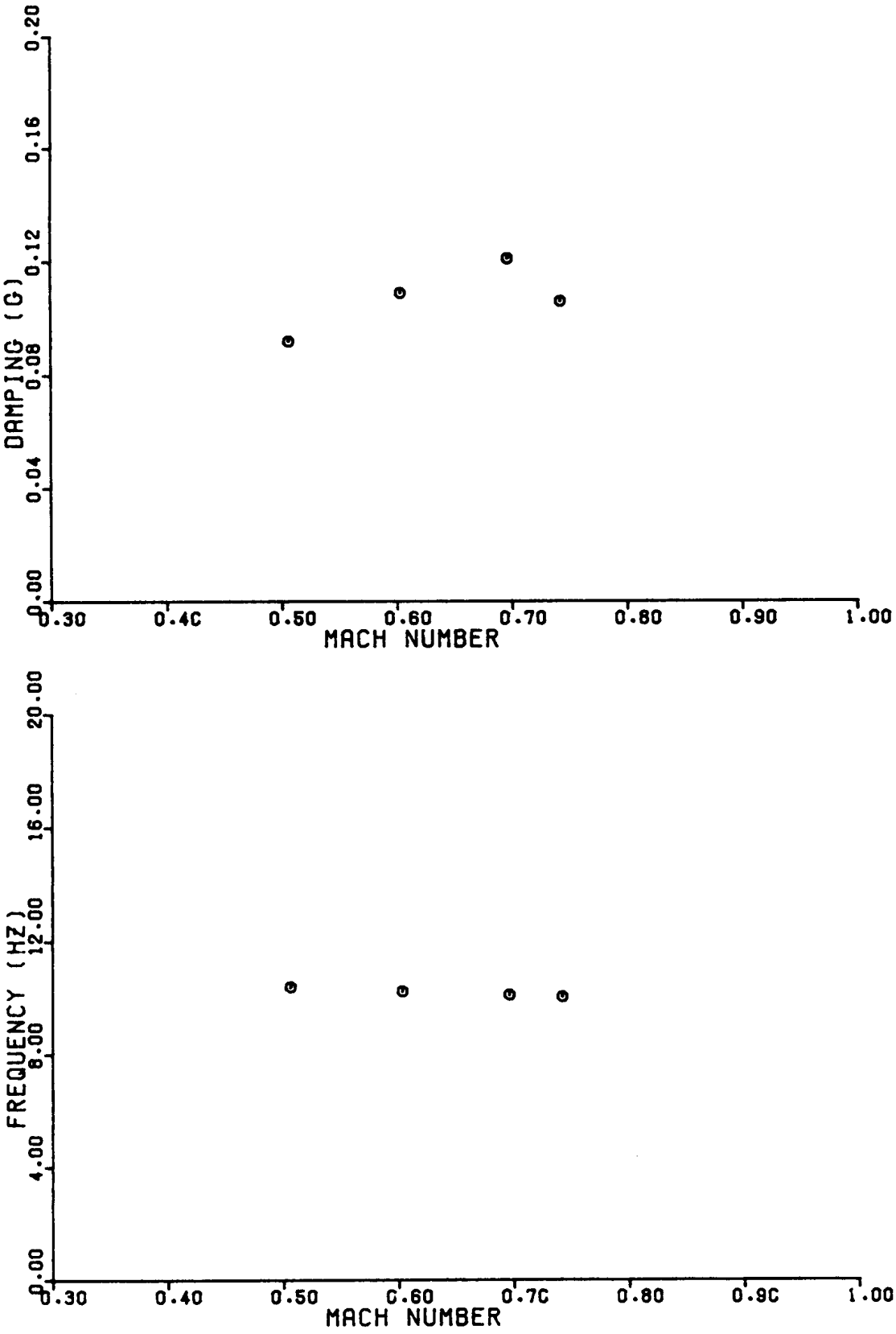

Figure 33. Left wing fore-and-aft bending modal data at 5000 ft for 35° wing sweep.

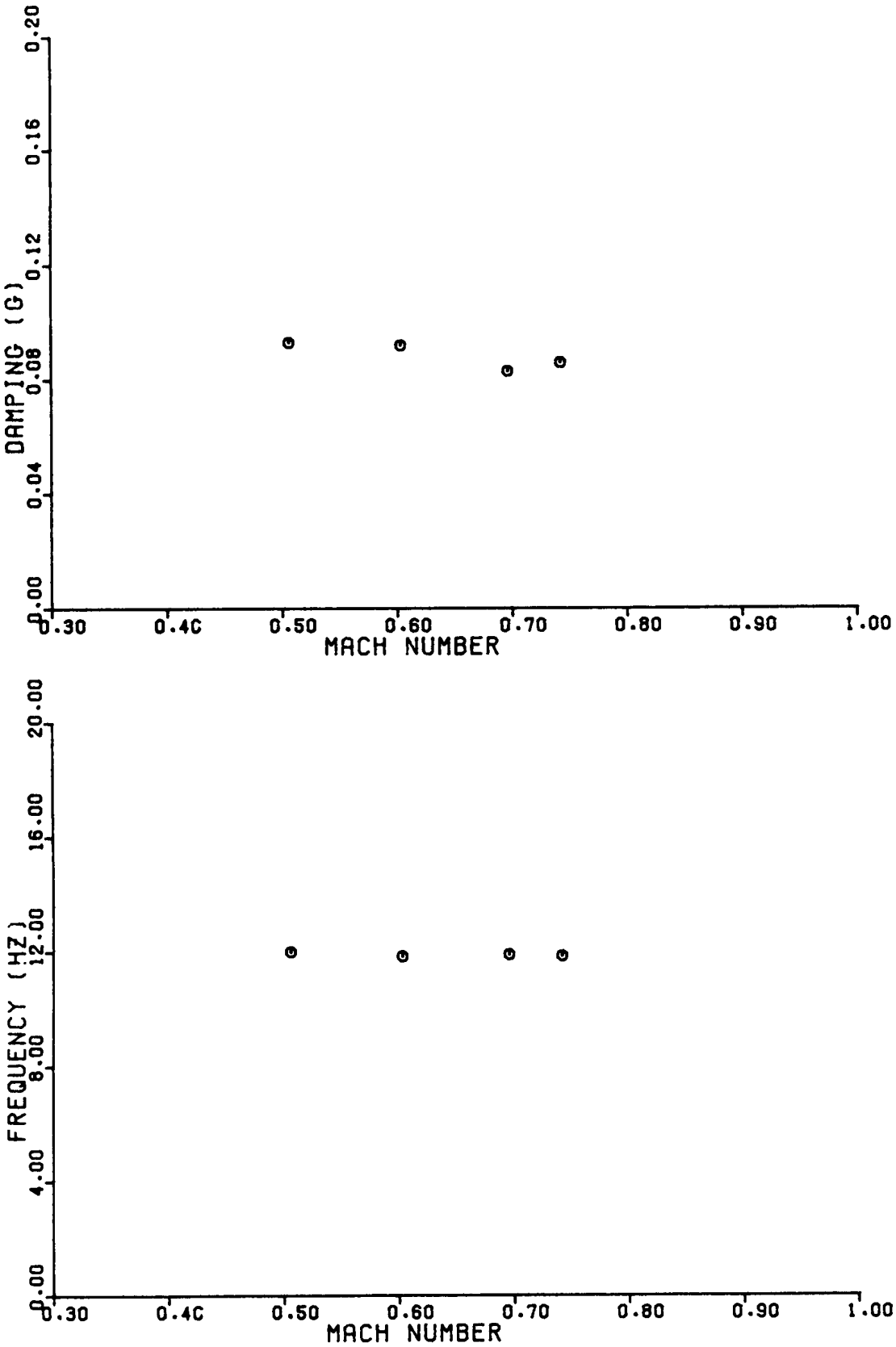

Figure 34. Right wing fore-and-aft bending modal data at 5000 ft for 35° wing sweep.

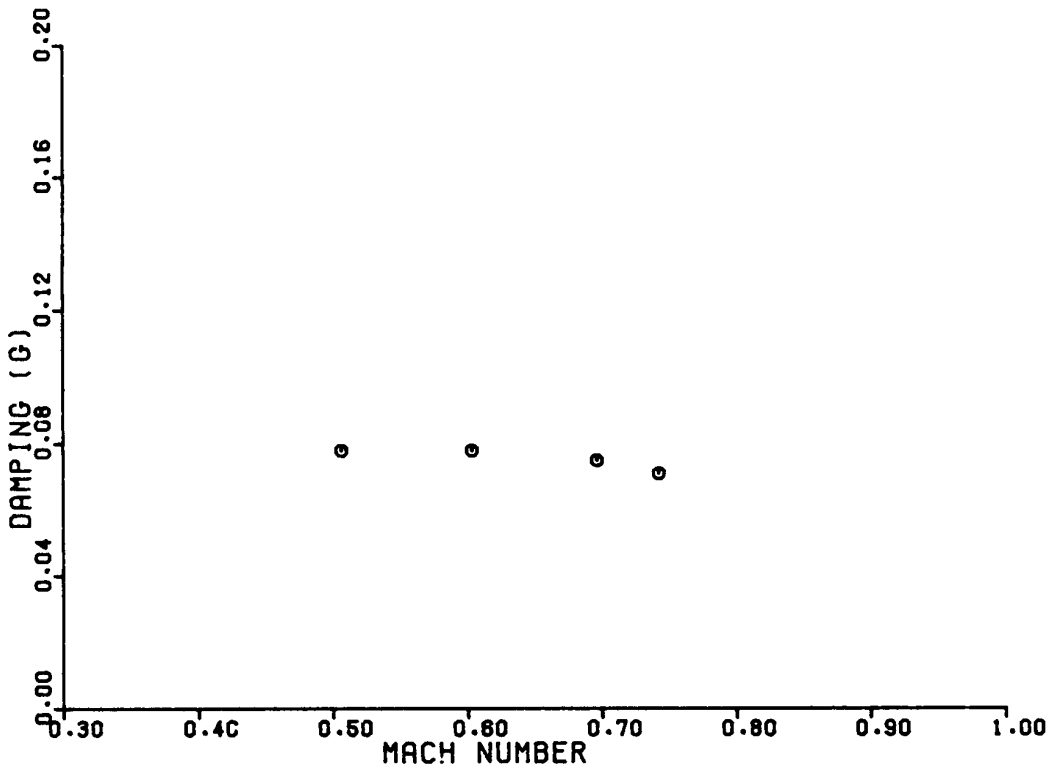

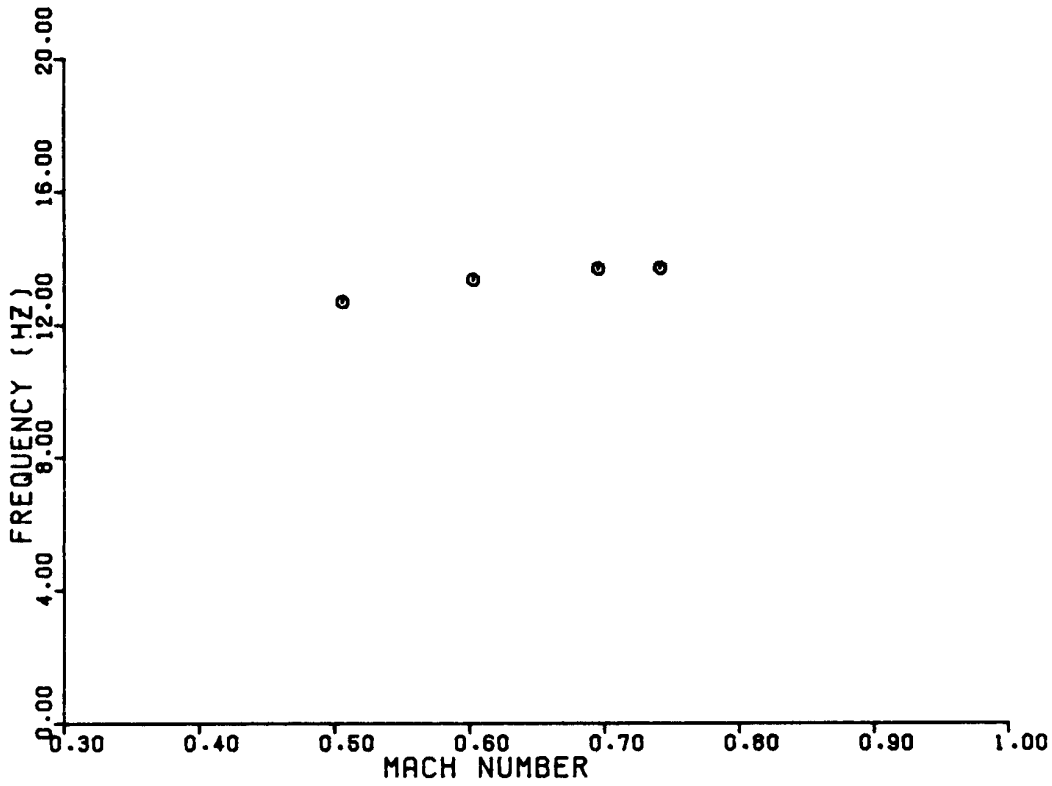

Figure 35. Veritcal fin bending modal data at 5000 ft for 35° wing sweep.

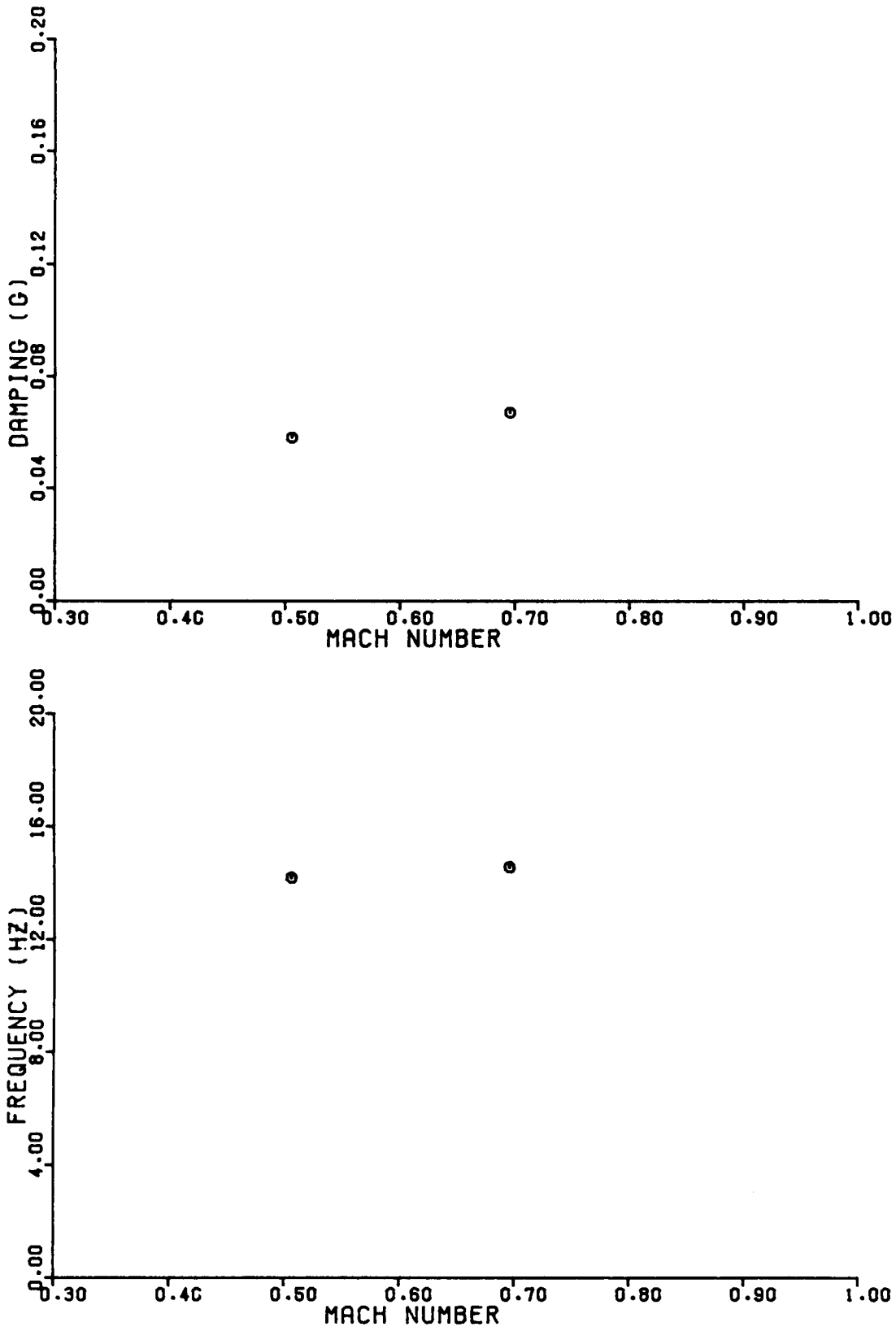

Figure 36. Second symmetric wing bending modal data at 5000 ft for 35° wing sweep.

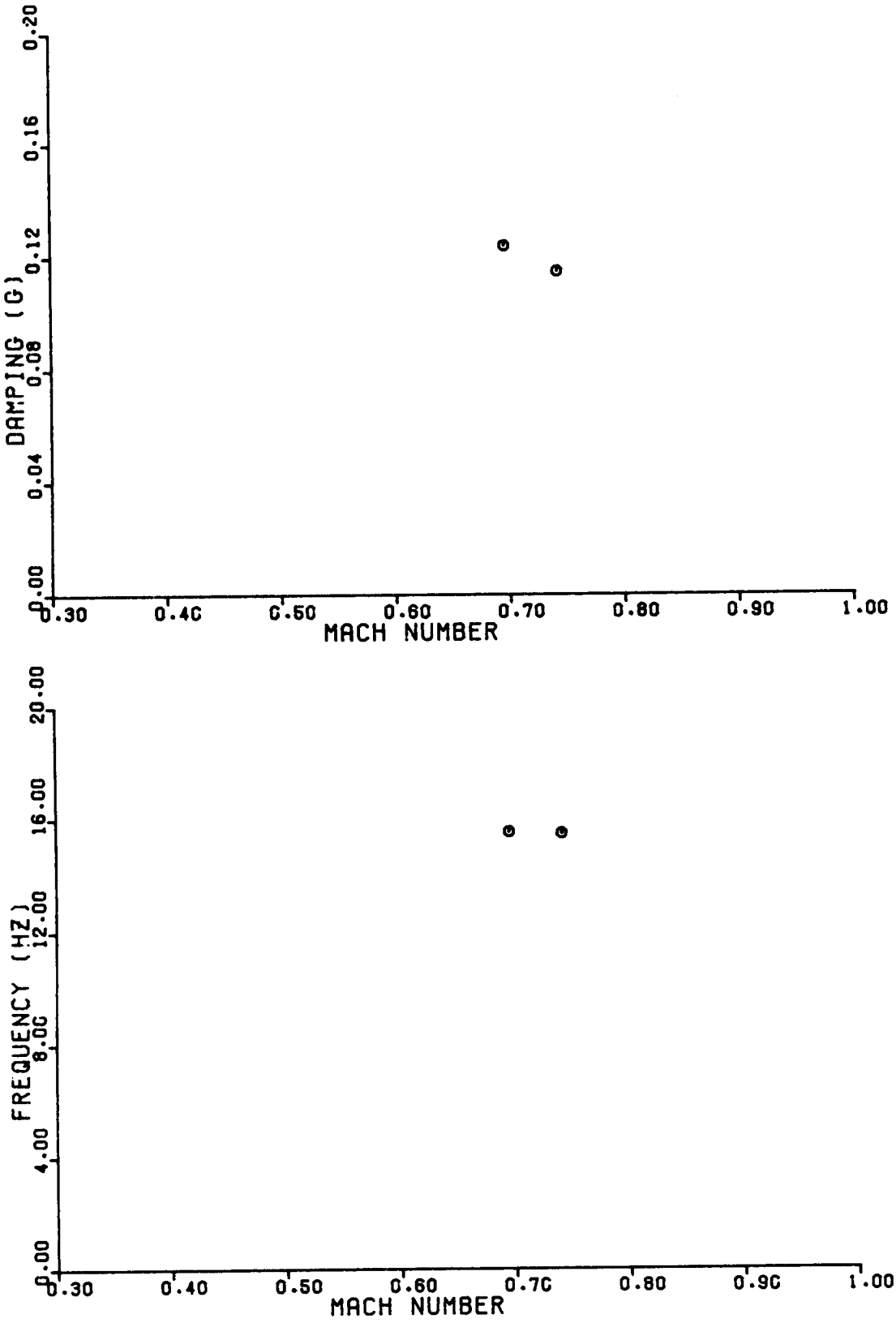

Figure 37. Second antisymmetric wing bending modal data at 5000 ft for 35° wing sweep.

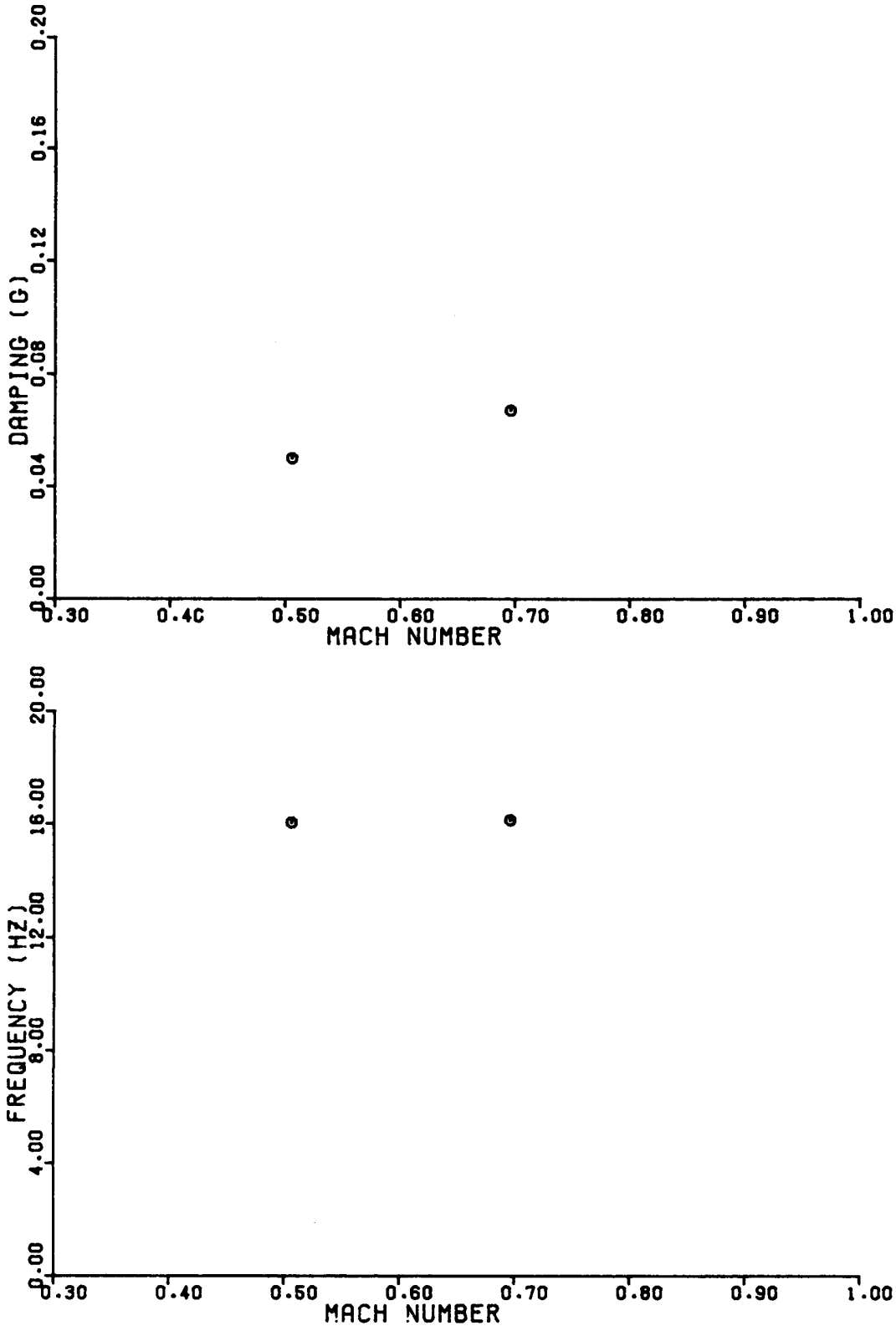

Figure 38. Horizontal stabilator bending modal data at 5000 ft for 35° wing sweep.

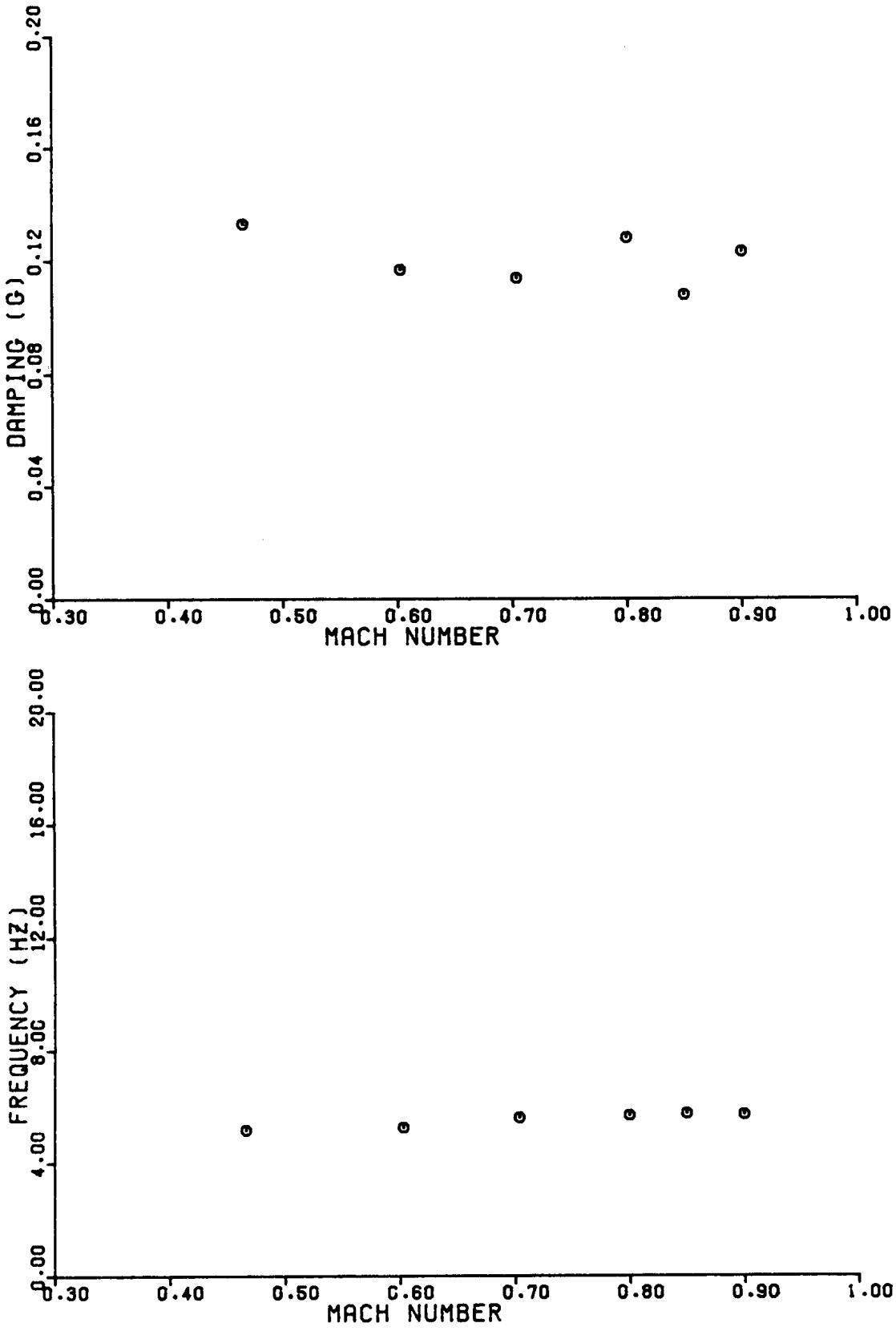

Figure 39. Symmetric wing bending modal data at 17,000 ft for 35° wing sweep.

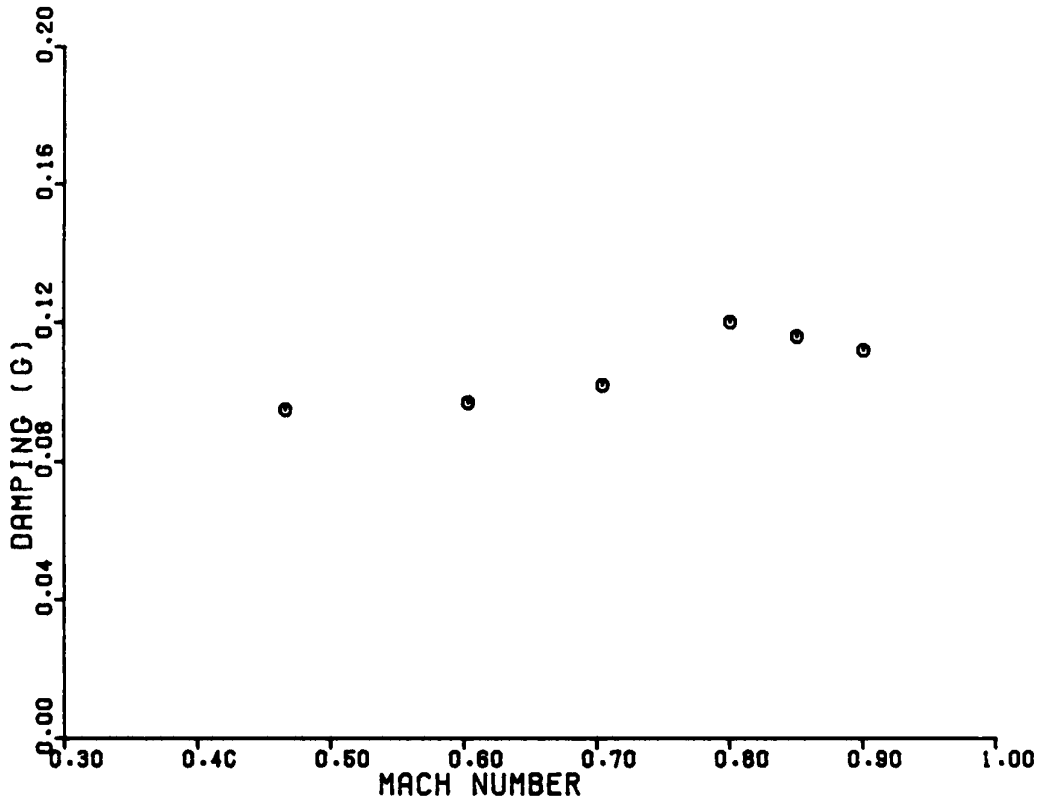

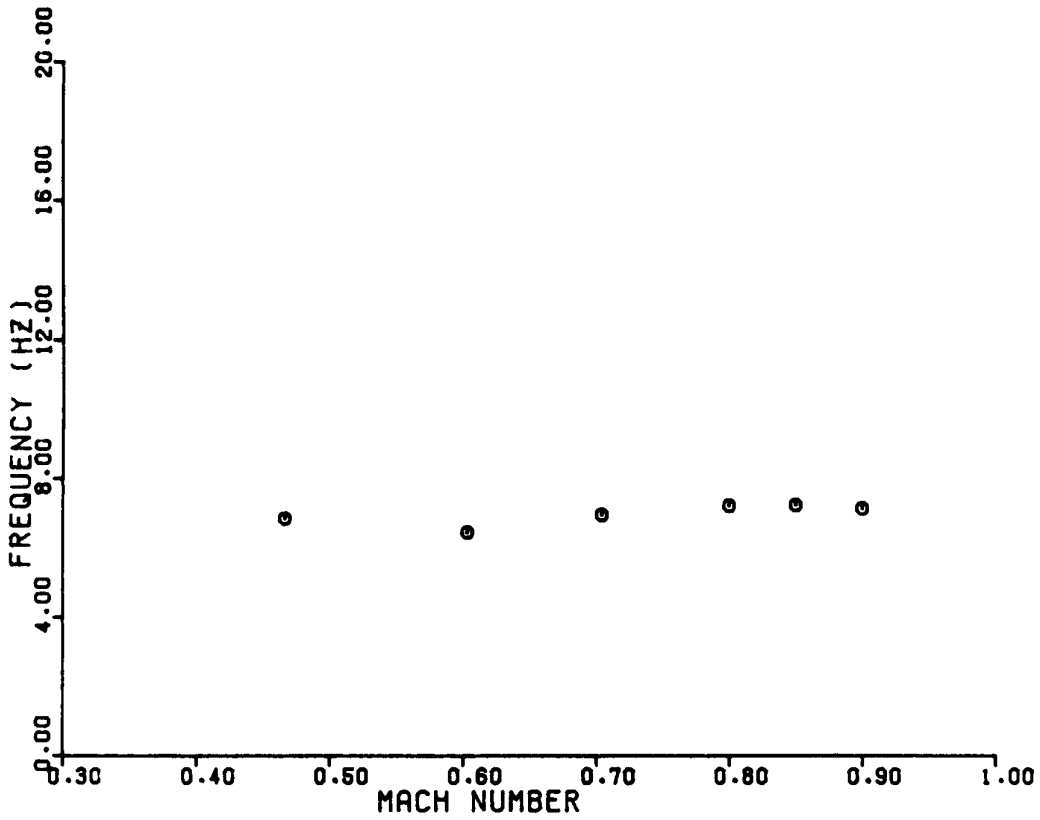

Figure 40. Antisymmetric wing bending modal data at 17,000 ft for 35° wing sweep.

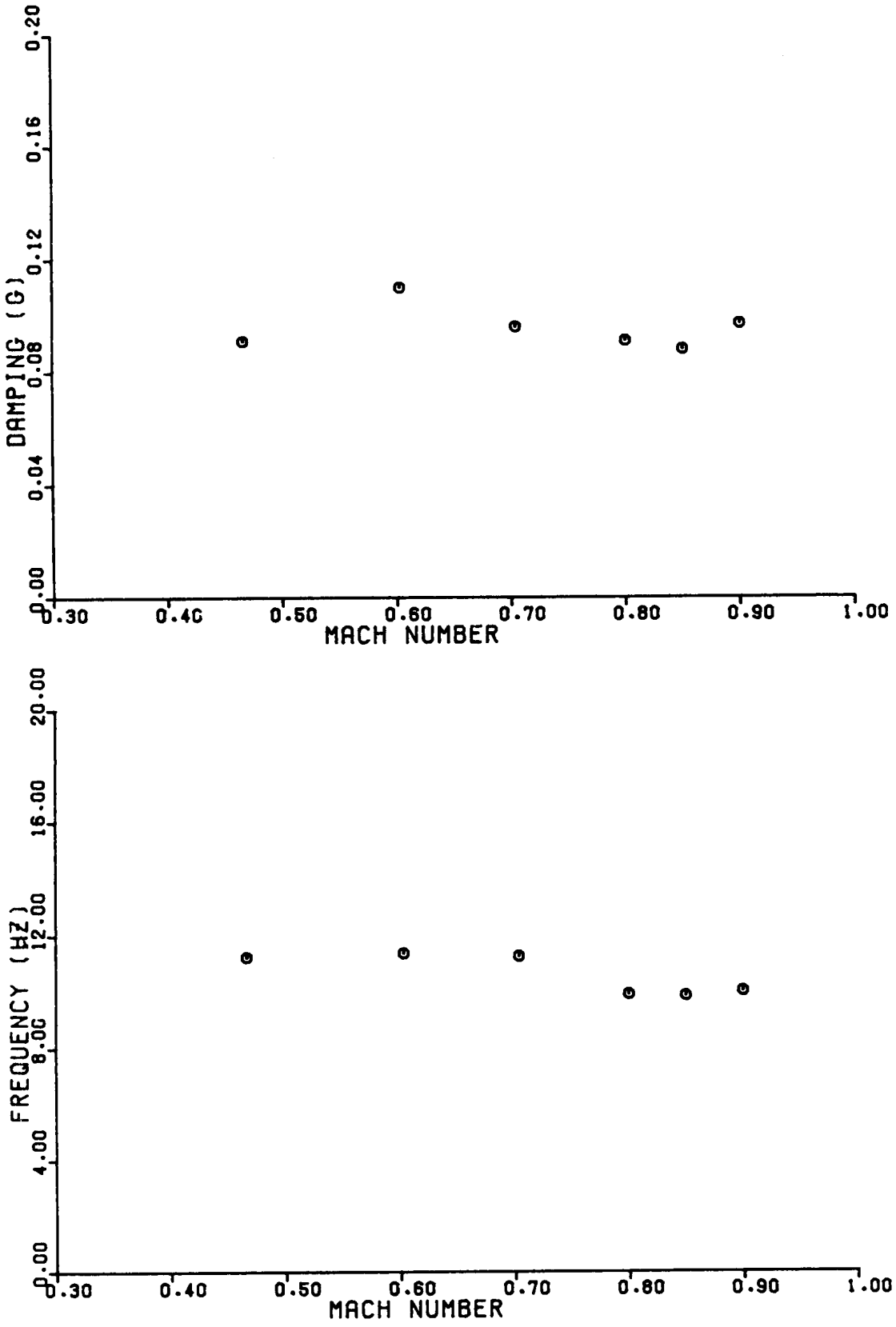

Figure 41. Left wing fore-and-aft bending modal data at 17,000 ft for 35° wing sweep.

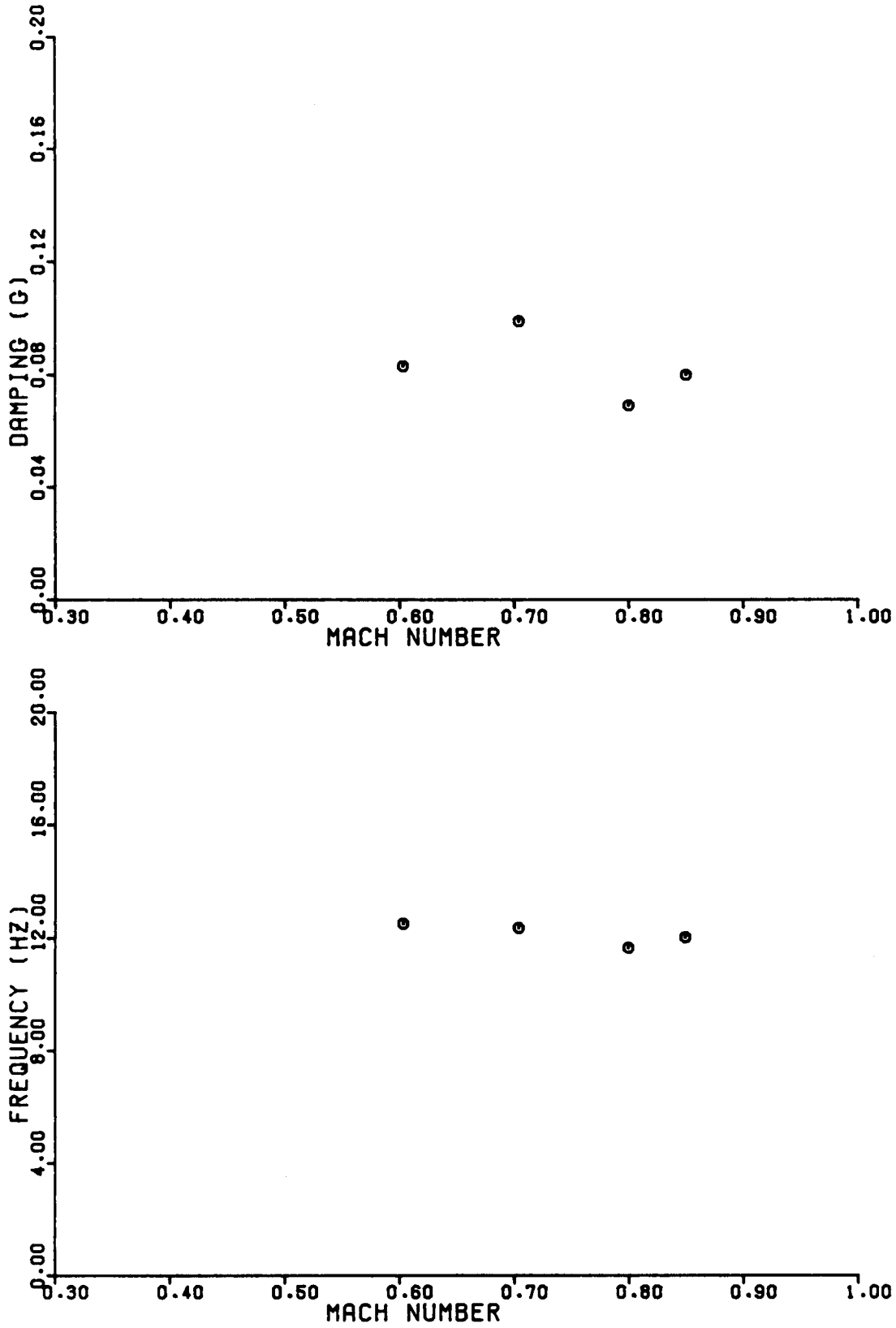

Figure 42. Right wing fore-and-aft bending modal data at 17,000 ft for 35° wing sweep.

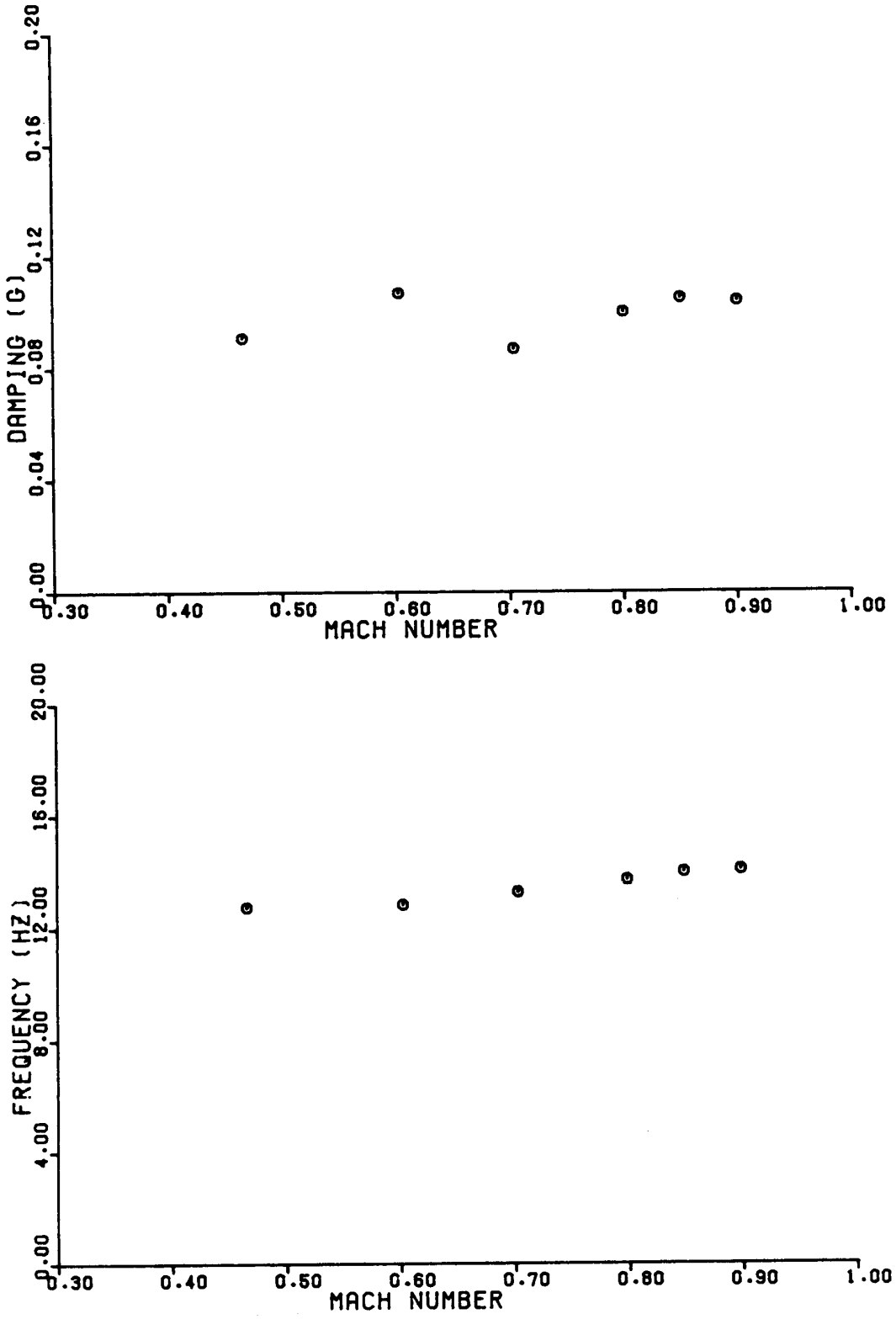

Figure 43. Vertical fin bending modal data at 17,000 ft for 35° wing sweep.

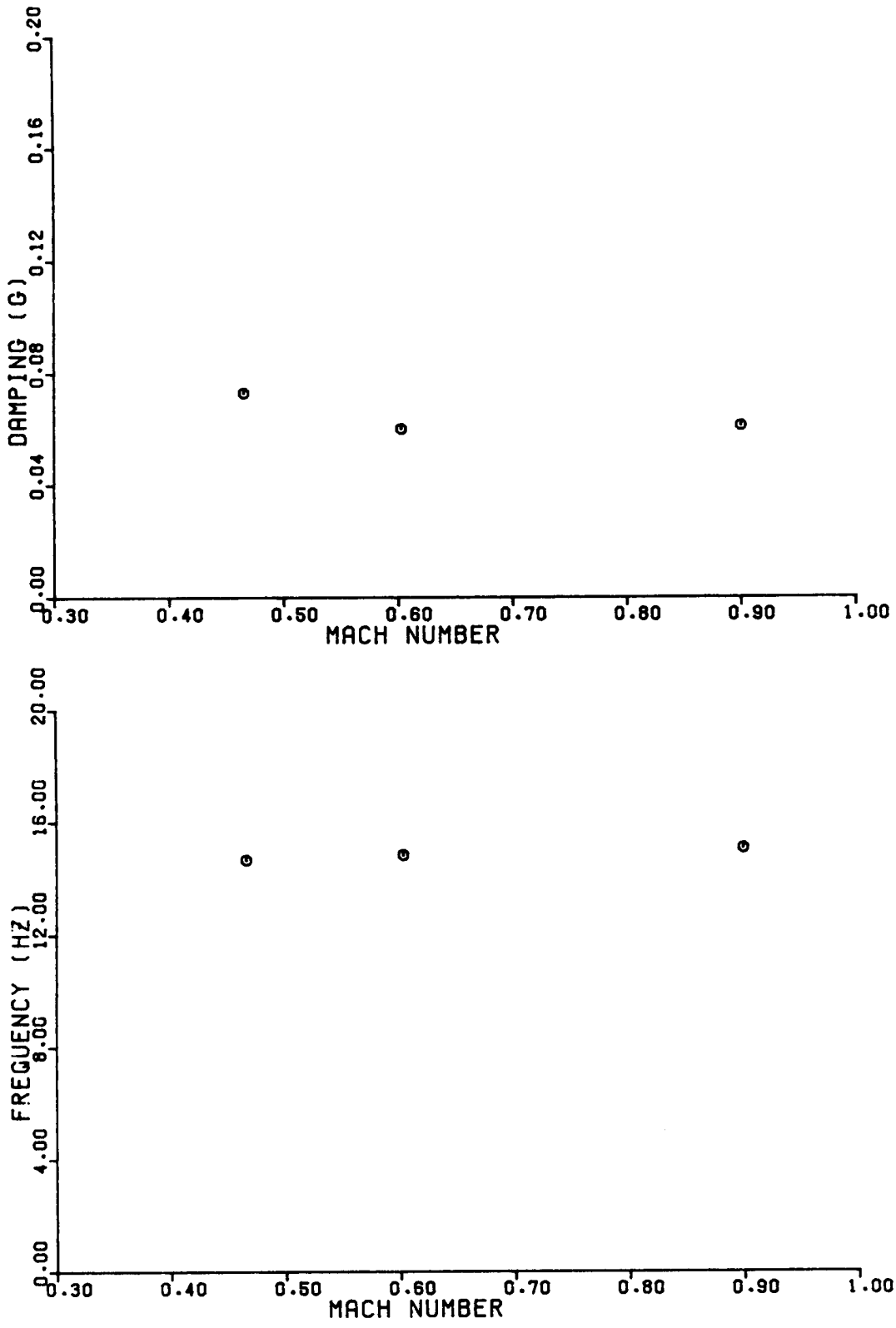

Figure 44. Second symmetric wing bending modal data at 17,000 ft for 35° wing sweep.

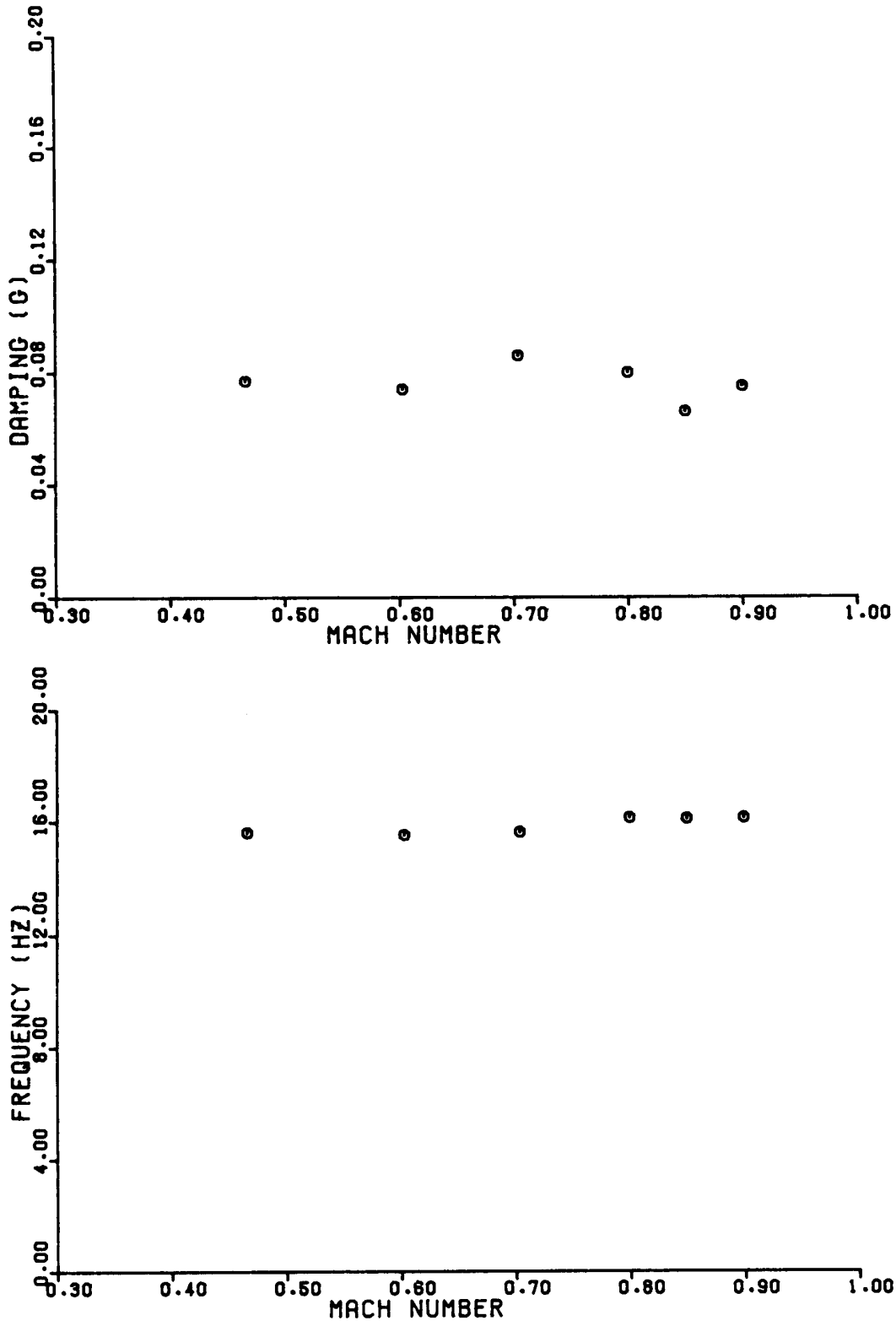

Figure 45. Second antisymmetric wing bending modal data at 17,000 ft for 35° wing sweep.

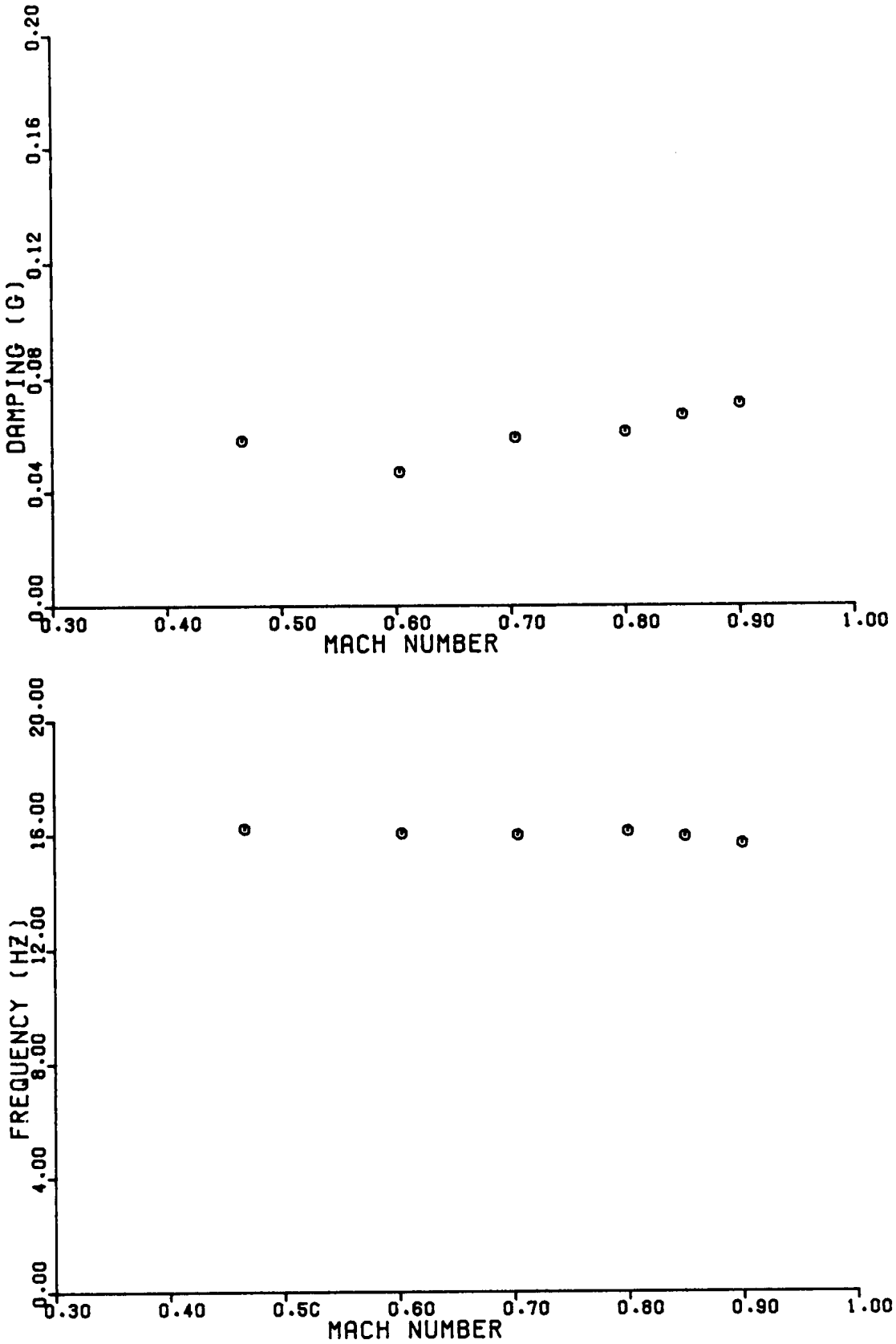

Figure 46. Horizontal stabilator bending modal data at 17,000 ft for 35° wing sweep.

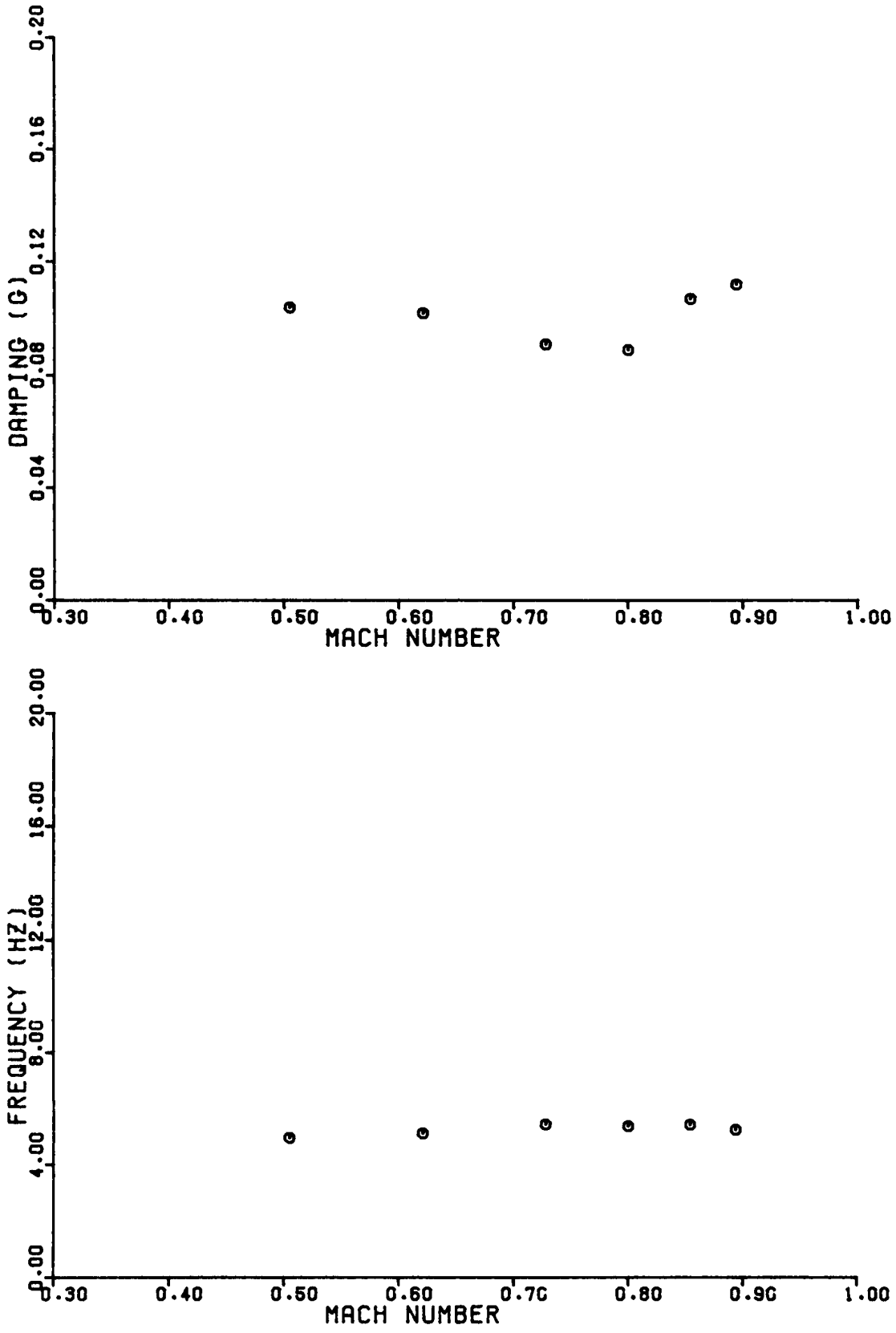

Figure 47. Symmetric wing bending modal data at 27,500 ft for 35° wing sweep.

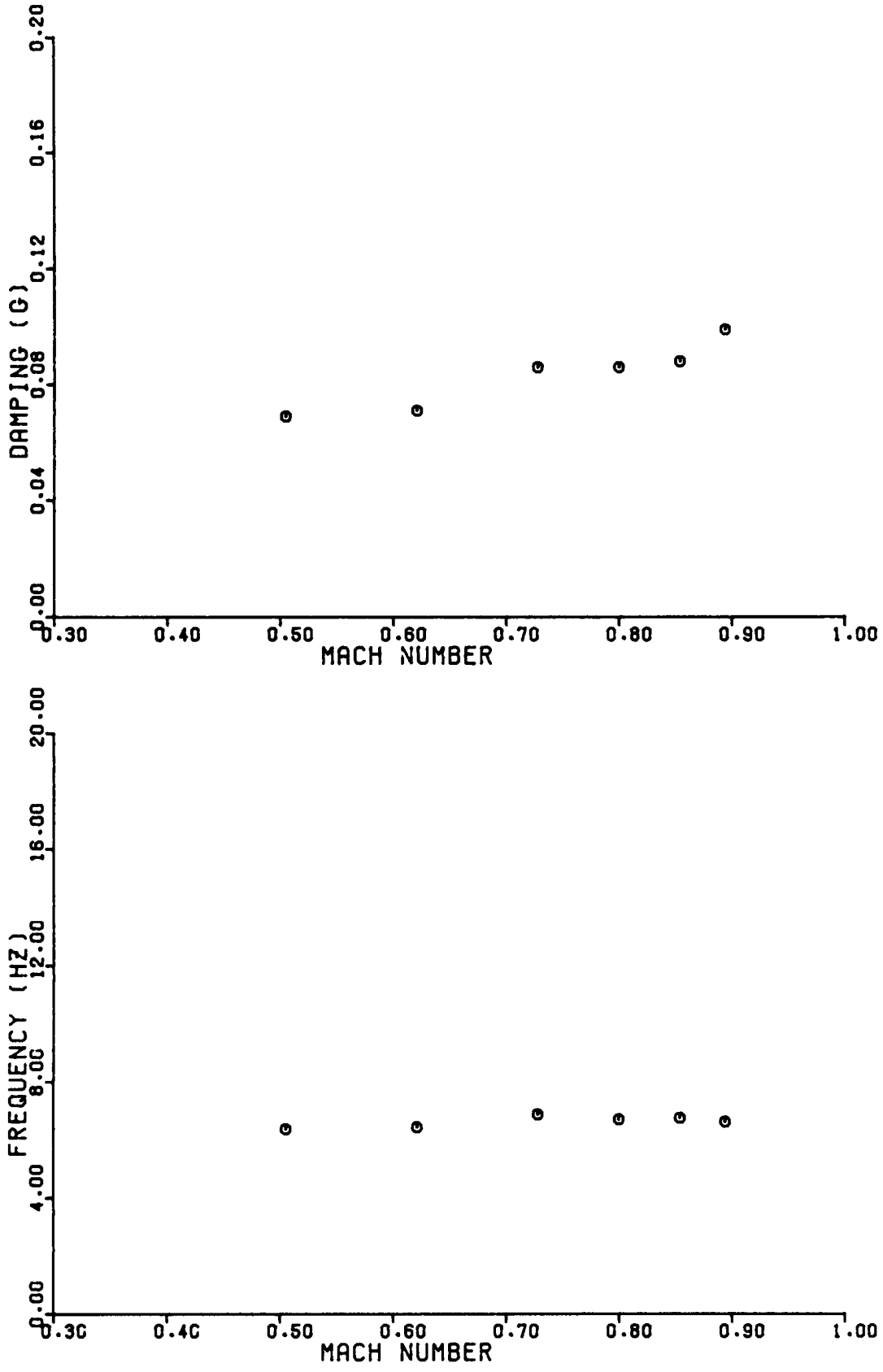

Figure 48. Antisymmetric wing bending modal data at 27,500 ft for 35° wing sweep.

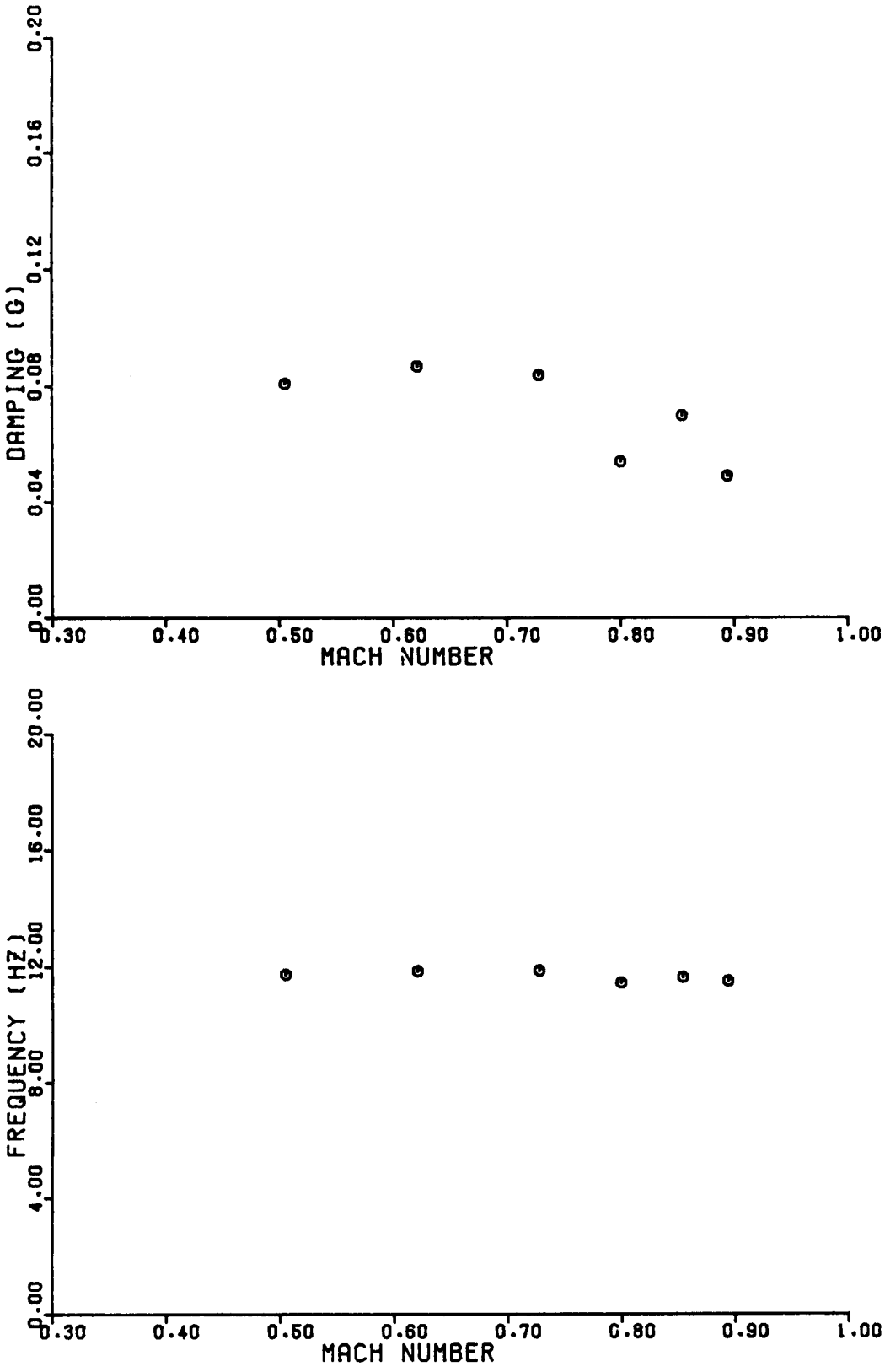

Figure 49. Left wing fore-and-aft bending modal data at 27,500 ft for 35° wing sweep.

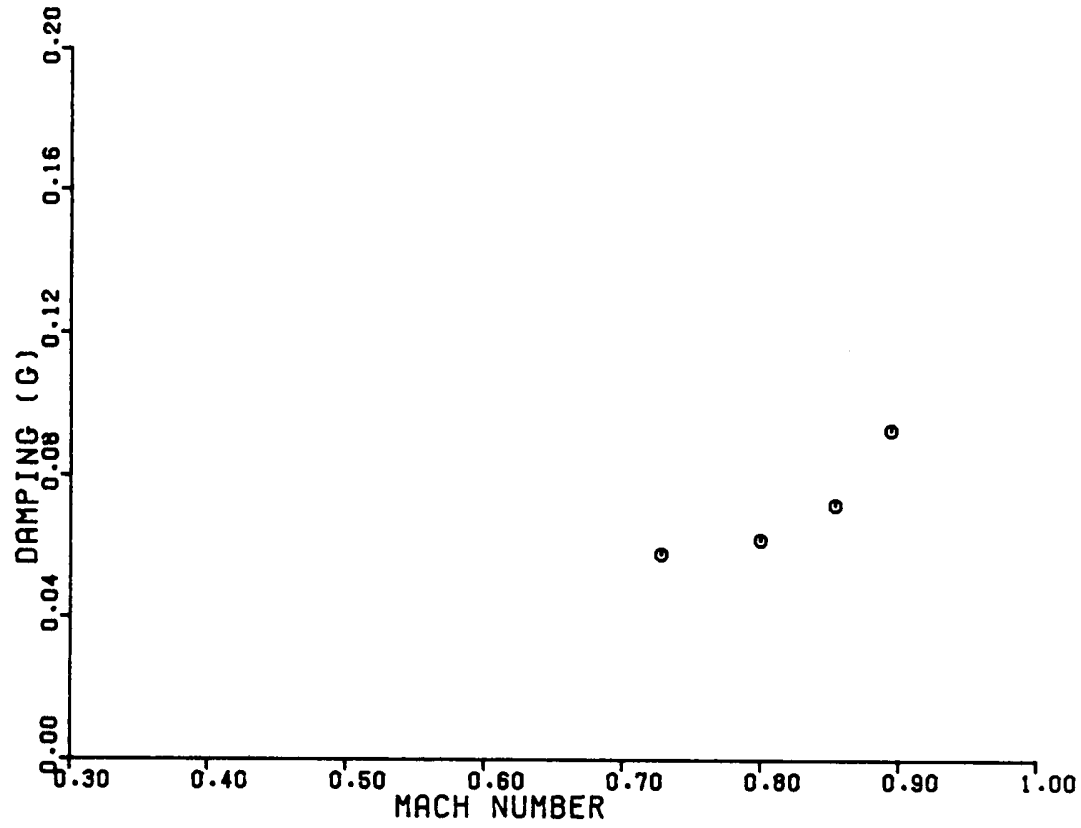

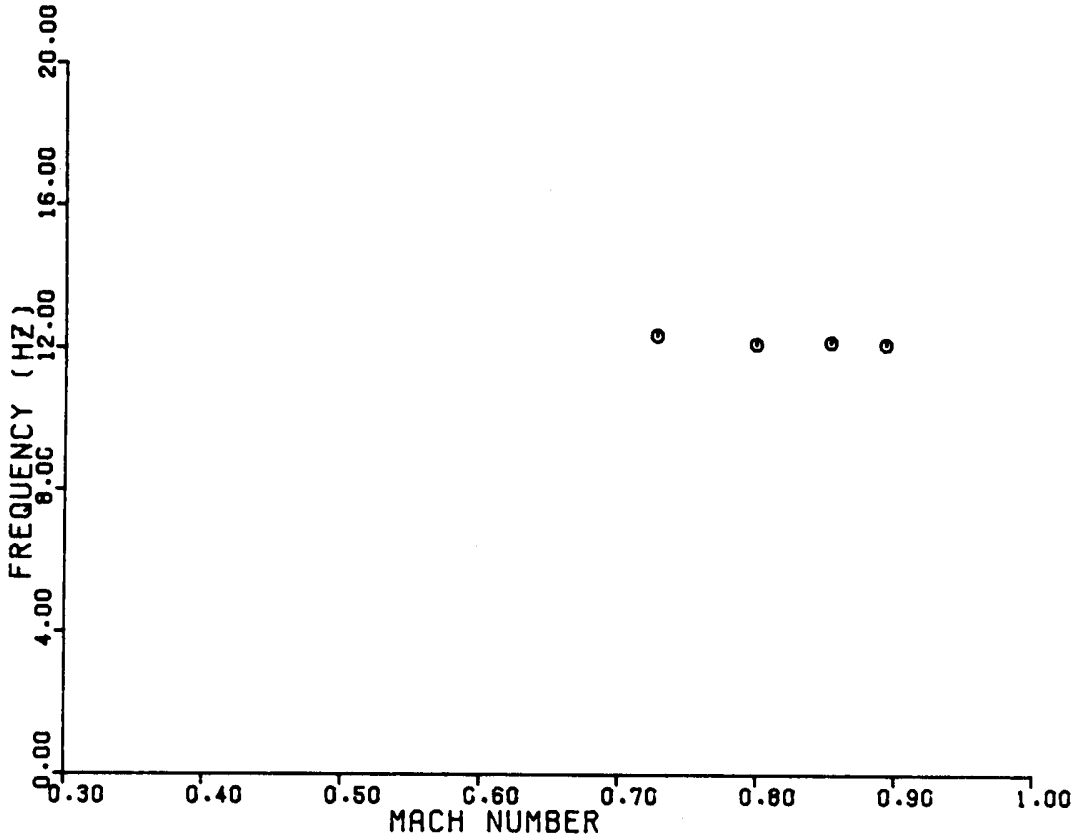

Figure 50. Right wind fore-and-aft bending modal data at 27,500 ft for 35° wing sweep.

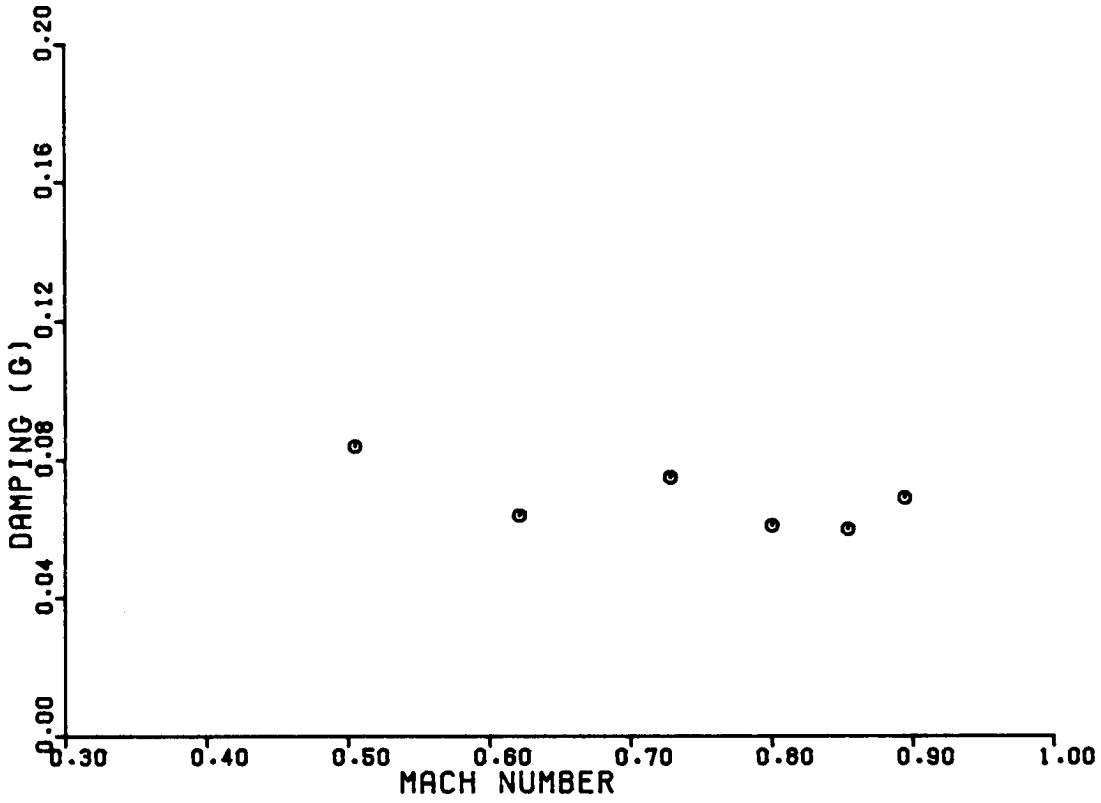

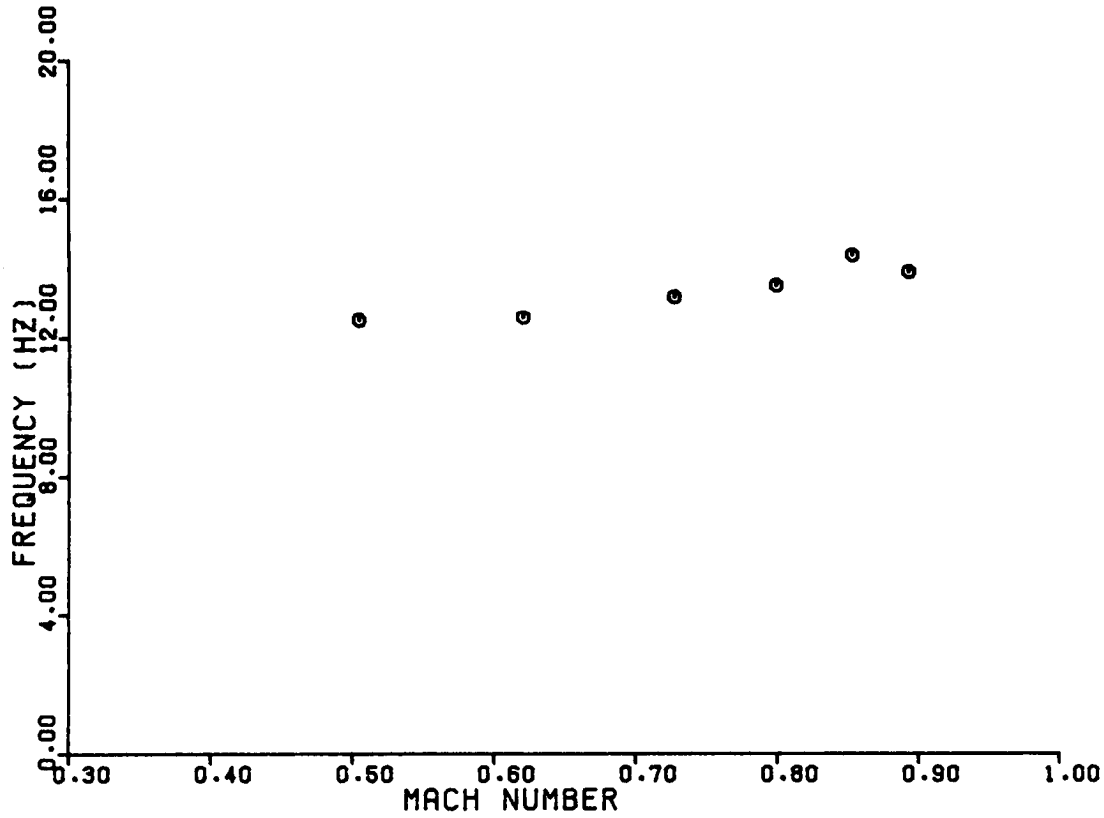

Figure 51. Vertical fin bending modal data at 27,500 ft for 35° wing sweep.

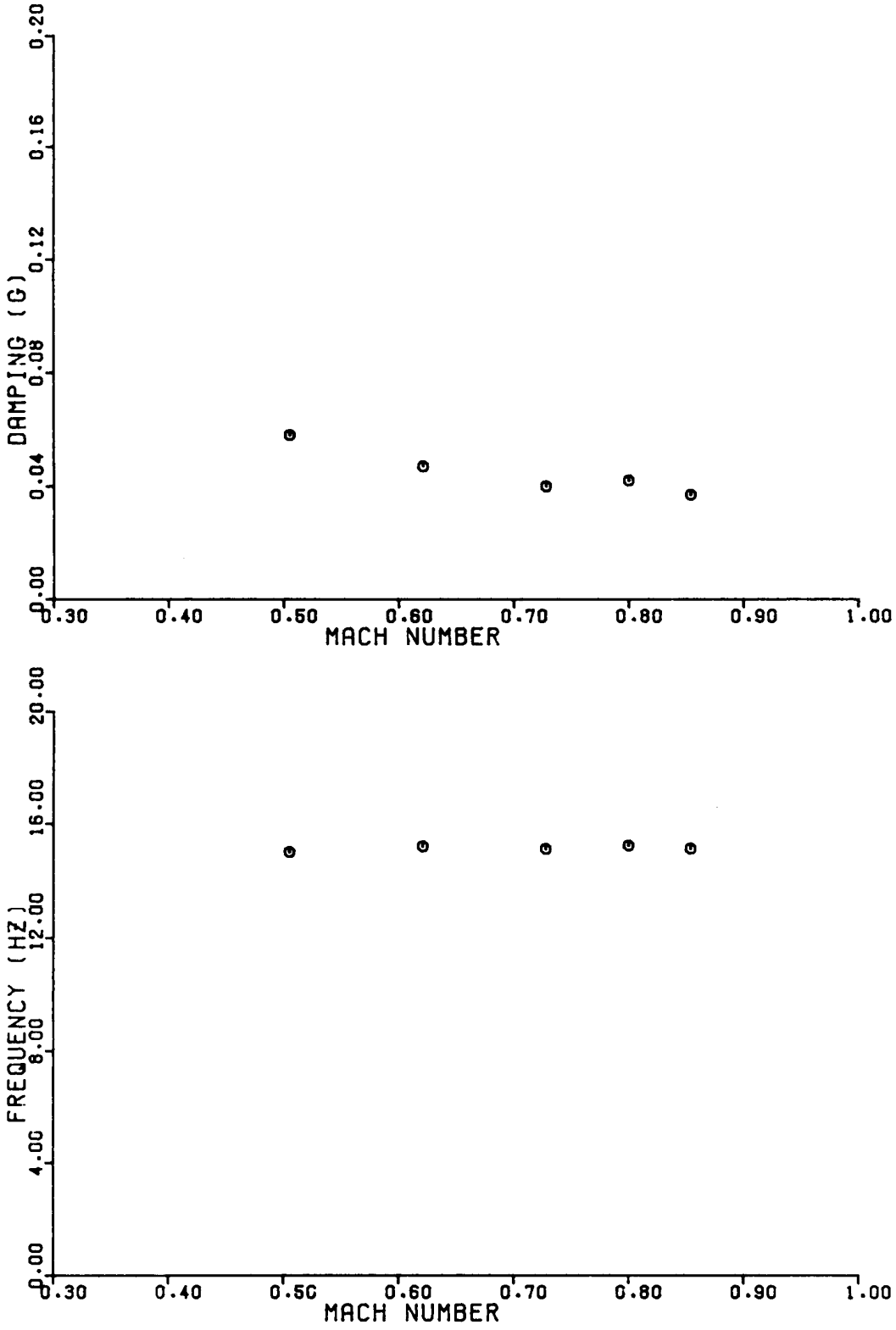

Figure 52. Second symmetric wing bending modal data at 27,500 ft for 35° wing sweep.

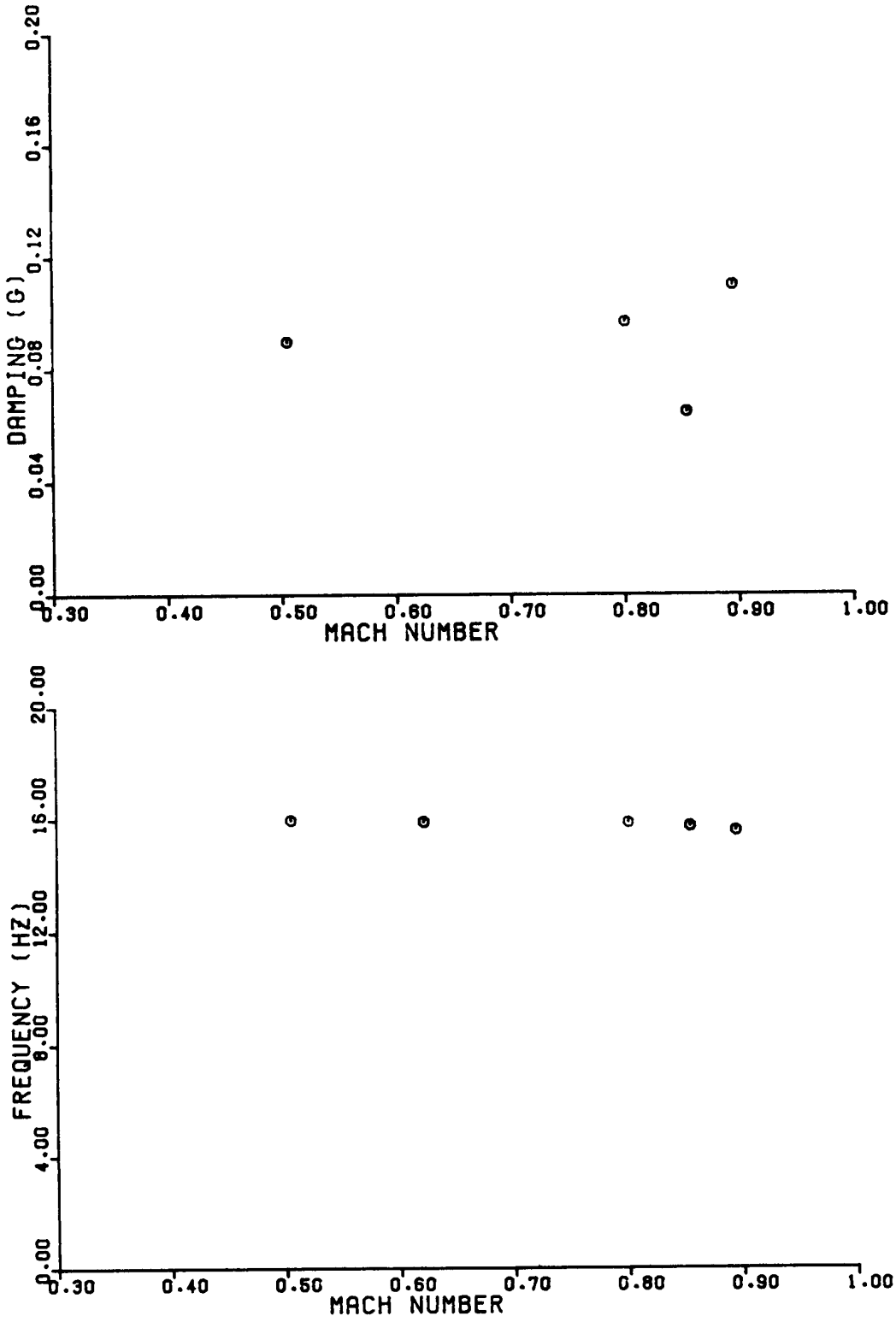

Figure 53. Second antisymmetric wing bending modal data at 27,500 ft for 35° wing sweep.

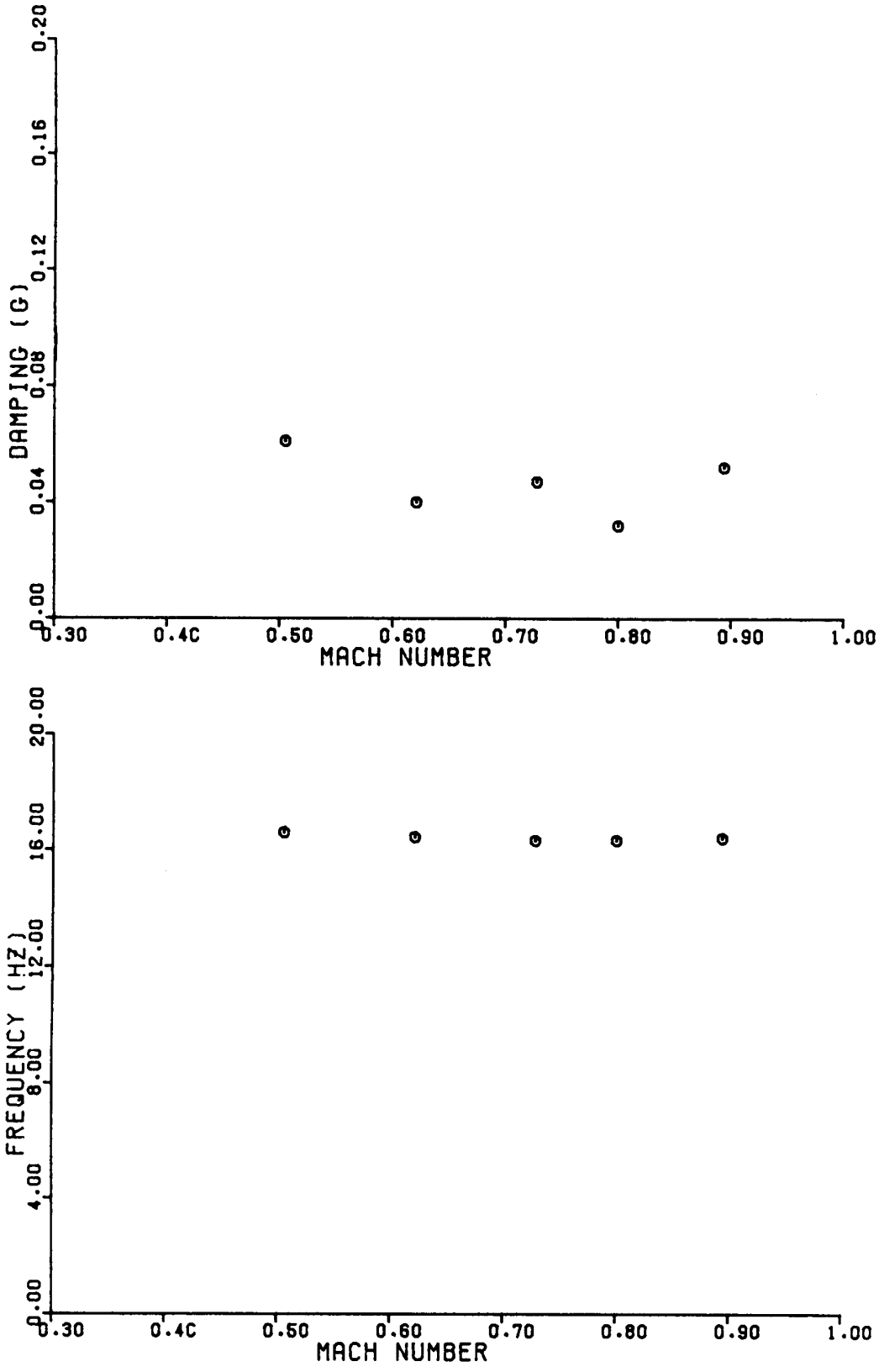

Figure 54. Horizontal stabilator bending modal data at 27,500 ft for 35° wing sweep.

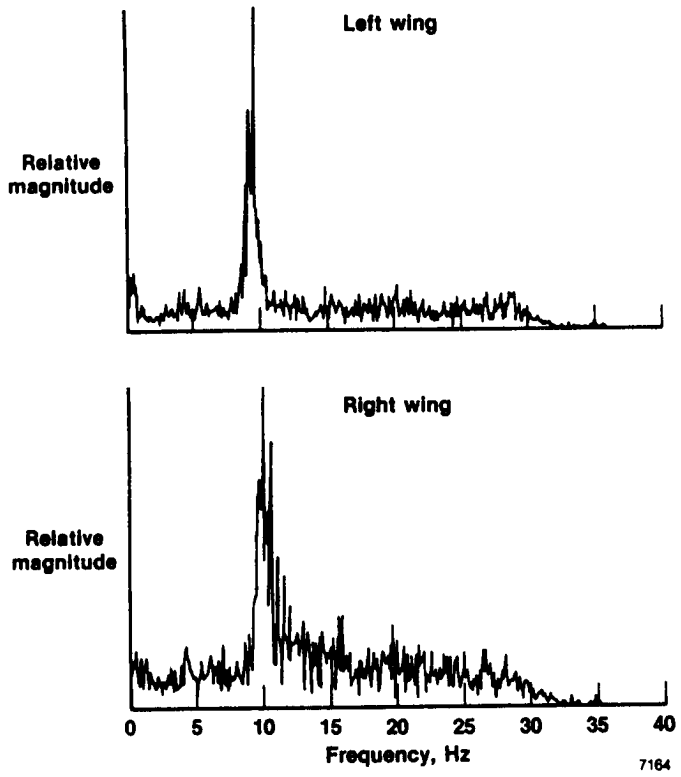

Figure 55. Wingtip fore-and-aft acceleration power spectra for Mach 0.7 at 17,000 ft.

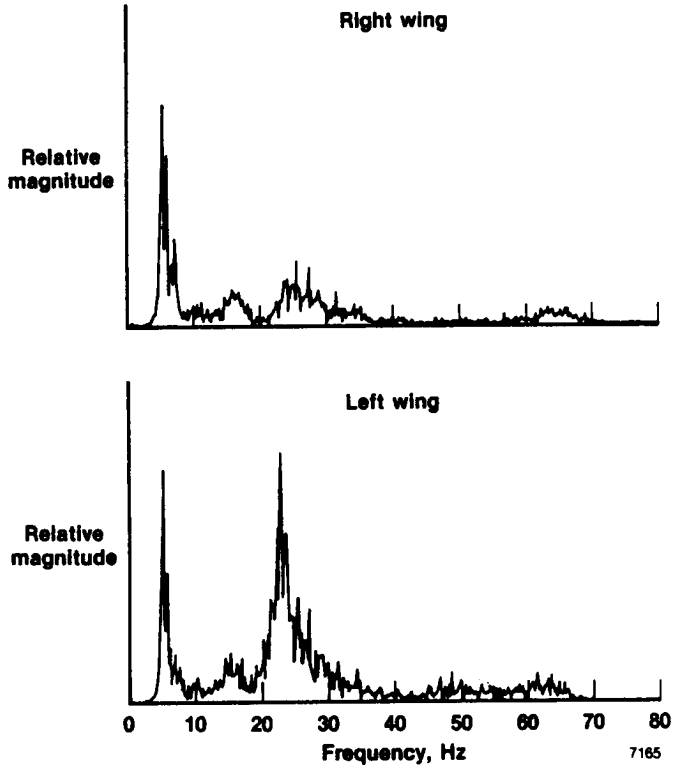

Figure 56. Wingtip vertical acceleration power spectra for Mach 0.85 at 27,500 ft.

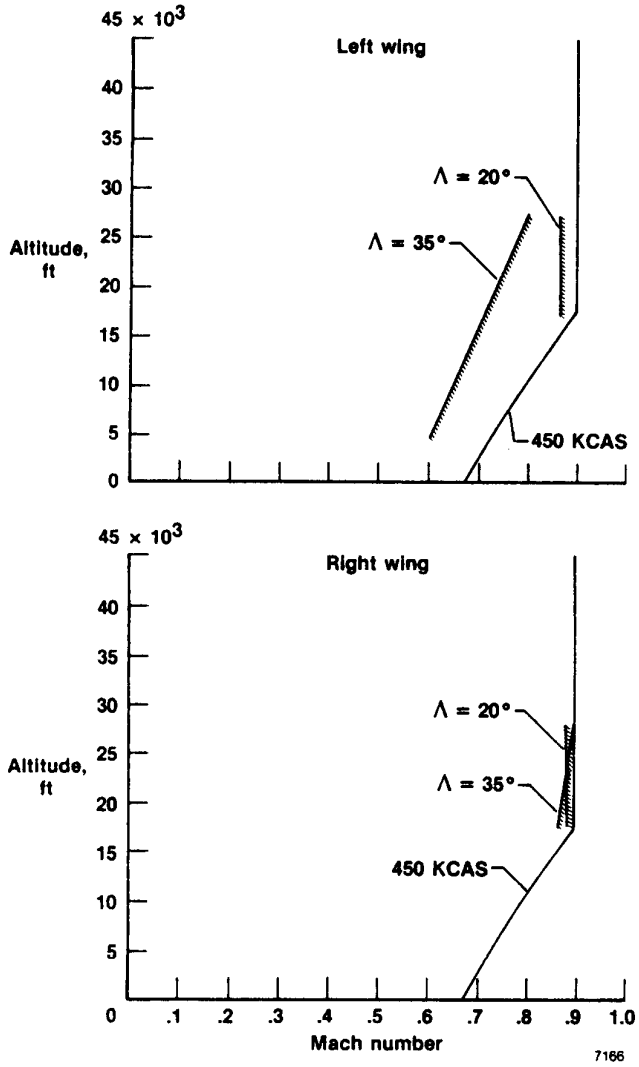

Figure 57. Spoiler resonance onset boundaries.

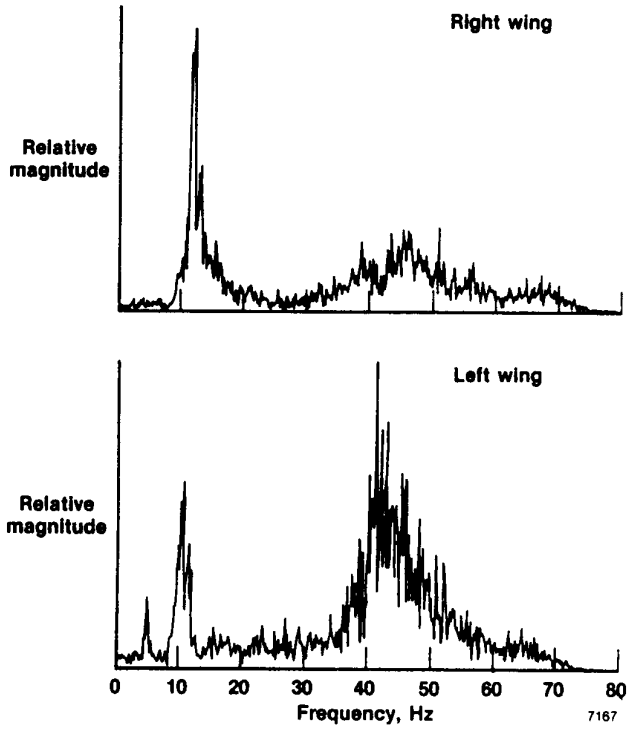

Figure 58. Wingtip fore-and-aft acceleration power spectra for Mach 0.85 at 27,500 ft.

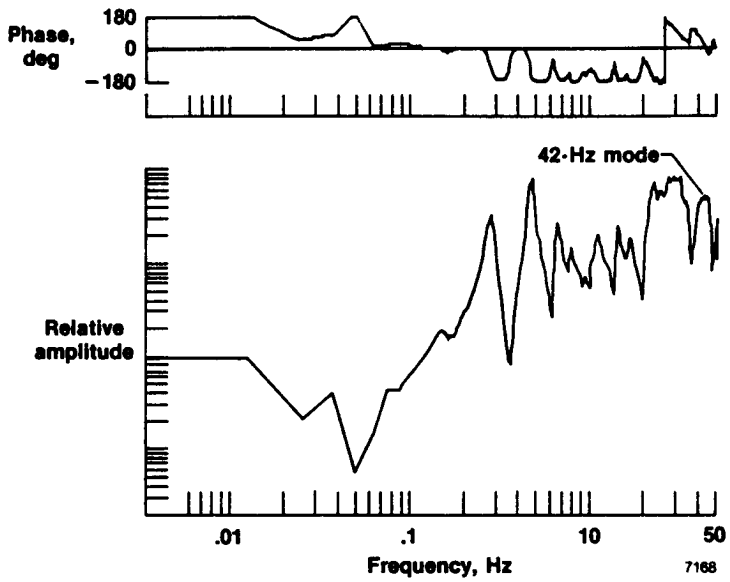

Figure 59. Wing outboard spoiler frequency response.

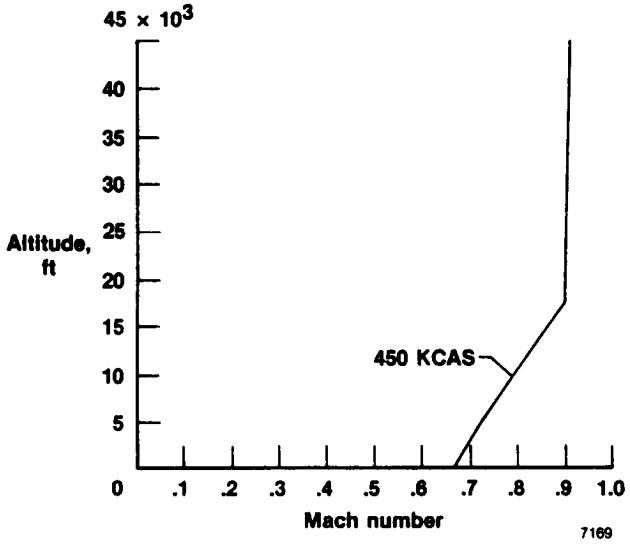

Figure 60. Cleared flutter envelope for the F-14 VSTFE airplane.

1. Report No.	2. Government Accession No.	3. Recipient's Catalog No.
NASA TM-88287		

4. Title and Subtitle	5. Report Date
Flutter Clearance of the F-14 Variable-Sweep Transition Flight Experiment Airplane — Phase I	September 1987
	6. Performing Organization Code
7. Author(s)	8. Performing Organization Report No.
Michael W. Kehoe	H-1402
	10. Work Unit No.
9. Performing Organization Name and Address	RTOP 505-60-31
NASA Ames Research Center Dryden Flight Research Facility P.O. Box 273 Edwards, CA 93523-5000	11. Contract or Grant No.
	13. Type of Report and Period Covered
12. Sponsoring Agency Name and Address	Technical Memorandum
National Aeronautics and Space Administration Washington, DC 20546	14. Sponsoring Agency Code

15. Supplementary Notes

16. Abstract

An F-14 airplane was modified to become the test bed aircraft for the variable-sweep transition flight experiment (VSTFE) program. The VSTFE program is a laminar flow program designed to measure the effects of wing sweep on boundary layer transition from laminar to turbulent flow. The airplane was modified by adding an upper surface foam-fiberglass glove over a portion of the left wing. Ground vibration and flight flutter testing were accomplished to clear a sufficient flight envelope to conduct the laminar flow experiments. Flight test data indicated satisfactory damping levels and damping trends for the elastic structural modes of the airplane. The data presented in this report include frequency and damping as functions of Mach number.

17. Key Words (Suggested by Author(s))	18. Distribution Statement
Flutter Ground vibration test Modal analysis	Unclassified — Unlimited Subject category 05

19 Security Classif. (of this report)	20. Security Classif. (of this page)	21. No. of Pages	22. Price*
Unclassified	Unclassified	64	A04

*For sale by the National Technical Information Service, Springfield, Virginia 22161.